AFRL-SR-AR-TR-03-

0363

REPORT DOCUMENTATION PAGE

1. REPORT DATE (DD-MM-YYYY)	2. REPORT TYPE	3. DATES COVERED (From - To)
12/31/2002	Final Report	6/1/2001-11/30/2002

4. TITLE AND SUBTITLE

Multi-physics Modeling and Simulation of Process-Induced Stresses in Polymer Matrix Composites

5a. CONTRACT NUMBER

F49620-01-1-0431

5b. GRANT NUMBER

5c. PROGRAM ELEMENT NUMBER

6. AUTHOR(S)

Kishore V. Pochiraju

5d. PROJECT NUMBER

5e. TASK NUMBER

5f. WORK UNIT NUMBER

7. PERFORMING ORGANIZATION NAME(S) AND ADDRESS(ES)

Stevens Institute of Technology
Castle Point on Hudson
Hoboken, NJ 07030

8. PERFORMING ORGANIZATION REPORT NUMBER

9. SPONSORING/MONITORING AGENCY NAME(S) AND ADDRESS(ES)

12. DISTRIBUTION/AVAILABILITY STATEMENT

Public Availability

13. SUPPLEMENTARY NOTES

14. ABSTRACT

A three-dimensional thermo-chemical simulation of the curing phase of Resin Transfer Molding (RTM) Process and process-induced stress and deformation analysis methodologies are developed. The mechanics model considers orthotropic and thermo-chemically varying viscoelastic stiffness of the composite material and varying boundary conditions during the process cycle. The residual stress and deformation profiles resulting from several processing histories including the effect of thermal expansion, and chemical shrinkage are studied. Several numerical simulations are performed to compare and validate the developed method with the existing solutions.

15. SUBJECT TERMS

Process Induced Stress and Deformation, Matrix Cure, Cure Dependent Viscoelasticity, Finite Element Method, Three Dimensional, Micro-Mechanical Structure-Property Relationships.

16. SECURITY CLASSIFICATION OF:			17. LIMITATION OF ABSTRACT	18. NUMBER OF PAGES	19a. NAME OF RESPONSIBLE PERSON
a. REPORT	b. ABSTRACT	c. THIS PAGE			19b. TELEPHONE NUMBER (Include area code)

Multi-Physics Modeling and Simulation of Process-Induced Stresses in Polymer-Matrix Composites

Project Report
June 2001 - 2002

Program Manager: Dr. H. T. Hahn
AFOSR

Principal Investigator: Dr. Kishore Pochiraju

Graduate Students: A. Cheung
Y. Yu

AFOSR Contract# F49620-01-1-0431

STEVENS
Institute of Technology

Department of Mechanical Engineering
Stevens Institute of Technology, Hoboken, NJ 07030

SUMMARY FACT SHEET

Multi-Physics Modeling and Simulation of Process-Induced Stresses in Polymer-Matrix Composites / Dr. Kishore Pochiraju

Summary:

A three-dimensional thermo-chemical simulation of the curing phase of Liquid Composite Molding Process coupled with process-induced stress and deformation analyses are developed. The mechanics model considers orthotropic and thermo-chemically varying viscoelastic stiffness of the composite material and varying boundary conditions during the process cycle. The residual stress and deformation profiles resulting from several processing histories including the effect of thermal expansion, and chemical shrinkage are studied. Several numerical simulations are performed to compare and validate the developed method with the existing solutions.

What Was Accomplished:

A Galerkin finite element with an Jacobi Conjugate Gradient (JCG) iterative solver is used to solve the thermal equilibrium and chemical kinetics during the curing phase of RTM process. The mold temperature history and molding process parameters are translated into initial and boundary conditions of the simulation. The temperature and degree of cure fields and their gradients are obtained during the curing process. Two material constitutive models describing the thermoelastic and viscoelastic behavior of the material are considered. Effective composite mechanical properties were computed using the instantaneous resin and fiber properties in a self-consistent field micromechanics model. For the viscoelastic constitutive equation, the cure and temperature dependent stress relaxation modulus was approximated as a Prony series of a number of Maxwell elements. The composite constitutive behavior is then implemented into a general purpose finite element software to determine the evolution of the residual stress and deformations with temperature and degree-of-cure dependent material behavior. Several numerical simulations are performed to compare the results with other numerical and approximate solutions available in the literature. Thus, a comprehensive methodology for predicting process-induced stress and deformations in composite materials is formulated, implemented and validated.

Why It Is Important:

Processing history strongly contributes to the residual stress development leading to part warpage and shrinkage and potential reduction in the absolute strength of the composite. Several applications, including modeling the residual stress and deformation evolution during RTM processing, analysis and optimization of process cycles for reduced process induced stress, and a novel use in the prediction of long term performance of the composites, are anticipated from the developed methodology.

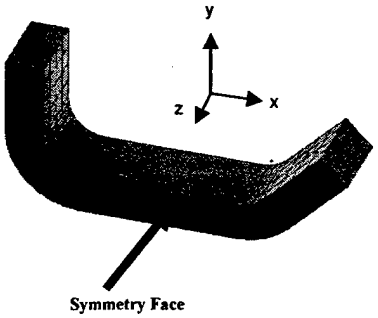

Three dimensional geometry of a typical part considered for numerical analysis.

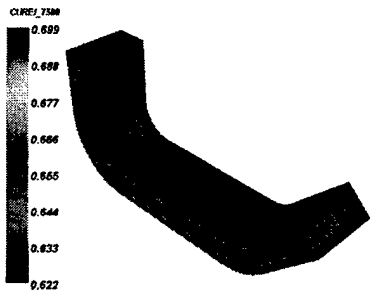

The degree of cure profiles shown at maximum exotherm point during cure

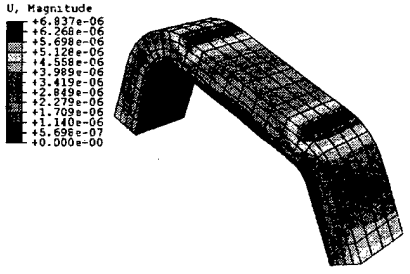

Residual deformations after demolding.

Abstract

The process-induced stress and deformation development in unidirectional composites was investigated. Processing history strongly contributes to the residual stress development leading to part warpage and shrinkage necessitating the ability to accurately simulate the manufacturing process of composites. The focus of this study is the development of a three-dimensional thermo-chemical cure simulation of the Resin Transfer Molding (RTM) process coupled with a process-induced stress and deformation analysis. A Galerkin finite element approach was used to solve the thermal equilibrium and chemical kinetics during the curing phase of RTM process. The part was subjected to mold temperature history corresponding to a specified manufacturing process plan. The temperature and degree of cure fields and their gradients are obtained during the curing process. The temperature and degree of cure fields obtained from the cure simulation are used to examine the residual stress and deformation developed during the curing phase. Two material constitutive models, thermo-elastic and viscoelastic, were studied. For the thermo-elastic approach, the rule of mixtures was used to depict the kinetic-viscoelastic behavior of the resin modulus. Effective composite mechanical properties were computed using the instantaneous resin and fiber properties in a self-consistent field micromechanics model. For the viscoelastic constitutive equation, the cure and temperature dependent stress relaxation modulus was approximated as a Prony series of a number of Maxwell elements. The

residual stress resulting from the processing history, thermal expansion, and chemical shrinkage were studied. For both models, ABAQUS finite element software was implemented to perform the stress and deformation analysis.

Contents

Tables

Table

Figures

Figure

NOMENCLATURE

$[\mathcal{A}]$	coefficient matrix
$\{\mathcal{B}\}$	right-hand-side vector of the linear system
$[\mathcal{C}]$	the capacity matrix
C_{pf}	specific heat of fiber
C_{pr}	specific heat of resin
H_r	resin heat of reaction
$[\mathcal{K}]$	the stiffness matrix
K_{xx}	thermal conductivity in x-direction
K_{yy}	thermal conductivity in y-direction
K_{zz}	thermal conductivity in z-direction
k_f	thermal conductivity of fiber
k_r	thermal conductivity of resin
N_e	total number of elements
N_n	total number of nodes
$[\mathcal{R}]$	the residual vector of linear system
R	ideal gas law constant
$\dot{R}$	rate of heat generation
r_α	reaction rate
T	temperature distribution
t	time
$\{\mathcal{T}\}$	temperature solution vector

α	degree of cure
Γ	boundary of the mold
Δt	time step size
θ	time integration coefficient
v_p	porosity
$v_f = 1 - v_p$	fiber volume fraction
ρ_f	density of fiber
ρ_r	density of resin
$\{\Phi\}$	interpolation function vector
Φ_i	interpolation function at the ith node
Ω	the computational domain
Ω_m	the domain of mold
Ω_p	the domain of part
$\partial/\partial n$	the outward normal derivative to Γ
E_m	instantaneous matrix modulus
E_m^0	fully uncured matrix modulus
E_m^∞	fully uncured matrix modulus
γ	matrix modulus fitting parameter
V_{ch}	volumetric shrinkage
V_{ch}^T	total volumetric shrinkage of matrix
ε^Δ	time-dependent non-mechanical strain
ε_{ch}	strain due to chemical shrinkage
κ_{jk}	effective chemical shrinkage coefficient
ϕ_{jk}	effective thermal expansion coefficient
σ	time-dependent stress

Q	time-dependent effective stiffness matrix of composite
Q^u	fully unrelaxed (elastic) stiffness matrix of composite
Q^∞	fully relaxed stiffness matrix of composite
R_f	partition factor
t, t'	present and past time
ξ, ξ'	present and past reduced time
a_T	shift function
T_g	glass transition temperature
τ^p	peak stress relaxation time
τ_ω	discrete stress relaxation time
W_ω	weight factor
$\vec{X}$	location vector

Superscripts

e	element
i, j	the ith and jth element
n	the nth time step

Chapter 1

INTRODUCTION

The use of composite materials offers the attractive quality of high strength-to-weight ratios. This characteristic is beneficial especially in applications such as the tail or wing of an aircraft. Although, composite materials offer tremendous advantages, the use of composite structures in many applications has not been widespread and has been limited to small components. This lack of use can be attributed to the complexity involved in accurately predicting the behavior of the composite part. The manufacturing process has a significant effect on the overall mechanical properties of the part. In addition, the phases of the manufacturing process are tightly coupled adding to the complexity of the manufacturing process model. During the manufacturing process, process-induced residual stress and deformation develop, which leads to detrimental effects such as part warpage and dimensional instability.

The objective of this study is to determine the residual stress and deformation states for fiber-reinforced composite structures arising from the manufacturing process, particularly the curing phase. During the curing phase, the mechanisms of thermal expansion and chemical shrinkage drive the evolution of

residual stress and deformation. In addition, the material behavior is viscoelastic necessitating the need of an accurate constitutive relation in terms of the process variables of time, temperature, and degree of cure. In order to determine the residual stress, the following approach was utilized:

- Simulate the thermo-kinetic cure cycle process
- Obtain temperature and degree of cure fields during process cycle
- Model fiber reinforcement structure to obtain effective mechanical properties
- Implement a time, temperature, and degree of cure dependent viscoelastic constitutive model in a generalizable stress simulation and obtain residual stress and deformation

The methodology of the present study is summarized in Figure 1.1. In this methodology, the simulation of the cure phase and stress development are not performed simultaneously. The temperature and cure fields obtained from the cure simulation are inputs to the residual stress simulation.

The following study will review the modeling and simulation of residual stress and deformation in polymer matrix composites during the cure cycle. Chapter 2 focuses on the development and implementation of the cure simulation, in which the Galerkin finite element method is employed. Numerical examples for a flat plate and curve-shaped geometry are presented. In Chapter 3, a discussion on the residual stress and deformation is presented, which includes a thermo-elastic

and viscoelastic formulation. For the viscoelastic formulation, a study of the behavior of an isotropic and orthotropic material was conducted. In addition, a time, temperature, and cure dependent viscoelastic constitutive relation was investigated. Numerical results of the three different approaches are also presented after each section. Chapter 4 is devoted to a discussion of the results.

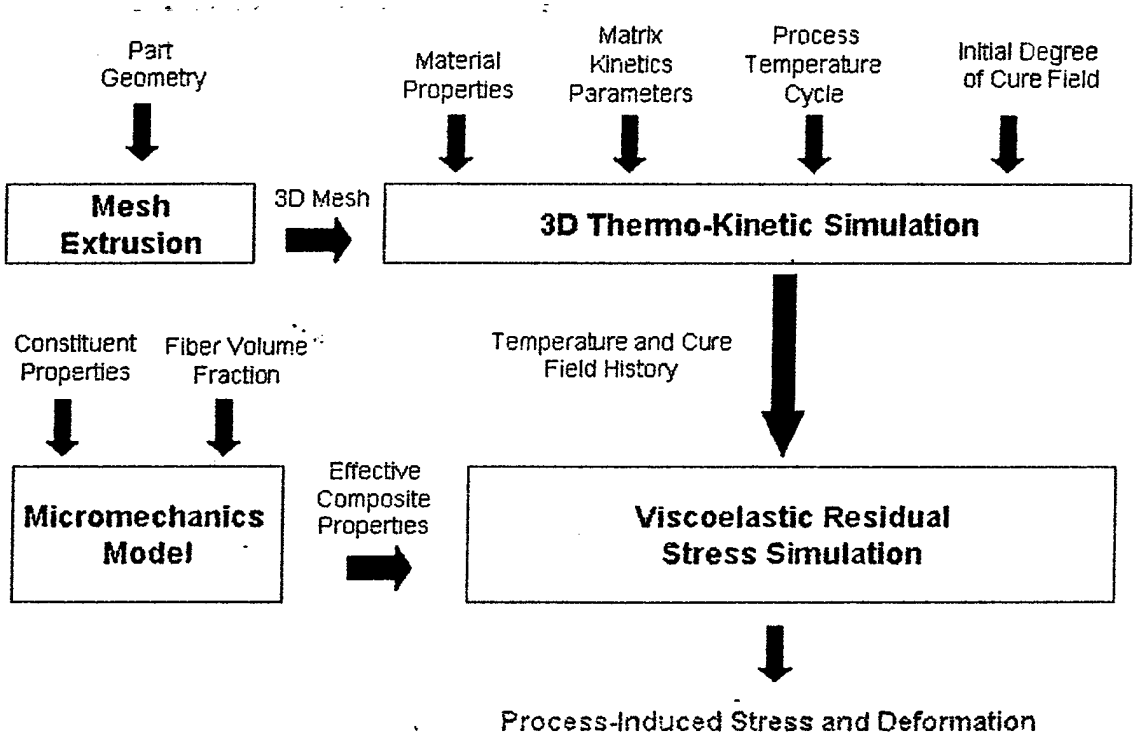

Figure 1.1: Methodology of Coupled Cure and Stress Simulation

Chapter 2

CURE SIMULATION

2.1 Introduction

The utilization of polymer composite materials in many of today's industrial, space, and military applications has brought the understanding of the various liquid composite molding (LCM) processes to the forefront of engineering and science. In addition to high strength-to-weight ratios, the use of composite materials offer an increased fatigue life, improved corrosion and wear resistance, low thermal conductivity, and design flexibility. Unfortunately, this design flexibility introduces greater design challenges not seen with conventional homogeneous materials. The various combinations of fiber and matrix configuration, manufacturing process and conditions, etc. enhance the complexity of characterizing its mechanical properties. Several models have been developed to determine the mechanical properties based on the constituents and fiber volume fraction. Moreover, the input parameters of the LCM process greatly affect the performance and quality of the final part. As a result, the process presents the manufacturing challenge of producing a high quality product at minimum cost. Because of

the complexity in the characterization of composites, computer simulations of the process are necessary to reduce the time and cost of experiments and trial and error manufacturing.

One of the typical LCM processes used to develop composites is resin transfer molding (RTM). RTM is often used to produce large, net-shaped parts yielding high strength-to-weight ratios. The process entails a thermosetting resin injected into a heated mold packed with a fiber preform and cured under controlled temperatures. The process cycle for polymer matrix composites (PMCs) with a thermosetting resin matrix consists of the following stages: 1) mold filling, 2) curing, 3) mold cooling, and 4) demolding. During the mold filling stage, the injection pressure, temperature of the mold, permeability of the matrix, resin viscosity, flow rate, location of gates, etc. dictate the quality of the part. While this stage of the process plays an important role in the outcome of the final part, the mold filling and curing stages are decoupled and the curing stage is the main focus of this study.

A typical cure cycle consists of two dwell temperatures. In a two-step cure cycle, the material temperature is raised from room temperature to the first dwell temperature and held constant for about an hour. During the first dwell, excess gases are removed and the viscosity of the matrix material is lowered to facilitate flow and compaction of the part. The temperature is increased to the second dwell temperature which allows the cross-linking of the polymer to take place. [1] There is a minimum temperature required before cross-linking begins. High

cure temperatures increase the reaction rate and lower the cycle time and cost. However, higher cure temperatures lead to the development of process-induced residual stresses, which result in part warpage and dimensional instability. Therefore, it is important to understand and simulate the mechanisms contributing to the curing phase stress development.

A distinction between thin and thick section composites must be made before proceeding with any type of residual stress analysis. Thick section composites experience a number of manufacturing problems that do not appear in thin section laminates such as thermal spiking, non-uniform consolidation, and non-uniform curing [2]. The heat released from the exothermic cross-linking reaction causes the temperature increase in the interior of the part. With thin section composites, the heat is quickly transmitted to the outer edges. However, in thick section composites, the low thermal conductivity prevents the quick dissipation of the heat resulting in thermal spiking and large thermal gradients.

2.2 Literature Review

Large thermal gradients create differential degree of cure and cause varying thermal expansions from the mismatch of coefficients of thermal expansion (CTE) and chemical shrinkage, especially in thick section composites [3], which lead to significant residual stress development. Various studies have been conducted in order to gain an understanding of the curing phase. Early work by Loos and Springer [4] involved the development of a one-dimensional cure simulation of a

flat plate using an implicit finite difference method. Bogetti and Gillespie [5] conducted a two-dimensional cure simulation in thick anisotropic thermosetting composites with a coupled thermal and chemical kinetics formulation using the finite difference method. Yi et. al. [6] developed a nonlinear transient heat transfer finite element model where material parameters are both temperature and degree of cure dependent. In the work of Park and Lee [7], a two dimensional cure simulation was also developed and introduced a degeneration method to build the thermal conductivity matrix. Zhu et. al [8] presented a full three-dimensional coupled thermo-chemo-viscoelastic model simulating the heat transfer, curing, residual stresses and deformation of a composite part. For the cure simulation, the thermal and cure mass matrices were lumped via the HRZ lumping scheme [9] to prevent negative degree of cure values. The Newton-Raphson method and an adaptive time stepping technique are employed in the finite element solution.

The thermo-chemo equilibrium equation includes the internal heat generation term resulting from the exothermic cure reaction. Different reaction rate models have been presented for several material systems, particularly glass/polyester and graphite/epoxy. The model for the Hercules 3501-6 epoxy resin was developed by Loos and Springer [4]. Bogetti and Gillespie [5] modeled the glass/polyester system. Later cure models [1],[6]-[8], and [10] used the same models for the polyester and epoxy systems.

2.3 Problem Description

In a study of the residual stress and deformations of PMCs, the temperature and degree of cure history throughout the part is necessary. The Galerkin finite element formulation was used for the coupled thermo-kinetic simulation in this effort. This methodology is suited for solving large meshes using element-free and iterative solution techniques for increased computational efficiency when dealing with large mesh sizes [11]. The paper presents the formulation, illustration of typical results, and examples used for verification of the implementation. Two numerical examples are presented for which prior results and experimental data are available in the literature. The next section presents the thermo-kinetic formulation proceeded by the two numerical examples. The cure simulation is then followed by different approaches to model the residual stresses and deformations during the curing phase

2.4 Cure Simulation Formulation

The in-mold curing phase of the RTM process is formulated as a coupled thermo-kinetic analysis. The presence of separate and dissimilar material phases (fiber and matrix) is modeled using effective property homogenization. The effective physical and thermal properties are determined from the fiber and matrix properties, the fiber volume fraction and orientation. Two separate kinetics models are used to simulate the cure reaction, one appropriate for the glass/polyester and the other for carbon/epoxy systems. The temperature cycle used for the

curing of part is translated into time-dependent mold boundary conditions.

2.4.1 Energy Balance

The three-dimensional time dependent energy balance with orthotropic material conductivity is given as follows:

$$(v_p\rho_r C_{pr} + v_f\rho_f C_{pf})\frac{\partial T}{\partial t} = (K_{xx}\frac{\partial^2 T}{\partial x^2} + K_{yy}\frac{\partial^2 T}{\partial y^2} + K_{zz}\frac{\partial^2 T}{\partial z^2}) + \rho_r v_p \dot{R} \qquad (2.1)$$

where $\dot{R}$ is the rate of heat generation from the chemical reaction, which is related to the total heat of reaction (H_r) and rate of reaction (r_α) as given by the following equation:

$$\dot{R} = H_r r_\alpha \qquad (2.2)$$

The equivalent thermal conductivities, K_{xx}, K_{yy} and K_{zz}, are computed from the fiber and matrix properties. K_{xx} is calculated from rule of mixtures [12] using the fiber volume fraction v_f. The transverse (K_{yy}) and through-the-thickness (K_{zz}) conductivity values are similarly calculated based on the fiber orientation details.

$$k_t = \frac{k_r - k_f}{k_r + k_f + v_f(k_r + k_f)} \qquad (2.3)$$

$$K_{xx} = v_f k_f(1 + v_p k_t) + v_p k_r(1 - v_f k_t) \qquad (2.4)$$

The governing equation is solved subjected to the mold-wall temperature boundary conditions and vanishing heat flux conditions on symmetry boundaries:

$$T = T^{applied}(t) \;\; on\ mold\ surfaces \qquad (2.5)$$

$$-K\frac{\partial T}{\partial n} = 0 \;\; on\ symmetry\ surfaces$$

2.4.2 Cure Kinetics

Curing of polymers is temperature dependent as the reaction kinetics vary with temperature. Also, the reactions are exothermic hence the coupling between thermal balance and cure kinetics. The reaction rate and the degree of cure, α are related by the following rate equation:

$$\frac{\partial \alpha}{\partial t} = r_\alpha \tag{2.6}$$

with the initial condition, $\alpha_0 = \alpha_i$ at $t = t_i$.

For different types of polymerization appropriate kinetic models are required to determine the rate and heat of reaction. Two different models were used for modeling the glass/epoxy and graphite/epoxy systems. The kinetic model used for the glass/polyester material is as follows [5]:

$$\frac{d\alpha}{dt} = (K_1 + K_2\alpha^m)(1-\alpha)^n \tag{2.7}$$

$$K_1 = A_1 e^{\frac{-E_1}{RT}} \tag{2.8}$$

$$K_2 = A_2 e^{\frac{-E_2}{RT}}$$

The model for the graphite/epoxy is a three-term rate equation as shown below [4]:

$$\frac{d\alpha}{dt} = (K_1 + K_2\alpha)(1-\alpha)(0.47-\alpha) \;\; for \;\; (\alpha \leq 0.3) \tag{2.9}$$

$$\frac{d\alpha}{dt} = K_3(1-\alpha) \;\; for \;\; (\alpha > 0.3) \tag{2.10}$$

$$K_1 = A_1 e^{\frac{-E_1}{RT}} \tag{2.11}$$

$$K_2 = A_2 e^{\frac{-E_2}{RT}}$$

$$K_3 = A_3 e^{\frac{-E_3}{RT}}$$

The thermal balance and kinetics equations are solved in an incremental/iterative time stepping scheme where the temperature and degree of cure is determined sequentially at each time step.

2.4.3 Galerkin Finite Element Method

The computational domain, Ω, is discretized by a union of finite elements $\Omega^{(e)}$ as $\Omega = \Sigma \cup_{e=1}^{N_e} \Omega^{(e)}$, where $\Omega^{(i)} \cap \Omega^{(j)} = \emptyset$, if $i \neq j$ and N_e is the total number of elements in Ω. The approximate element solution is defined as:

$$T = \{\Phi(x,y,z)\}^T \{\mathcal{T}(t)\} \tag{2.12}$$

For the Galerkin method, the weight function is chosen as:

$$w = \{\Phi(x,y,z)\} \tag{2.13}$$

Equation (2.1) can be integrated by multiplying the weight function and using Green's theorem,

$$[\mathcal{C}] \frac{\partial \{\mathcal{T}\}}{\partial t} + [\mathcal{K}] \{\mathcal{T}\} = \{\mathcal{R}\} \tag{2.14}$$

where

$$[\mathcal{C}] = \sum_e \int_{\Omega^{(e)}} \{\Phi\} \{\Phi\}^T d\Omega \tag{2.15}$$

$$[\mathcal{K}] = C_k \sum_e \int_{\Omega^{(e)}} \left[K_{xx} \frac{\partial \{\Phi\}}{\partial x} \frac{\partial \{\Phi\}^T}{\partial x} + K_{yy} \frac{\partial \{\Phi\}}{\partial y} \frac{\partial \{\Phi\}^T}{\partial y} + K_{zz} \frac{\partial \{\Phi\}}{\partial z} \frac{\partial \{\Phi\}^T}{\partial z} \right] d\Omega \tag{2.16}$$

$$C_k = \frac{1}{v_p \rho_r C_{pr} + v_f \rho_f C_{pf}} \tag{2.17}$$

$$\{\mathcal{R}\} = C_r \sum_e \int_{\Gamma^{(e)}} r_\alpha \Phi d\Omega \tag{2.18}$$

$$C_r = \frac{\rho_r v_p H_r}{v_p \rho_r C_{pr} + v_f \rho_f C_{pf}} \tag{2.19}$$

Equation (2.14) is discretized by the backward Euler method in time where $\Delta t = t^{(n+1)} - t^{(n)}$.

$$\{[\mathcal{C}] + \Delta t\,[\mathcal{K}]\}\,\{\mathcal{T}\}^{(n+1)} = [\mathcal{C}]\,\{\mathcal{T}\}^{(n)} + \Delta t\,\{\mathcal{R}\} \tag{2.20}$$

Equation (2.20) can be simply denoted as a system of linear algebraic equations defined by,

$$[\mathcal{A}]\,\{\mathcal{T}\}^{(n+1)} = \{\mathcal{B}\}^{(n)} \tag{2.21}$$

where,

$$[\mathcal{A}] = [\mathcal{C}] + \Delta t\,[\mathcal{K}] \tag{2.22}$$

$$\{\mathcal{B}\} = [\mathcal{C}]\,\{\mathcal{T}\}^{(n)} + \Delta t\,\{\mathcal{R}\} \tag{2.23}$$

By multiplying by the weight function, Φ. Eq. (2.6) can be integrated in the same fashion as the thermal balance equation.

$$[\mathcal{C}]\,\frac{\partial \alpha}{\partial t} = \{\mathcal{R}\} \tag{2.24}$$

The kinetics equation(2.24) is also discretized, where $\Delta t = t^{(n+1)} - t^{(n)}$.

$$[\mathcal{C}]\,\alpha^{(n+1)} = [\mathcal{C}]\,\alpha^{(n)} + \Delta t\,\{\mathcal{R}\} \tag{2.25}$$

where

$$[\mathcal{C}] = \sum_e \int_{\Omega^{(e)}} \{\Phi\}\,\{\Phi\}^T\,d\Omega \tag{2.26}$$

$$\{\mathcal{R}\} = \sum_e \int_{\Gamma^{(e)}} r_\alpha \Phi d\Omega \tag{2.27}$$

Equation (2.25) can be denoted as a system of linear algebraic equations defined by,

$$[\mathcal{C}]\,\alpha^{(n+1)} = \{\mathcal{B}\}^{(n)} \tag{2.28}$$

where,

$$\{\mathcal{B}\} = [\mathcal{C}]\,\alpha^{(n)} + \Delta t\,\{\mathcal{R}\} \tag{2.29}$$

HRZ mass lumping scheme [8] is employed to diagonalize the cure matrix, $[\mathcal{C}]$. The diagonalization leads to a inexpensive solution of Eq. 2.29 at each increment.

The solution is performed with a banded solver using Gibbs-Poole-Stockmeyer bandwidth (ACM CALGO Algorithm:582) reduction. The computational times recorded for a 363 degree of freedom problem are 154 milliseconds per time step on a 500 MHZ Pentium III class processor. For a problem with a larger mesh 10125 degrees of freedom and initial band width of 5343, the bandwidth reduction algorithm reduced the bandwidth to 287, and the computational time required was 700 milliseconds per time step.

2.5 Numerical Examples

Two numerical examples are presented to illustrate the results obtained. The results from the current method are compared with those available in the literature and experimental data when available. Two geometry choices, namely a flat plate and a curve-shaped part, and two material systems, namely glass/polyester and carbon/epoxy, are used for the numerical examples.

Table 2.1: Material Properties of Glass/Polyester

Density (ρ)	1890 kg/m^3
Polymer specific heat (C_p)	1260 J/kg-K
Thermal Conductivity (K_{zz})	0.2163 W/m-K
K_{xx}/K_{zz}	2

2.5.1 Curing of a Flat Plate

A flat plate with dimensions of 15.24 cm x 15.24 cm and a uniform thickness of 2.54 cm is considered. Due to symmetry, a quarter of the plate is meshed. The geometry of the model analyzed was 7.62 cm x 7.62 cm and 1.27 cm thick. The thermal and kinetic properties for the glass/polyester can be found in Tables 2.1 and 2.2, respectively. The finite element model used composed of a 200 element 8 node brick mesh. The part was subjected to a prescribed temperature cycle for which experimental results were available [5]. The cycle entails a 60 minute dwell at 78°C, a rise to 90°C and a 70 minute dwell at 126°C as seen in Figure 2.1. Figures 2.2 and 2.3 show the temperature and cure evolution at the center of the plate for the glass/polyester system. These results are in good agreement with the published experimental results. Figure 2.2 shows a maximum temperature of 128°C (a thermal spike) occurring at 165 minutes into the cure cycle due to the exothermal curing reaction. There was a 38°C temperature difference between the boundary and the center of the part. The accuracy of the maximum temperature was found to be sensitive to the time step utilized in the numerical analysis. A time increment of 1 sec was adequate to capture the effects of the exotherm in the simulation. The simulation of the glass/polyester plate was completed with

Table 2.2: Cure Kinetics for Glass/Polyester

A_1 (min^-1)	0
A_2 (min^-1)	3.7 x 10^{22}
E_1 (J/mole)	0
E_2 (J/mole)	1.674 x 10^5
m	0.524
n	1.476
R (J/mol-K)	8.31434
H_r (J/kg)	77,500

13,920 increments (4 hours of simulation time) with a CPU time of 2146 seconds (36 minutes) on a personal computer. From the plot of the degree of cure in Figure 2.3, the value of the degree of cure goes from 0 to 0.99 in a short period of time from 130-150 minutes. This rapid change occurs during the period of the thermal spike further emphasizing the sensitivity of the simulation to the time step.

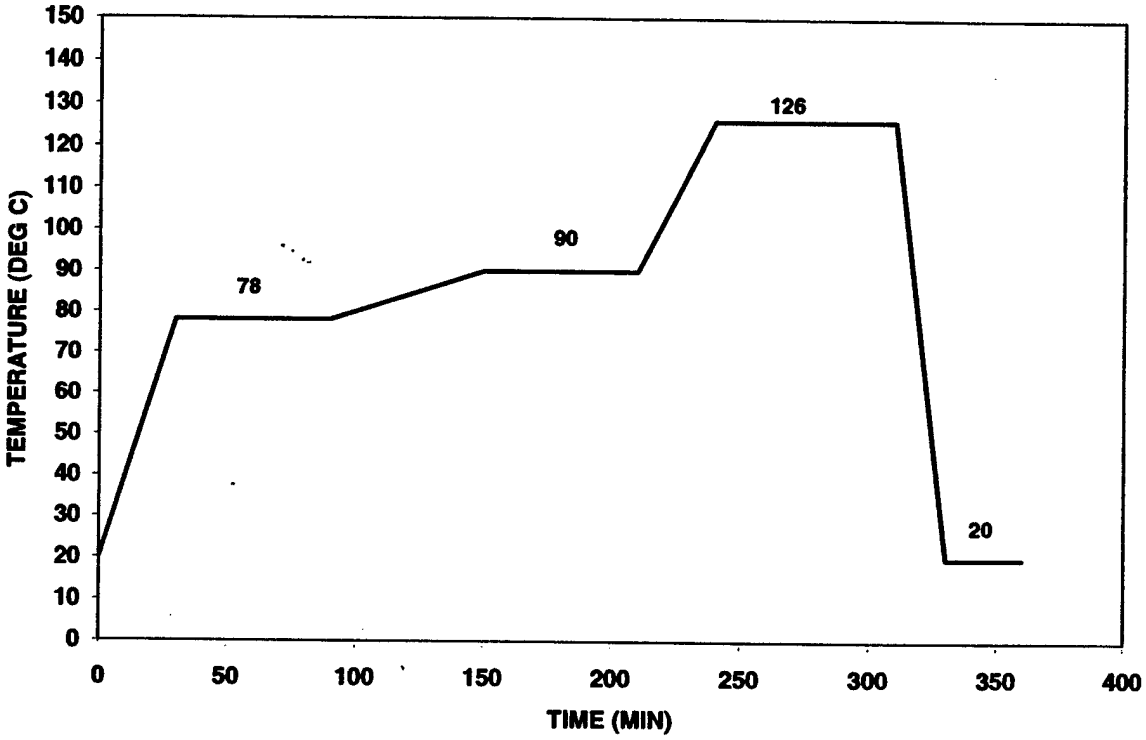

Figure 2.1: Boundary Temperature Cycle for Glass/Polyester Material

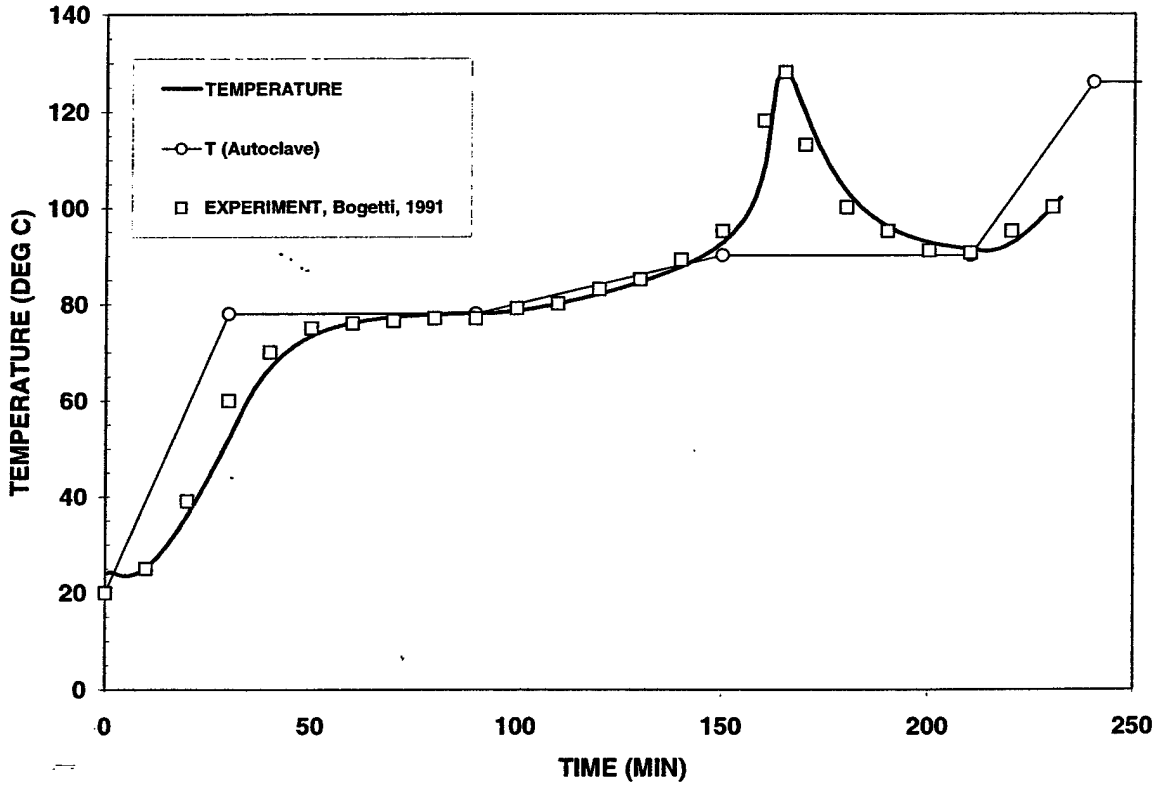

Figure 2.2: Temperature Profile for Center-point Node for Glass/Polyester Plate

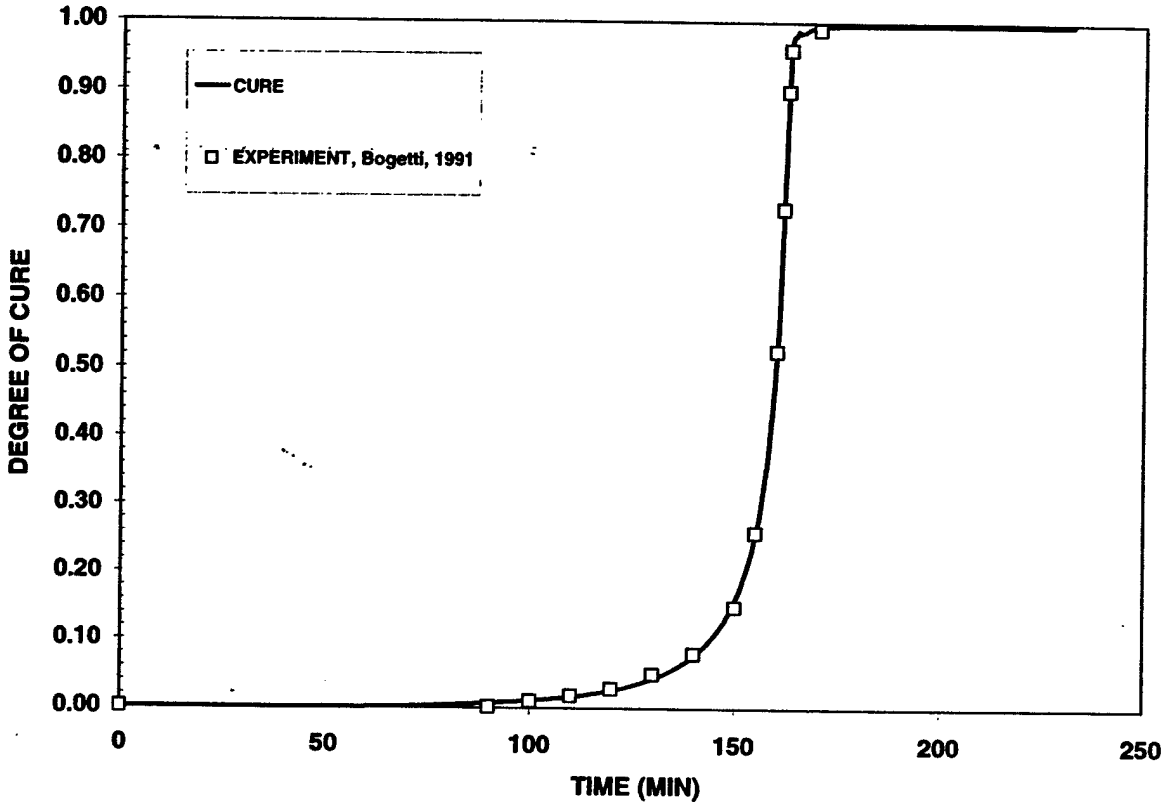

Figure 2.3: Degree of Cure Profile for Center-point Node for Glass/Polyester Plate

The plate curing simulation was also run with graphite/epoxy material properties as given in Tables 2.3 and 2.4. The temperature cycle for the graphite/epoxy material [13] found in Figure 2.4 had a 1 hour dwell at 116°C and a 2 hour dwell at 177°C. The graphite/epoxy plate results in Figures 2.5 and 2.6 were also in agreement with the experiment in [13]. Because of the change in cure kinetic models when the degree of cure reaches above 0.3, the degree of cure profile appears to have two peaks with the transition at 104 minutes. There are two thermal spikes in the temperature profile of the center point node in Figure 2.5. For the first spike, there was a 9°C difference compared to the boundary. There was a 31°C difference for the second spike. The cure simulation for the graphite/epoxy plate required 10,000 iterations (26 minutes of CPU time) with a 1 sec time step. Although the flat plate geometry with uniform thickness may not warrant a three-dimensional analysis, this case was used to benchmark and verify the performance of the present method.

Table 2.3: Material Properties of Graphite/Epoxy

Density (ρ)	1578 kg/m^3
Polymer specific heat (C_p)	862 J/kg-K
Thermal Conductivity (K_{zz})	0.4135 W/m-K
K_{xx}/K_{zz}	1, 5, 10

Table 2.4: Cure Kinetics for Graphite/Epoxy

A_1 (min^-1)	2.102 x 10^9
A_2 (min^-1)	-2.014 x 10^9
A_3 (min^-1)	1.960 x 10^5
E_1 (J/mole)	8.07 x 10^4
E_2 (J/mole)	7.78 x 10^4
E_3 (J/mole)	5.66 x 10^4
R (J/mol-K)	8.31434
H_r (J/kg)	198.6 x 10^3

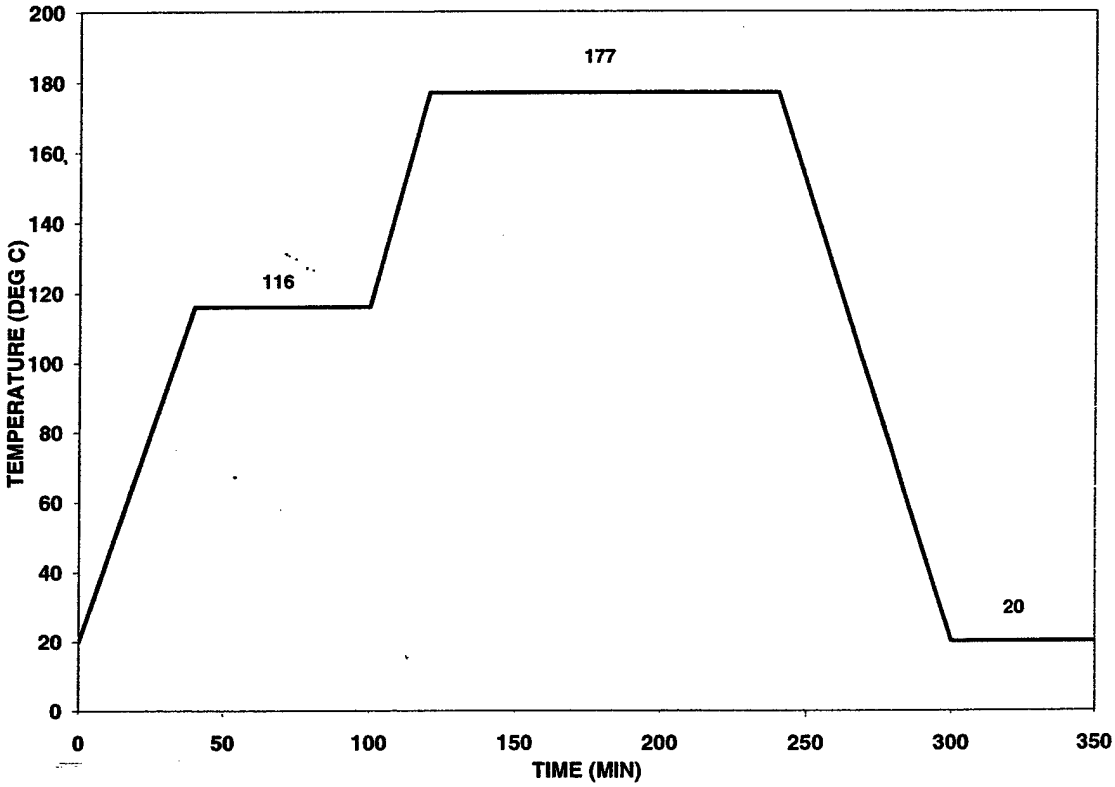

Figure 2.4: Boundary Temperature Cycle for Graphite/Epoxy Material

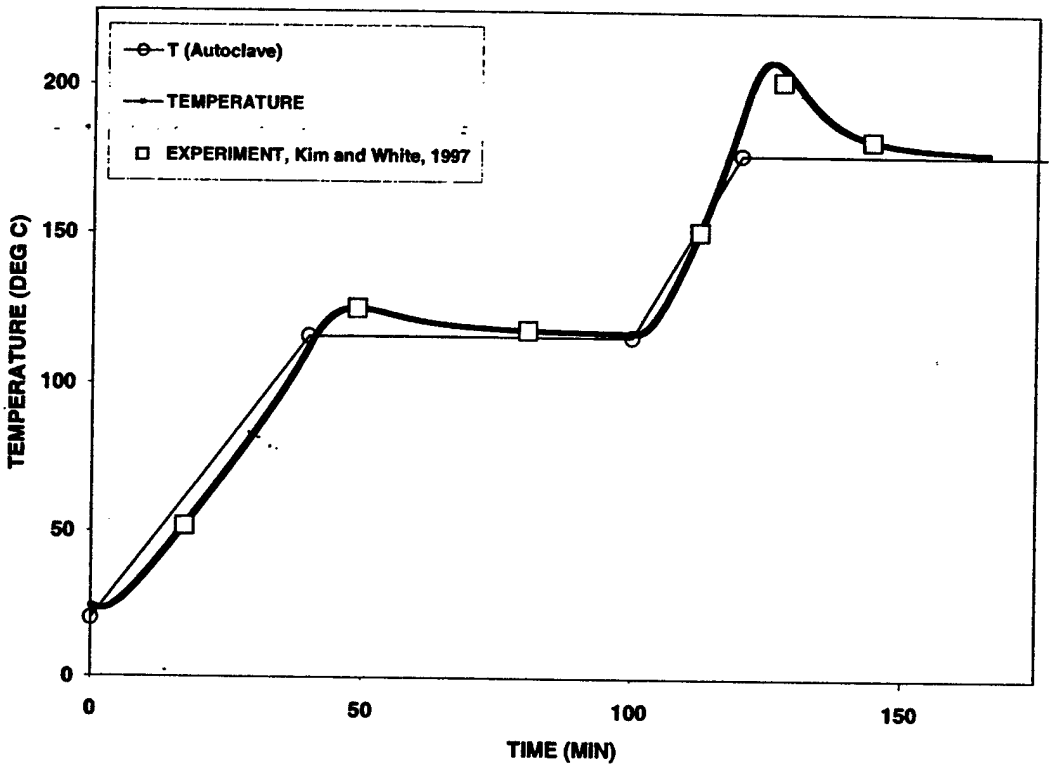

Figure 2.5: Temperature Profile for Center-point Node for Graphite/Epoxy Plate

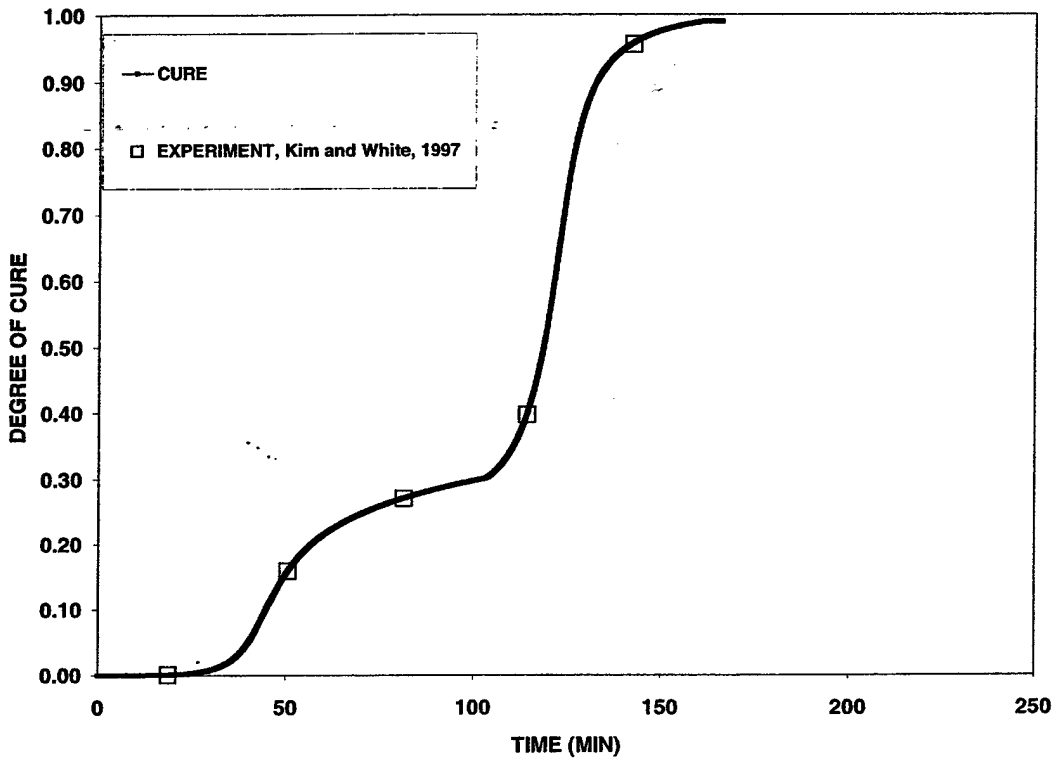

Figure 2.6: Degree of Cure Profile for Center-point Node for Graphite/Epoxy Plate

2.5.2 Curve-Shaped Part

As the second example, the curve-shaped part presented in [8] is analyzed. The dimensions of the cross section are shown in Figure 2.7. The part had an overall width of 8 cm. Because of half-symmetry, the model had a width of 4 cm. The material system used for the part is graphite/epoxy with properties shown in Tables 3 and 4. The temperature cycle in Figure 2.4 was applied to all the boundaries except the front face because of symmetry. The mesh employed has 448 elements and 725 nodes with a bandwidth of 34. The temperature and degree of cure profiles for a node in the center of the part can be found in Figures 2.8 and 2.9, respectively. Using a 1 sec time step, the simulation was complete after 9,960 iterations. The computational time required was in the order of 130 milliseconds per iteration.

For this example we present a series of results detailing temporal and spatial variation of the temperature and degree of cure within the part. Three points in time are selected for obtaining the spatial variations of temperature and cure in the part. The first point, t_a, is at 100 minutes into the cure cycle, before the thermal rise. The other two are at t_b= 113 min and t_c = 125 minutes. The final time, t_c, is at the peak of the thermal spike, while the second point is the midpoint. These points correspond to the rapid reaction phase of the cure cycle as seen in Figure 2.8. The temperature and degree of cure contours are shown on four separate cut-planes in the part seen in Figures 2.10-2.13. As seen in these figures, the temperature increases from a low temperature of 116°C to a high

temperature of 195°C within a short period of time, approximately 25 minutes. The temperature difference is 79°C. Also in this time period, the degree of cure rises from 0.276 to 0.699, a difference of 0.41. The contour plots also show that the highest temperature and degree of cure occur mainly in the middle portion of the part. At point 1 and 2, the temperature and degree of cure is mainly uniform throughout the part, whereas point 3 displays a temperature difference of 18°C.

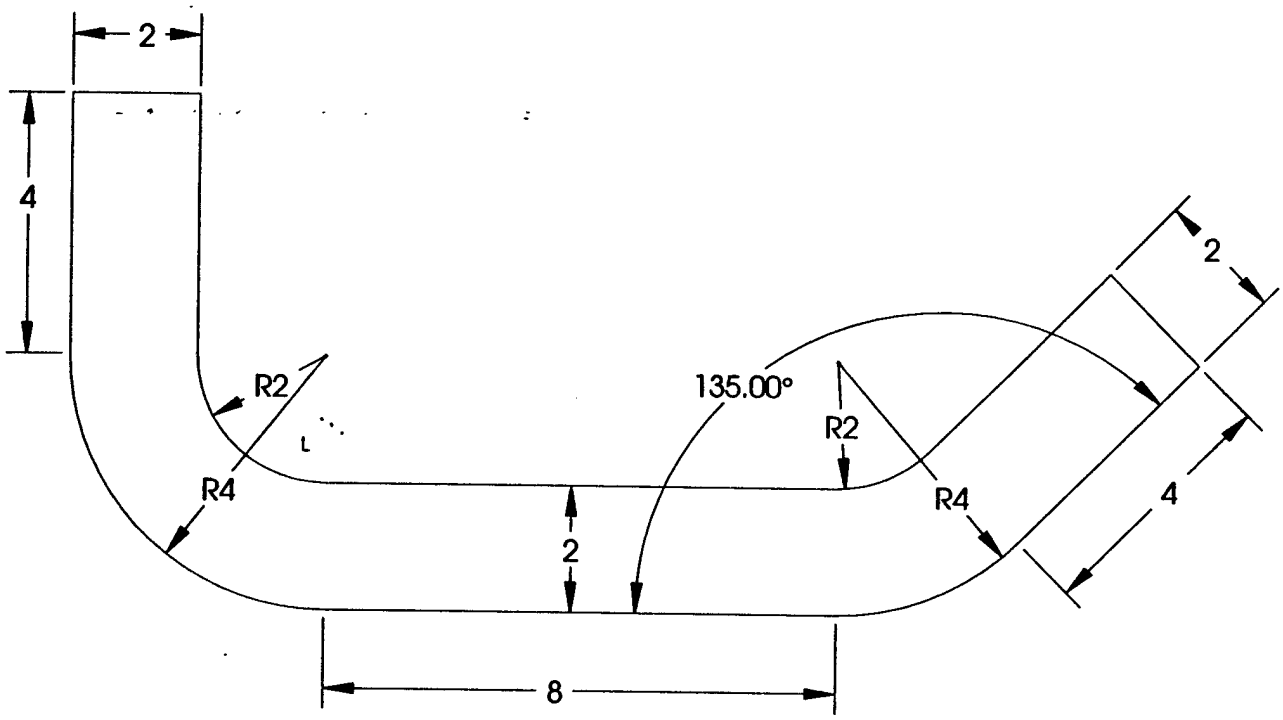

Figure 2.7: Dimensions for Cross-Section of Curve Shaped Part (units in cm)

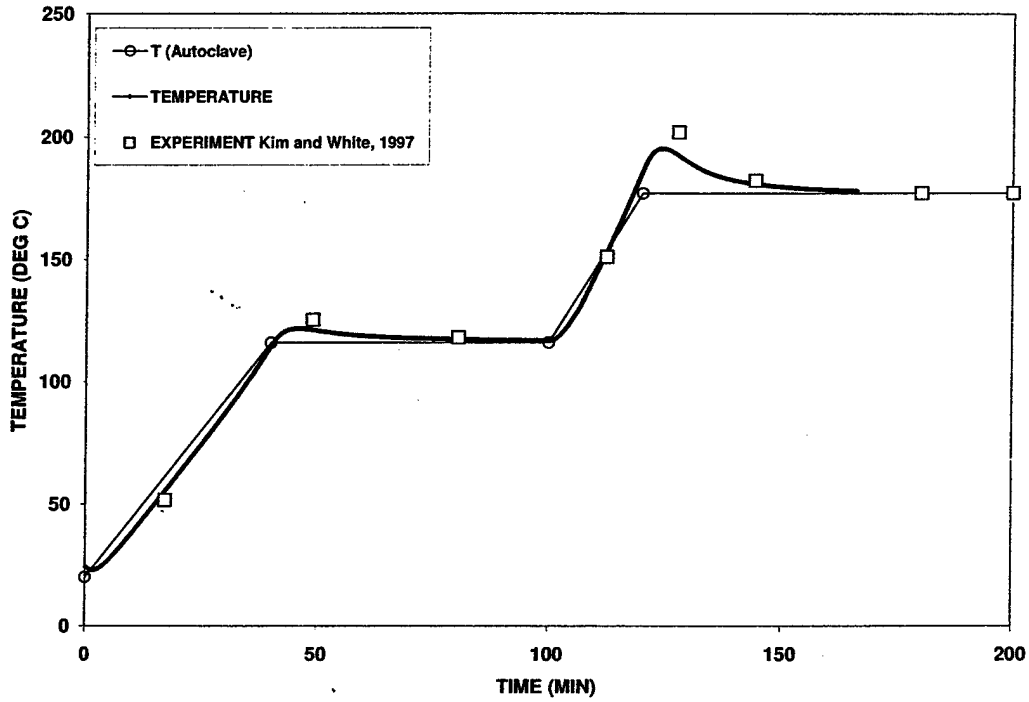

Figure 2.8: Temperature Profile for Center-point Node for Curve Shaped Part

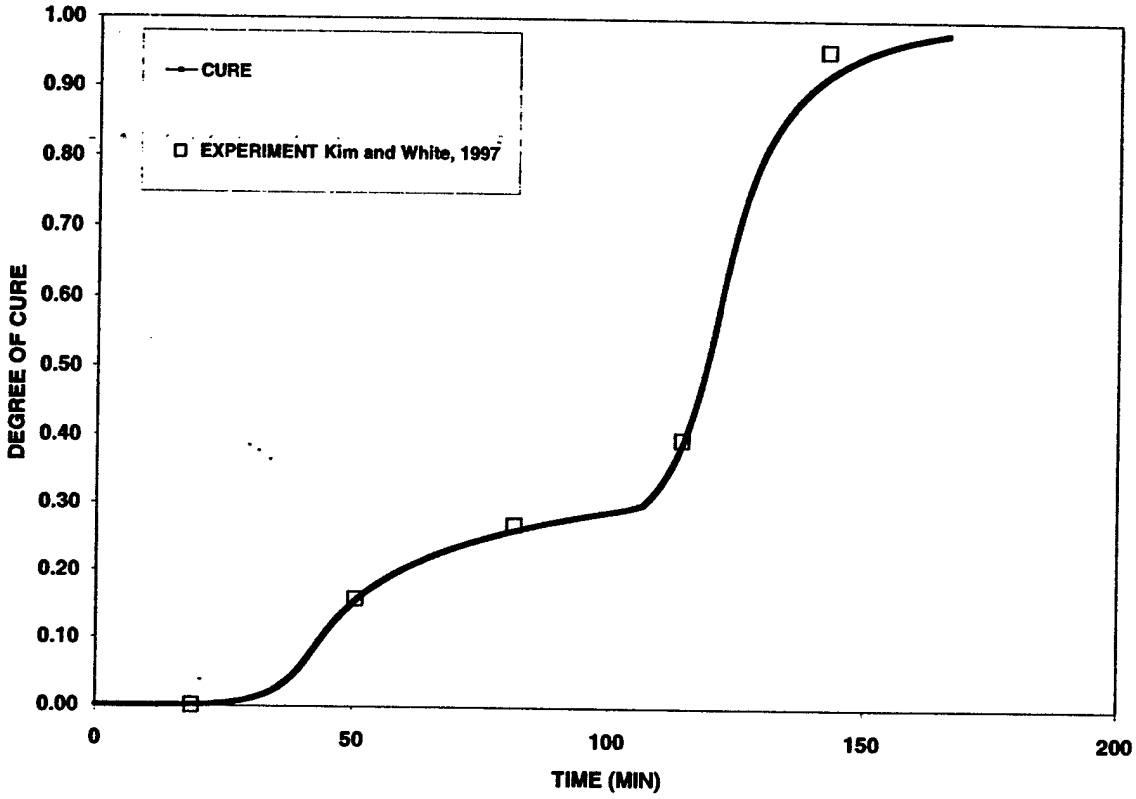

Figure 2.9: Degree of Cure Profile for Center-point Node for Curve Shaped Part

time = 100 min

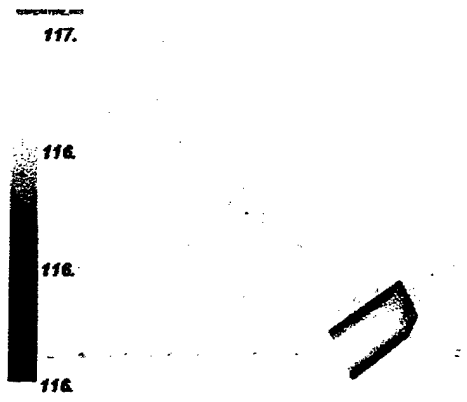

(a)

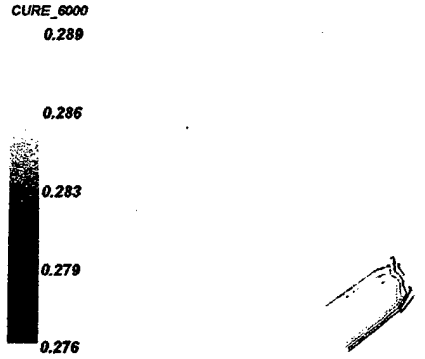

(d)

time = 113 min

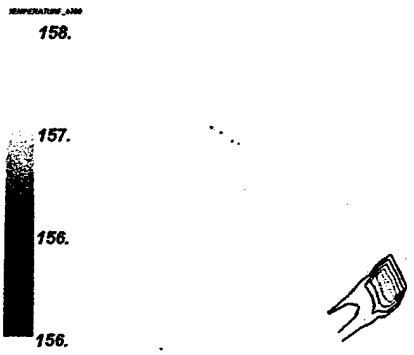

(b)

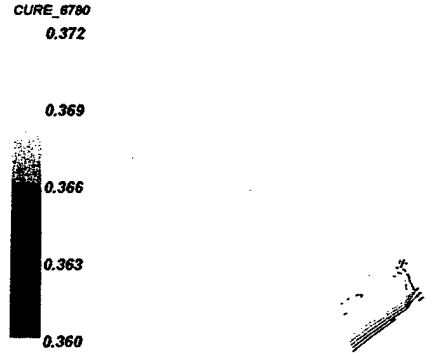

(e)

time = 125 min

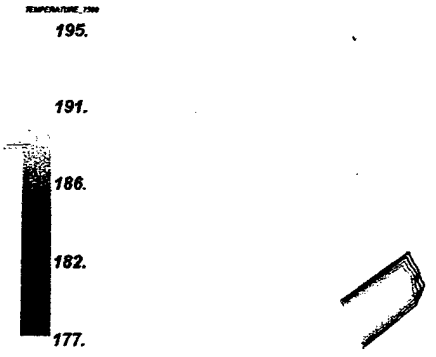

(c)

(f)

Figure 2.10: Curved Section: Temperature (left) and Degree of Cure (right) Contours

time = 100 min

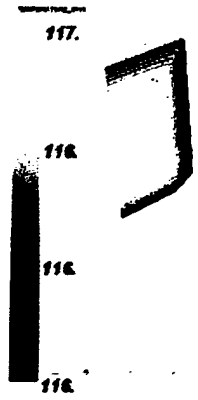

(a)

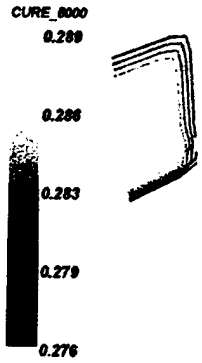

(d)

time = 113 min

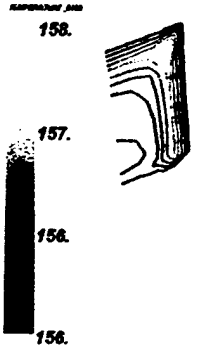

(b)

(e)

time = 125 min

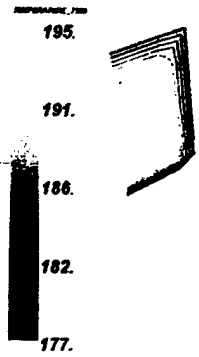

(c)

(f)

Figure 2.11: Vertical Section: Temperature (left) and Degree of Cure (right) Contours

time = 100 min

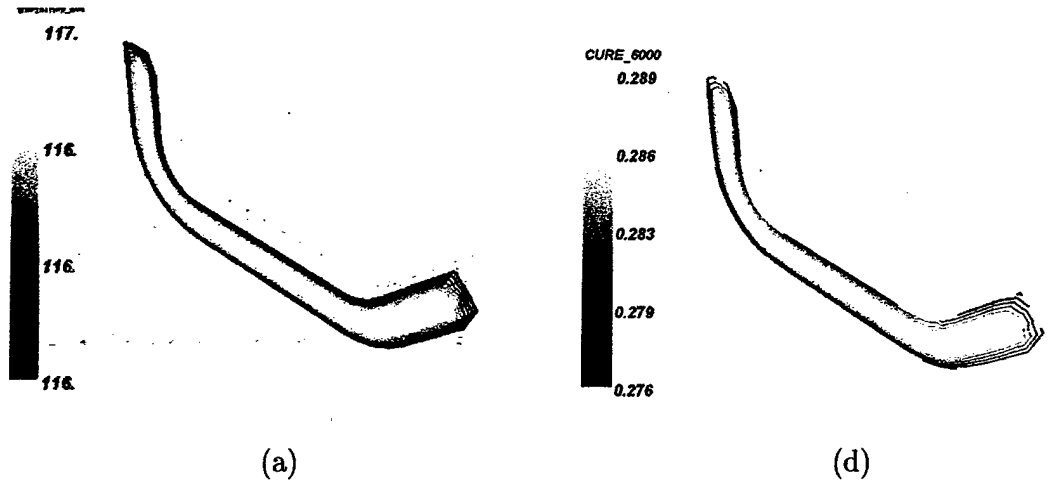

(a) (d)

time = 113 min

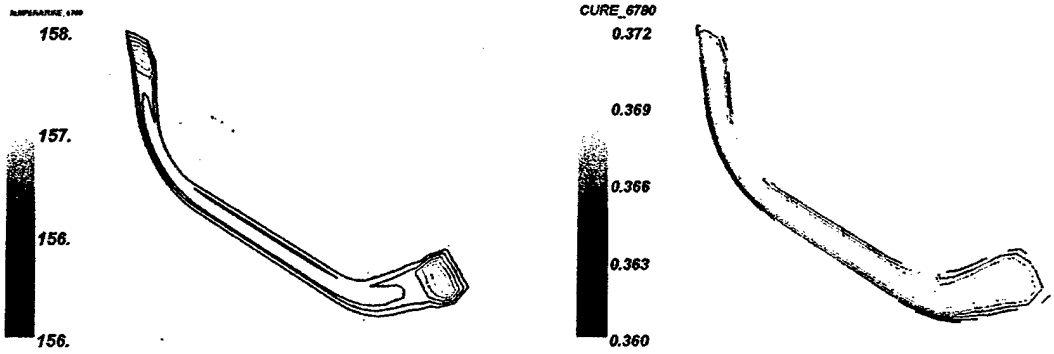

(b) (e)

time = 125 min

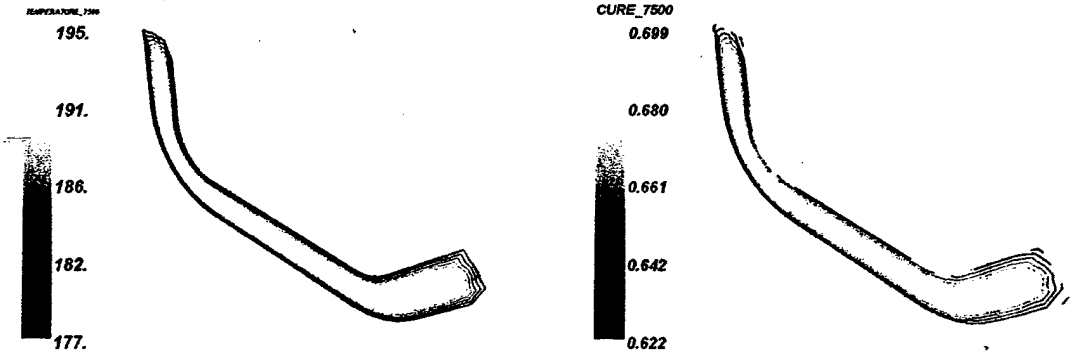

(c) (f)

Figure 2.12: Mid- Section: Temperature (left) and Degree of Cure (right) Contours

time = 100 min

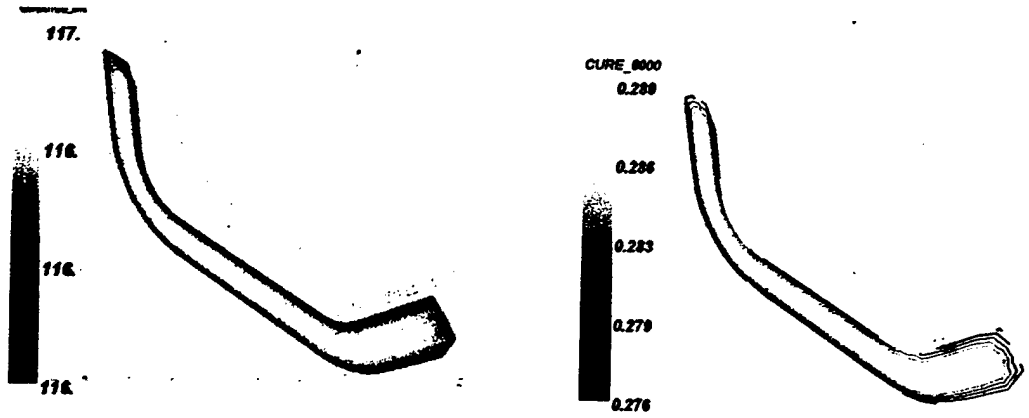

(a) (d)

time = 113 min

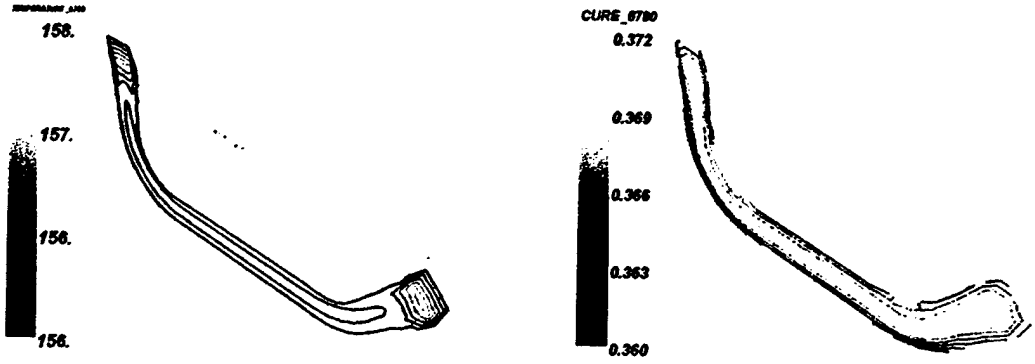

(b) (e)

time = 125 min

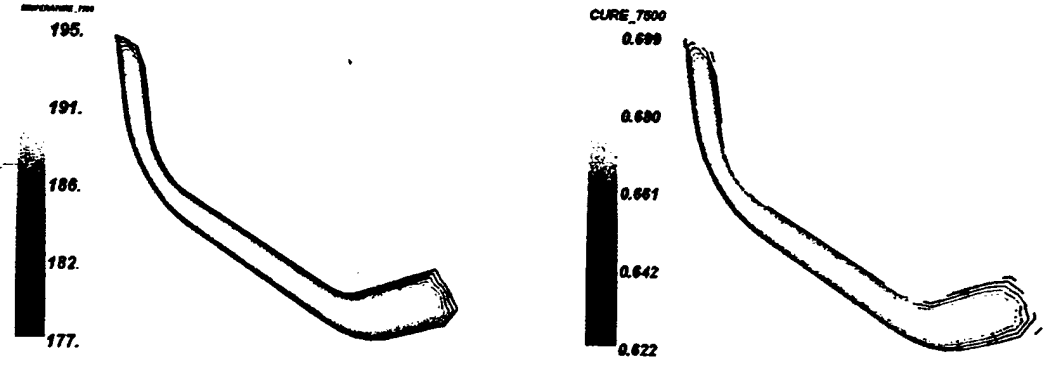

(c) (f)

Figure 2.13: Symmetry Plane: Temperature (left) and Degree of Cure (right) Contours

Chapter 3

RESIDUAL STRESS AND DEFORMATION

3.1 Introduction

Composite materials offer a number of desirable qualities as previously stated. However, their use has been limited by the complex issues involved in manufacturing a dimensionally accurate part. The residual stress and deformation development during the curing phase has a significant effect on both the dimensions and mechanical performance of the part. Residual stresses can result in warpage, matrix cracks, and delamination causing part failure earlier than expected. The ability to predict the behavior of composite materials is necessary especially when being used in applications such as aircrafts and space shuttles. The predictability of the composite strength would aid in the the design of composite parts with better dimensional stability. In addition, an accurate prediction of composite behavior would eliminate the expenses involved in manufacturing by trial and error. Therefore, understanding the mechanisms involved in residual stress development and creating computer simulations of the process is important and this is the focus of this research. Residual stresses mainly arise from thermal

expansion coefficient mismatch between the composite constituents, volumetric chemical shrinkage of the resin, and non-uniform curing. These factors are especially significant in the case of thick section composites where large thermal and degree of cure gradients exist. These gradients induce spatially varying thermal expansions and chemical hardening effects where there is nonuniform mechanical property development across the laminate thickness [13].

3.2 Literature Review

Several studies have been conducted in the analysis of process induced residual stresses. The earliest study of residual stresses in thermoset matrix composites was performed by Hahn and Pagano [14]. In their study, a classical lamination theory (CLT) was applied to their elastic analysis of a thin laminate, in which a stress-free state before cool-down was assumed. Other studies employing the same technique simulated the in-plane stresses and curvatures [15]-[17]. Radford [18] also used the classical laminated plate theory with volume fraction variations to study the cure shrinkage induced warpage in flat uni-axial carbon/epoxy composites. Results showed that the volume fraction gradients induced from the manufacturing process were an important component to part warpage.

Early work by Weitsman [19] showed that the viscoelastic response of the resin must be taken into account. The residual stresses resulting from cool-down was reduced by twenty percent in comparison to a linear elastic analysis. An optimal cool down path was derived based on this analysis in a follow up study[20].

In the work of Hodges et al. [21], the effect of cure temperature on the residual stresses for an epoxy resin (Cyanamid-Fothergill)was studied. A lower cure temperature was proposed to reduce the mismatch in the thermal expansions. A number of curing cycles were considered and monitored with measurements of viscosity and volume changes using differential scanning calorimetry (DSC). Stango and Wang [22] studied the viscoelastic response of a laminate by examining the interlaminar stresses at the free edge due to cool-down.

Kim and Hahn [23] monitored the warpage of unsymmetric cross-ply laminates and used an elastic method to relate the warpage to residual stress. Bogetti and Gillespie [24] investigated the development of residual stresses during cure in thick composites for a glass/polyester material system. Their model took the matrix shrinkage and thermal expansion into account by contributing to the total strains. From the incremental total strains, the stress and deformations were calculated based on a cure-dependent resin modulus. Their work was based on an elastic model, which coupled a one-dimensional cure simulation with laminated plate theory. This method of determining residual stresses was later adopted in the work of Teplinksy and Gutman [10], in which the effects of stacking geometry and laminate thickness on stresses and strains were examined. A linear, viscoelastic stress model was derived by White and Hahn [1] to include the effects of chemical and thermal strains during autoclave or hot press processing of PMCs. The mechanical properties had a functional dependence on the degree of cure and the transverse compliance was assumed to be the only time dependent compliance.

The residual moments and curvatures for unsymmetric cross-ply laminates were calculated and validated for a graphite/bismaleimide composite system in a companion paper [25]. The study showed that the contribution of the chemical strains to residual stress was less than 4%. Unfortunately, this model was restricted to thin laminates.

In the work of Kim and White [26] and [13], residual stresses in thick graphite/epoxy laminates were studied using a viscoelastic analysis, where the time-dependent stiffnesses were modeled using a series of exponential functions and based on cure dependent relaxation times. It was found that the residual stress developed in thick section composites was significant especially in the transverse direction. The model included the effects of strain from thermal, moisture and chemical expansions. The effect of chemical shrinkage was found to be negligible for the material system analyzed. Also, an elastic model was found to be adequate if the stress development is confined to the cool-down stage and chemical shrinkage and hardening effects aren't significant. A recent study using the same methodology as Kim and White was conducted by Zhu et al. [8]. A three-dimensional coupled thermo-chemo-viscoelastic model was developed to simulate the heat transfer, curing, residual stress and deformation during the entire cure cycle. Numerical results yielded significant stress development prior to cool-down.

In order to describe the viscoelastic response of composites, Kim and White [27] conducted a study into the stress relaxation of 3501-6 epoxy resin at cure states ranging from 0.57 to 0.98. A Prony series was used to describe the relaxation

modulus and shift functions used to obtain reduced times were derived based on curve fitted data. The experimental study showed that the cure state had a profound effect on the stress relaxation of epoxy. Further study of the stress relaxation of 3501-6 epoxy resin was done by White and Hartman [28] in which the specimens were tested in three-point bending to obtain creep compliance over a wide temperature range. Direct inversion and the Hopkins-Hamming method were used to calculate the stress relaxation modulus mater curves from the creep compliance curves. Chemical aging effects were also taken into account. Another experimental method for viscoelastic characterization was presented by O'Brien et al [29] using parallel plate rheometry to measure the material behavior prior to the gel point.

The development of the mechanical properties during cure was also examined by Simon et al. [30] by using a methodology combining the principles of time-temperature superposition, time-cross-link density superposition, and the rubbery elasticity of networks. The shift factors in this formulation followed the Williams-Landel-Ferry (WLF) equation. The viscoelastic model was extended to predict the isotropic residual stresses in a commercial epoxy in [31]. Like previous viscoelastic models, the shear modulus was modeled as a sum of Maxwell elements each having a characteristic relaxation time. The results of the study showed that cure shrinkage contributes significantly to the total residual stresses and an elastic analysis overestimates the residual stresses. Chemical shrinkage was found to be a major contributor to the spring-forward effect in L-shaped continuous fiber lam-

inates in Wiersma et al. [32]. The prediction of the spring-forward was sensitive to the amount of cure shrinkage and viscosity profile during the cure cycle using a viscoelastic model.

Extensive studies in the viscoelastic stress analysis of composites was also conducted by Yi et al. In [33] and [34], a finite element formulation for analyzing interlaminar stress fields in nonlinear anisotropic viscoelastic composites was presented. Schapery's single integral formulation was extended to account for viscoelastic anisotropy and multiaxial stress states. The finite element procedure was also used to study the behavior during cool-down in [35]. Hilton and Yi [36] performed a stochastic delamination simulation of nonlinear viscoelastic composites. A similar methodology using Schapery's nonlinear viscoelastic model was presented in [37] and [38] for unidirectional carbon/epoxy composites.. A nonlinear three-dimensional viscoelastic analysis was performed for unidirectional and cross-ply laminates by Chen et al. [39]with a viscoelastic model represented by a finite series of Kelvin elements coupled with an elastic spring. A representative volume element was analyzed rather than the whole composite geometry. The investigation showed that the viscous behavior of the matrix plays an important role in the evaluation of the residual stresses. Fisher and Brinson [40] also performed a micromechanical investigation using the Mori-Tanaka (MT) method and the Benveniste solution to include the effects of viscoelastic interphase regions.

3.3 Problem Description

The contribution of the spatial and temporal variance of the composite material behavior during the curing phase to the evolution of stress and deformation is the focus of the present study. Most of the models on process-induced stress from previous studies are limited to the cool-down phase of the composite. In addition, several finite element codes were developed. However, presently, a generic platform to simulate the manufacturing process does not exist. The objective is to study the behavior of the composite and evolution of residual stress and deformation during the curing phase to aid in the development of a generic architecture to simulate the coupled phases of the composite manufacturing process.

The material constitutive models adopted are coupled with the three-dimensional cure simulation to understand the mechanisms involved in the stress development. The models take into account the effects of thermal expansion, chemical cure shrinkage, and non-uniform curing, which are all important sources of internal loading. The graphite/epoxy composite system was used to illustrate the significant stress development during the curing phase; thereby emphasizing the need for a stress analysis prior to cool-down. Two material constitutive models, thermo-elastic and viscoelastic, were studied. For the thermo-elastic approach, the rule of mixtures was used to depict the kinetic-viscoelastic behavior of the resin modulus. Effective composite mechanical properties were computed using the instantaneous resin and fiber properties in a self-consistent field micromechanics model. For the viscoelastic constitutive equation, the cure and temperature

dependent stress relaxation modulus was approximated as a Prony series of a number of Maxwell elements. For both models, ABAQUS finite element software was implemented to perform the stress and deformation analysis on a composite system of unidirectional fibers.

3.4 Thermo-Elastic Formulation

During the curing process, the state of the thermosetting resin dictates the effective mechanical properties of the composite system. The modulus of the resin goes from low to high as the resin changes from a liquid viscous state to a viscoelastic/elastic solid. From Figure 3.1, the evolution of the resin modulus can be separated into three regions [41]. At the beginning of the cure cycle, the resin is assumed to be a fully uncured, viscous fluid where the stiffness is negligible. In the second region, significant increases in the stiffness and chemical shrinkage occur due to the cross-linking reaction. During this phase, the resin quickly goes from an uncured to a cured state. Also in this region, the chemical kinetic hardening and viscoelastic relaxation are competing mechanisms governing the mechanical properties of the resin. The behavior of the resin in the third region is observed to be viscoelastic at high temperatures and elastic at lower temperatures. For the thermo-elastic formulation, the properties of the fiber were assumed to be constant and independent of cure. The instantaneous resin modulus was modeled as a function of degree of cure and used in conjunction with the constant fiber properties and volume fraction in a micromechanics model to determine the effective composite properties. While the resin modulus was strongly influenced by the curing process, the resin Poisson ratio, ν_m, was assumed to be constant. In the following thermo-elastic formulation, chemical shrinkage and thermal expansion strains were taken into account with the assumption that the coefficients of thermal expansion and chemical shrinkage were constant. The thermal expansion

and chemical shrinkage strain were dependent on the change in temperature and degree of cure, respectively.

The equation to describe the instantaneous resin modulus, specifically in the second region, was a rule of mixtures model based on the degree of cure [41] as seen in the following:

$$E_m = (1-\alpha)E_m^0 + \alpha E_m^\infty + \gamma(1-\alpha)\alpha(E_m^\infty - E_m^0) \tag{3.1}$$

where α is the degree of cure and E_m^0 and E_m^∞ are the fully uncured and fully cured matrix moduli, respectively. γ is a fitting parameter corresponding to the speed at which the resin modulus approaches the fully cured modulus. The resin modulus approaches the fully cured modulus rapidly if the value of *gamma* is high. For the following analysis, γ was assumed to be zero to represent the gradual increase of the resin modulus. From [41], a study of Equation (3.1) showed reasonable agreement with experimental results with $\gamma = 0$. Similarly, the rule of mixtures was used to compute the longitudinal composite stiffness, E_1. With the matrix modulus, E_m, the instantaneous composite properties were computed using a self-consistent field micromechanics model from Whitney and McCullough [42] and presented in Appendix A.

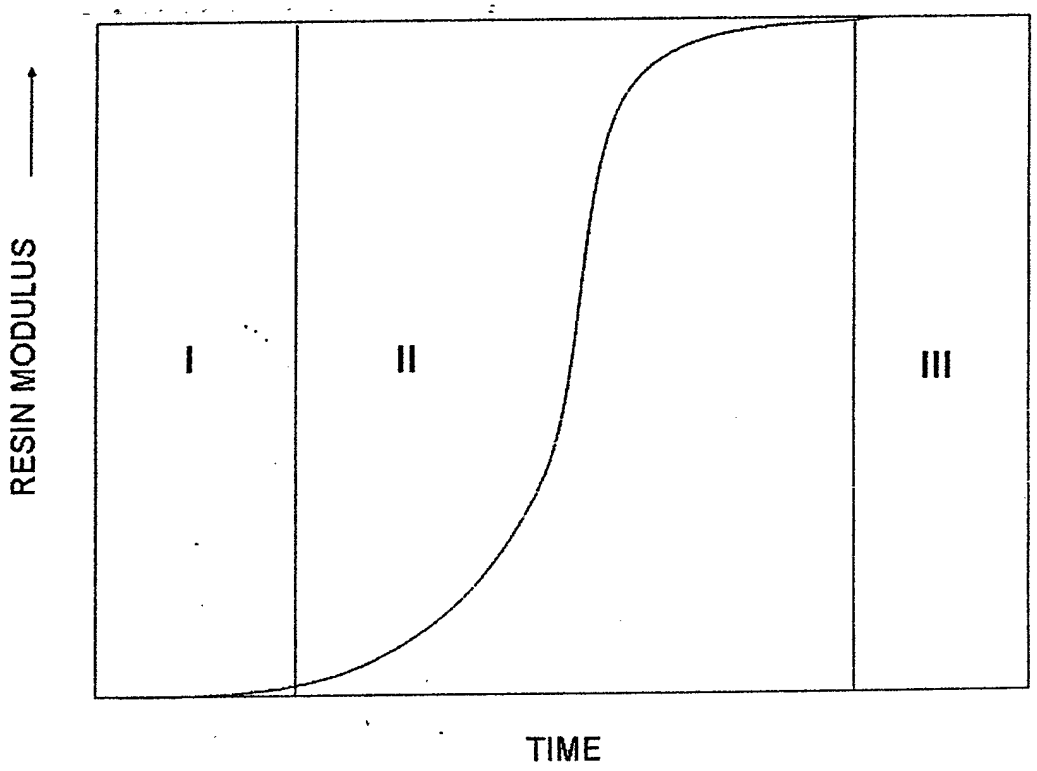

Figure 3.1: Behavior of Resin Modulus during Cure

3.4.1 Chemical Shrinkage

In early studies, the influence of chemical shrinkage on residual stresses was neglected by assuming that the chemical shrinkage occurs in the process where the mechanical properties are low [1]. However, recent work has found that the chemical shrinkage has significant effects on the residual stress development and contributing to the spring-forward effect in many composite parts [8]. The behavior of the chemical shrinkage strain during the curing process of several thermosetting resins, including AS4/3501-6 prepreg, was studied by Russell [43]. He reported that the volumetric shrinkage can be modeled as a linear function of degree of cure in which:

$$V_{ch}(\alpha) = V_{ch}^{T}\alpha \tag{3.2}$$

where V_{ch}^{T} is the total volumetric shrinkage of the resin. For the 3501-6 epoxy resin studied, the typical value of V_{ch}^{T} is 5% is used in the present study. Also, the model assumes a constant coefficient throughout the cycle. The relation between the volumetric shrinkage and the strain due to shrinkage is seen in the following expression:

$$\varepsilon_{ch} = \kappa_m = \sqrt[3]{1 + V_{ch}} - 1 \tag{3.3}$$

From Equation (3.3), the coefficient of chemical shrinkage (κ_m) for the resin can be obtained and used in the Whitney and McCullough micromechanics model to determine the effective coefficients in the principal directions, (κ_{ii}). The following expression for the chemical shrinkage strain is obtained based on the change in

degree of cure, $\Delta\alpha(t)$.

$$\varepsilon_j^{\Delta}(t) = \kappa_{jk}\Delta\alpha_k(t) \tag{3.4}$$

3.4.2 Thermal Expansion

Thermal expansion is a major mechanism contributing to the residual stress development specifically in thick section composites where large thermal gradients exist. In addition, the thermal expansion coefficient mismatch between the resin and the fiber produce significant stress and deformation. The expression for thermal expansion strains is modeled as a linear function based on the temperature difference. The coefficients of thermal expansion in the principal directions were assumed to be constant throughout the cure cycle and obtained using the micromechanics model knowing the coefficients of the constituents.

$$\varepsilon_j^{\Delta}(t) = \phi_{jk}\Delta T_k(t) \tag{3.5}$$

3.4.3 ABAQUS Implementation

ABAQUS finite element software was used for the stress and deformation analysis. The methodology involves the utilization of the temperature and degree of cure distributions obtained from the Galerkin FEM cure simulation in conjunction with a thermo-mechanical model in ABAQUS. In order to model the thermal expansion and the chemical shrinkage, a user subroutine, UEXPAN, was developed. In addition, The temperature and degree of cure fields were obtained via the subroutines, UTEMP and UFIELD, respectively, which interpolated the

Table 3.1: 3501-6 Resin Properties

E_m^0 (MPa)	3.447
E_m^∞ (MPa)	3.447 x 10^3
V_{shrink} (%)	5.0

values by calling and reading the data from files generated by the cure simulation. The user subroutines developed for ABAQUS are located in Appendix B. To model the degree of cure dependent modulus, a table of effective composite properties based on the micromechanics model for different degrees of cure was generated in Excel and used in the ABAQUS input file.

3.4.4 Numerical Example

The residual stress and deformation development of the curve-shaped part simulated in Section 2.5.2 was studied. The part is a graphite/epoxy composite with unidirectional fibers. Figure 3.2 shows the mesh detailing the coordinate system used. In this case, the fibers are oriented along the x-direction. The values of the initial and final modulus of the resin needed to calculate the instantaneous modulus is in Table 3.1. The effective composite properties were determined using the instantaneous cure dependent resin modulus and the constant fiber properties in Table 3.2 in a micromechanics model. The top face of the curve-shaped part was constrained to simulate the influence of the mold. A uniform pressure, 167 kPa, was applied to the bottom face of the part. The stress and strain behavior of an element located at the centermost region of the composite was studied. At this location, the element's temperature goes above the mold

Table 3.2: Elastic Material Properties of AS4 Fiber and 3501-6 Epoxy Resin

Property	AS4 Graphite	3501-6 Epoxy
ϕ_1 ($\mu\varepsilon/^oC$)	-0.9	57.6
ϕ_2 ($\mu\varepsilon/^oC$)	7.2	57.6
κ_{11} ($\mu\varepsilon$)	0.0	-0.0164
κ_{22} ($\mu\varepsilon$)	0.0	-0.0164
ν_{12}	0.2	0.35
ν_{13}	0.2	0.35
ν_{23}	0.3	0.35
E_1 (GPa)	206.8	3.2
E_2 (GPa)	20.68	3.2
G_{12} (GPa)	27.58	1.185
G_{13} (GPa)	27.58	1.185
G_{23} (GPa)	6.894	1.185

temperature because of the heat generated from the cross-linking polymerization. To study the mechanisms driving the residual stress development, the following three simulations were performed:

(1) Case 1: Only thermal expansion

(2) Case 2: Only chemical shrinkage

(3) Case 3: Both thermal expansion and chemical shrinkage

From the simulation, the most significant stress development occurred along the fiber direction. The maximum normal stress in the x-direction (σ_{11}) was approximately 2 MPa for Case 3. Figures 3.3 and 3.4 show the resulting plots of the normal stress and normal strain, respectively, for all three cases. When the thermal expansion effects are only taken into account, the strain development closely follows the temperature profile since thermal strain is driven by the temperature difference. Likewise, the chemical shrinkage strain behavior is similar to the degree of cure profile. The stress obtained from the thermal expansion case shows that the part is in a state of compression reaching a maximum stress of -2.5 MPa. In the chemical shrinkage case, the stress is doubled compared to Case 3 where the effects of both strains are taken into account. The stress and strain profile for Case 3 always falls in between Case 1 and 2. From this, one can see how the mechanisms of chemical shrinkage and thermal expansion compete with one another. As a result, one can design the process temperature cycle so that the thermal and chemical strains cancel each other out and reduce the residual stress.

The shear stress and strain for Case 3, σ_{23} and ε_{23} are plotted in Figure 3.5. The part experiences a sharp dip in the shear strain (about $-7.5x10^{-6}$) early in the cycle. This can be attributed to the low viscosity of the resin at the beginning of the cure cycle. The contour plots of the displacement and Von Mises stress at the end of the cure cycle is presented in Figures 3.6. A maximum displacement of $6.8x10^{-}6$ m was experienced on the bottom face, particularly along the edges of the curvature. In contrast, the maximum stress was on the top face of the part, mostly in the areas of the curvature. Because studies have shown that an elastic analysis overestimates the residual stress, a fully anisotropic viscoelastic model is desired.

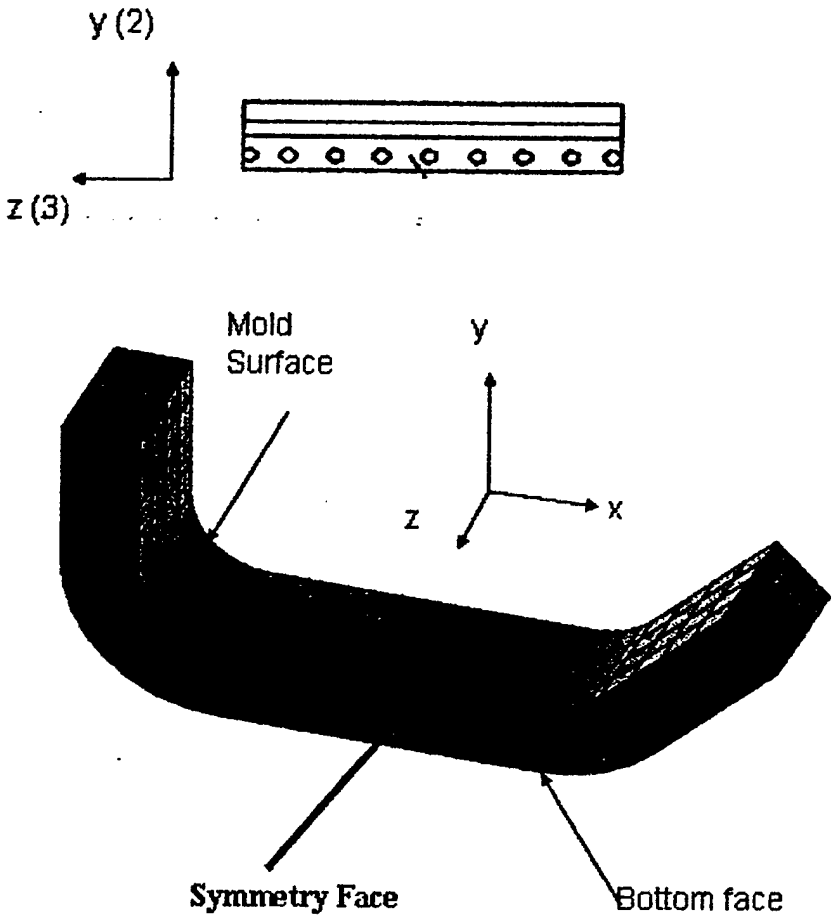

Figure 3.2: Curve-Shaped Part Mesh

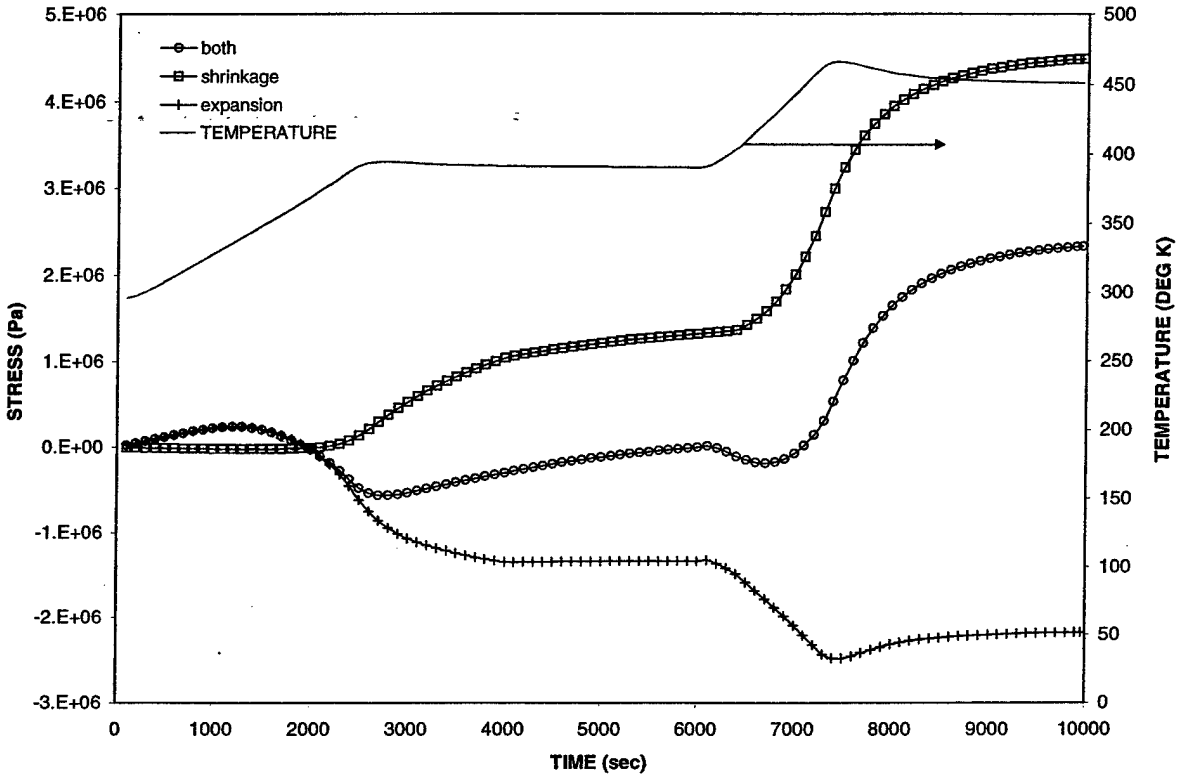

Figure 3.3: Elastic Normal Stresses in X-Direction (σ_{11})

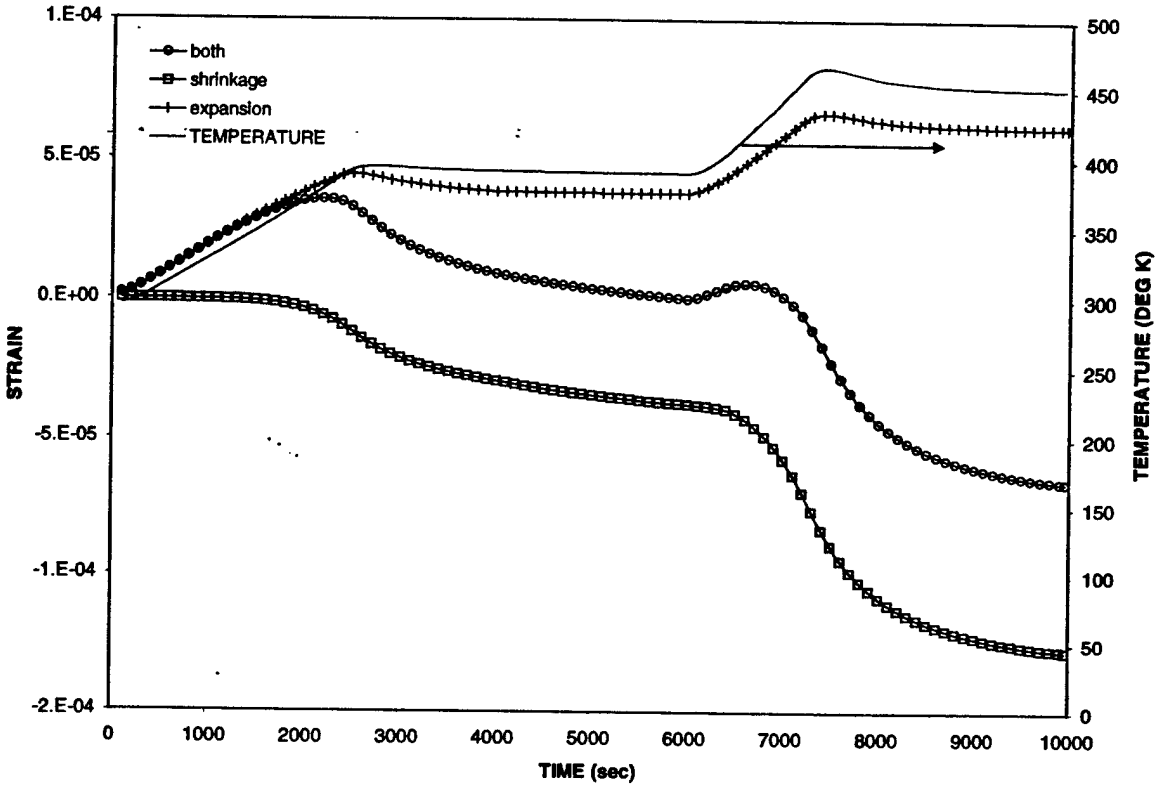

Figure 3.4: Elastic Normal Strains in X-Direction (ε_{11})

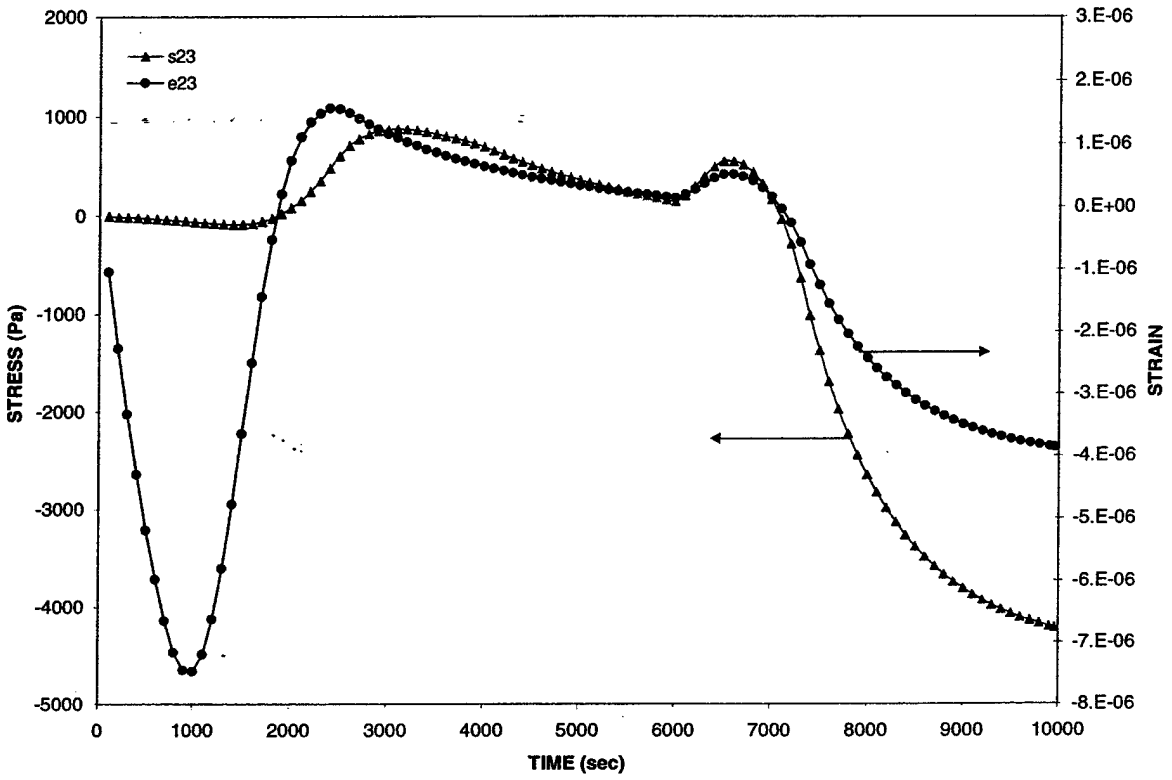

Figure 3.5: Elastic Shear Stress and Strain

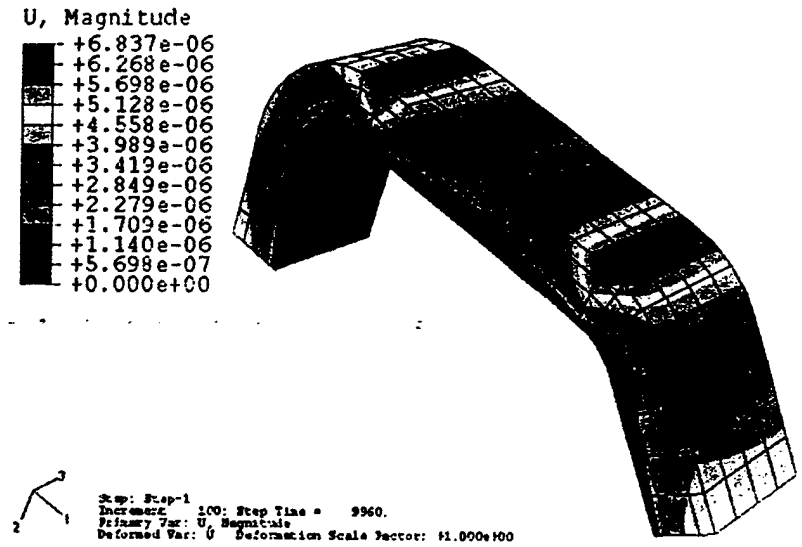

(a)

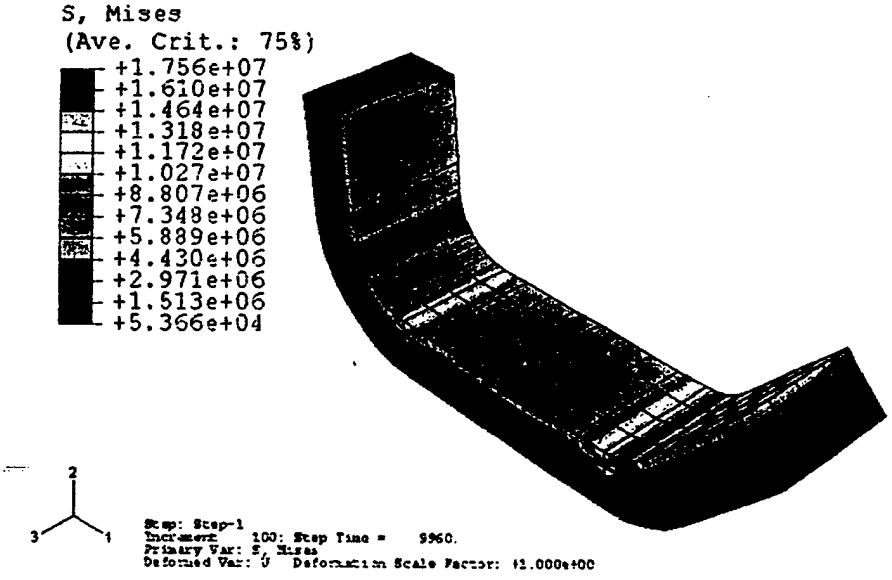

(b)

Figure 3.6: Elastic: Displacement (a) and Von Mises Stress (b) Contours at t=9960 sec

3.5 Viscoelastic Formulation

From various studies, it was reported that an elastic formulation overestimates the residual stress and deformation. Therefore, the viscoelastic behavior of the resin should not be neglected in an accurate process model. The model used to depict the viscoelastic behavior of the composite was based on the work by Kim and White, [2], [27], [13], and [26]. The general expression for the constitutive relationship for an anisotropic linear viscoelastic material is [2]:

$$\sigma_{ij}(t) = \int_{-\infty}^{t} Q_{ijkl}(\alpha, T, \vec{X}, t, t') \frac{\partial}{\partial t'} (\varepsilon_{kl}(\vec{X}, t') - \varepsilon_{kl}^{\Delta}(\vec{X}, t') dt' \qquad (3.6)$$

where σ_{ij} is the stress tensor. ε_{kl} and $\varepsilon_{kl}^{\Delta}$ are the mechanical and non-mechanical strains, respectively while $\vec{X}$ is the location vector. α and T represent the degree of cure and temperature while t and t' are the present and past times, respectively. Equation (3.6) can be expressed in matrix form to yield the following:

$$\sigma_i(t) = \int_{-\infty}^{t} Q_{ij}(\alpha, T, \vec{X}, t, t') \frac{\partial}{\partial t'} (\varepsilon_j(\vec{X}, t') - \varepsilon_j^{\Delta}(\vec{X}, t') dt' \quad (i, j = 1 - 6) \qquad (3.7)$$

Using the chemical shrinkage and thermal expansion strain analysis in Section 3.4.1 and 3.4.2, the expression for the non-mechanical strains can be described in Equation (3.8). Typically moisture concentration contributes to the total non-mechanical strain, but for this study, the effects are ignored.

$$\varepsilon_j^{\Delta}(\vec{X}, t) = \phi_{jk} \Delta T_k(\vec{X}, t) + \kappa_{jk} \Delta \alpha_k(\vec{X}, t) \qquad (3.8)$$

Equation (3.7) can be further simplified into the integral form in the following equation assuming a zero stress history before $t = 0$ and thermorheologically

simple behavior at a constant degree of cure.

$$\sigma_i(t) = \int_0^t Q_{ij}(\alpha, T, \vec{X}, \xi - \xi') \frac{\partial}{\partial t'} (\varepsilon_j(\vec{X}, t') - \varepsilon_j^{\Delta}(\vec{X}, t') dt' \quad (i, j = 1 - 6) \tag{3.9}$$

where the reduced times, ξ and ξ', are described as the following with a_T as a degree of cure and temperature dependent shift factor.

$$\begin{aligned} \xi &= \int_0^t \frac{1}{a_T(\alpha, T(t''))} dt'' \\ \xi' &= \int_0^t \frac{1}{a_T(\alpha, T(t''))} dt'' \end{aligned} \tag{3.10}$$

3.5.1 Orthotropic Material

Prior to developing the model for the stress relaxation modulus, a brief summary of the viscoelastic stress-strain relation for orthotropic materials is presented in matrix form.

$$\begin{Bmatrix} \sigma_x \\ \sigma_y \\ \sigma_z \\ \sigma_{yz} \\ \sigma_{zx} \\ \sigma_{xy} \end{Bmatrix} = \begin{pmatrix} Q_{11} & Q_{12} & Q_{13} & & & \\ Q_{21} & Q_{22} & Q_{23} & & 0 & \\ Q_{31} & Q_{32} & Q_{33} & & & \\ & & & Q_{44} & & \\ & 0 & & & Q_{55} & \\ & & & & & Q_{66} \end{pmatrix} \begin{Bmatrix} \varepsilon_x \\ \varepsilon_y \\ \varepsilon_z \\ \varepsilon_{yz} \\ \varepsilon_{zx} \\ \varepsilon_{xy} \end{Bmatrix} \tag{3.11}$$

where the components of the Q matrix are functions of the relaxation and shear moduli and Poisson's ratios corresponding to the principal directions.

$\sigma_i = Q_{ij} \varepsilon_j$

$$
\begin{aligned}
Q_{11} &= \frac{1-\nu_{23}\nu_{32}}{\Delta}E_1 \qquad (3.12)\\
Q_{12} = Q_{21} &= \frac{\nu_{31}+\nu_{21}\nu_{23}}{\Delta}E_1\\
Q_{13} = Q_{31} &= \frac{\nu_{31}+\nu_{21}\nu_{32}}{\Delta}E_1\\
Q_{22} &= \frac{1-\nu_{13}\nu_{31}}{\Delta}E_2\\
Q_{23} = Q_{32} &= \frac{\nu_{32}+\nu_{12}\nu_{31}}{\Delta}E_2\\
Q_{33} &= \frac{1-\nu_{12}\nu_{21}}{\Delta}E_3\\
Q_{44} &= G_{23}\\
Q_{55} &= G_{31}\\
Q_{66} &= G_{12}\\
\Delta &= 1-\nu_{12}\nu_{21}-\nu_{23}\nu_{32}-2\nu_{21}\nu_{32}\nu_{13}
\end{aligned}
$$

For a transversely isotropic material in the y-z plane, Equation (3.11) reduces to a function of five independent time-dependent engineering properties, E_1, $E_2 = E_3$, $\nu_{12} = \nu_{13}$, ν_{23}, and $G_{12} = G_{13}$. The reduced stress-strain relation is seen in the following:

$$
\begin{Bmatrix} \sigma_x \\ \sigma_y \\ \sigma_z \\ \sigma_{yz} \\ \sigma_{zx} \\ \sigma_{xy} \end{Bmatrix} =
\begin{pmatrix}
Q_{11} & Q_{12} & Q_{13} & & & \\
Q_{12} & Q_{22} & Q_{23} & & 0 & \\
Q_{13} & Q_{23} & Q_{33} & & & \\
 & & & Q_{44} & & \\
 & 0 & & & \frac{Q_{22}-Q_{23}}{2} & \\
 & & & & & Q_{44}
\end{pmatrix}
\begin{Bmatrix} \varepsilon_x \\ \varepsilon_y \\ \varepsilon_z \\ \varepsilon_{yz} \\ \varepsilon_{zx} \\ \varepsilon_{xy} \end{Bmatrix} \qquad (3.13)
$$

3.5.2 Epoxy Resin Material Characterization

The challenge in modeling the viscoelastic behavior is describing the development of the stiffness matrix based on the processing parameters. Since all resins have different stress relaxation behavior, proper stress relaxation tests must be performed for each resin system. Since the implementation of a viscoelastic residual stress and deformation analysis is the focus of this study, the model described in [2] for the stress relaxation behavior of 3501-6 epoxy was used. Kim modeled the stress relaxation modulus as a generalized Maxwell model with a discrete exponential Prony series. The general form of the cure dependent expression is as follows:

$$E_m(\alpha,\xi) = E_m^{\infty}(\alpha) + E_m^{*}(\alpha)\sum_{\omega=1}^{N} W_\omega(\alpha) exp\left[\frac{-\xi(\alpha)}{\tau_\omega(\alpha)}\right] \tag{3.14}$$

where E_m^{∞} is the fully relaxed modulus and $E_m^{*} = E_m^{u} - E_m^{\infty}$, in which E_m^{u} is the unrelaxed modulus. Equation (3.14) is simplified by assuming E_m^{∞}, E_m^{*}, and W_ω are independent of degree of cure and temperature. W_ω are weight factors, τ_ω are discrete relaxation times, and ξ is the reduced time.

$$E_m(\alpha,\xi) = E_m^{\infty} + E_m^{*}\sum_{\omega=1}^{N} W_\omega exp\left[\frac{-\xi(\alpha)}{\tau_\omega(\alpha)}\right] \tag{3.15}$$

The reduced time of the resin, ξ, is depicted in the following expression:

$$\xi = \int_0^t \frac{1}{a_T(\alpha,T)} dt \tag{3.16}$$

In Kim and White's experimental studies, the slope of the shift function, a_T, increased as the degree of cure decreased. As a result, the following linear function of temperature with degree of cure dependent coefficients was developed. Figure

3.7 shows a plot of the shift factor for different temperatures. This plot displays the increasing slope of the shift factor as degree of cure decreases.

$$log(a_T) = c_1(\alpha)T + c_2(\alpha) \tag{3.17}$$

$$c_1(\alpha) = -a_1 exp\left(\frac{1}{\alpha - 1}\right)$$

$$c_2(\alpha) = -T^0 c_1(\alpha)$$

where $a_1 = 1.4/^oC$, $a_2 = 0.0712/^oC$, and $T^0 = 30^oC$.

To determine the stress relaxation times, the trend of peak relaxation times for different degree of cures was studied. The peak relaxation time is short at lower degree of cure and lengthens as the cure advances. Kim observed that the peak relaxation time increased approximately 6 orders of magnitude from a degree of cure of 0.57 to 0.98. This trend was then compared to the change in glass transition temperature (T_g) where temperature is in terms of degree Celsius. From the testing of samples of varying degree of cures, a curve fit of the glass transition temperature based on degree of cure was developed as seen in the following:

$$T_g(\alpha) = 10.344 + 11.859\alpha + 178.04\alpha^2 \tag{3.18}$$

This expression was normalized with the glass transition temperature of a reference degree of cure, $\alpha_{ref} = 0.98$, to obtain the chemical hardening function, $f(\alpha)$.

$$\frac{T_g(\alpha)}{T_g(\alpha_{ref})} = f(\alpha) = 0.0536 + 0.0615\alpha + 0.9227\alpha^2 \tag{3.19}$$

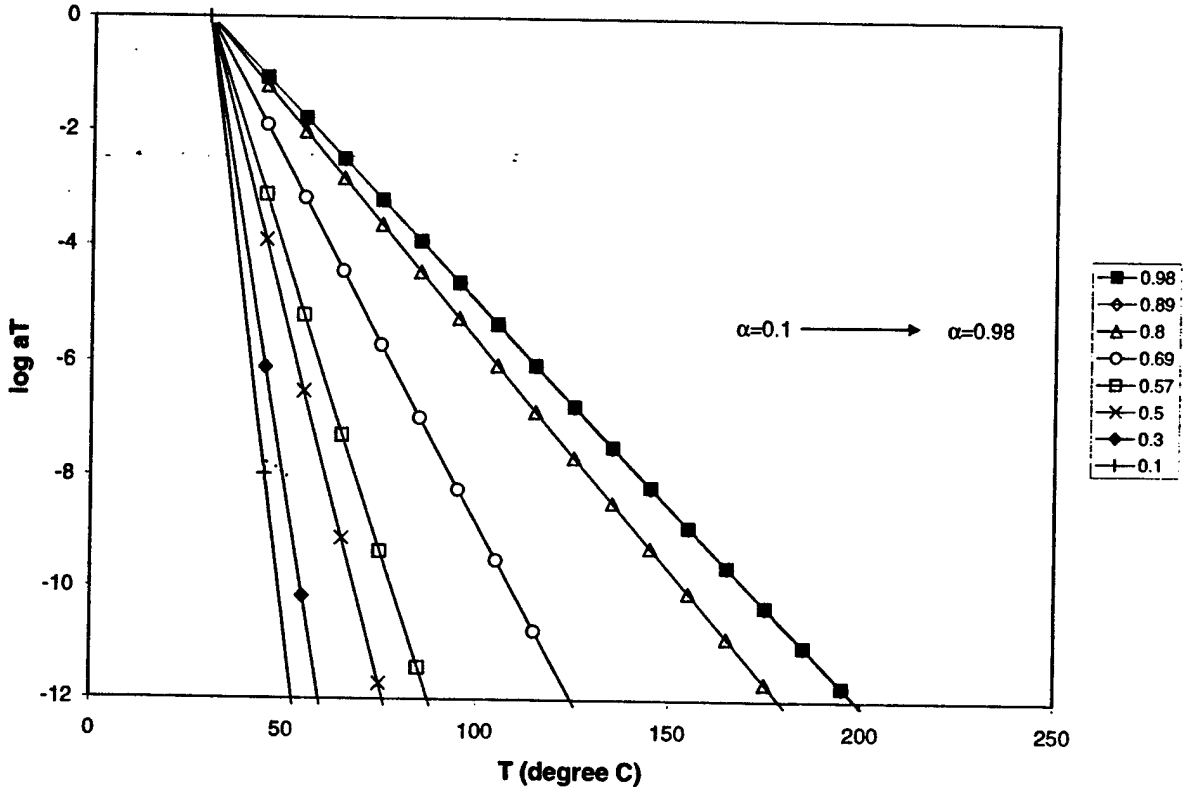

Figure 3.7: Kim Shift Function Model vs. Temperature for Different Degree of Cure

Table 3.3: Master Curve Parameters for $\alpha^0 = 0.98$ Degree of Cure

ω	τ_ω (min)	W_ω
1	2.922137×10^1	0.0591334
2	2.921437×10^3	0.0661225
3	1.82448×10^5	0.0826896
4	1.1031059×10^7	0.112314
5	2.8305395×10^8	0.154121
6	7.9432822×10^9	0.2618288
7	1.953424×10^{11}	0.1835594
8	3.3150756×10^{12}	0.0486939
9	4.9174856×10^{14}	0.0252258

With the assumption that the glass transition temperature as a function of cure behaves similarly to the peak stress relaxation times, the relaxation time at different degree of cures can be expressed as:

$$\frac{log(\tau^p(\alpha))}{log(\tau^p(\alpha = 0.98)} = f(\alpha) \tag{3.20}$$

Measuring that the peak stress relaxation time for $\alpha = 0.98$ is $10^{9.9}$ minutes, a plot of the peak relaxation time versus degree of cure can be seen in Figure 3.8. With the assumption that the other stress relaxation times followed the same behavior as the peak stress time, Equation 3.20 was rewritten as:

$$log(\tau_\omega(\alpha)) = f(\alpha) log(\tau_\omega(\alpha_{ref})) \tag{3.21}$$

Using the models of the shift function and stress relaxation times and the parameters of the reference degree of cure, $\alpha_{ref} = 0.98$, a semi-log plot of the resin modulus [Eq. (3.15] versus reduced time was generated as seen in Figure 3.9. The parameter values for α_{ref} are located in Table 3.3. The values used for E_m^∞ and E_m^* were 0.031 GPa and 3.169 GPa, respectively.

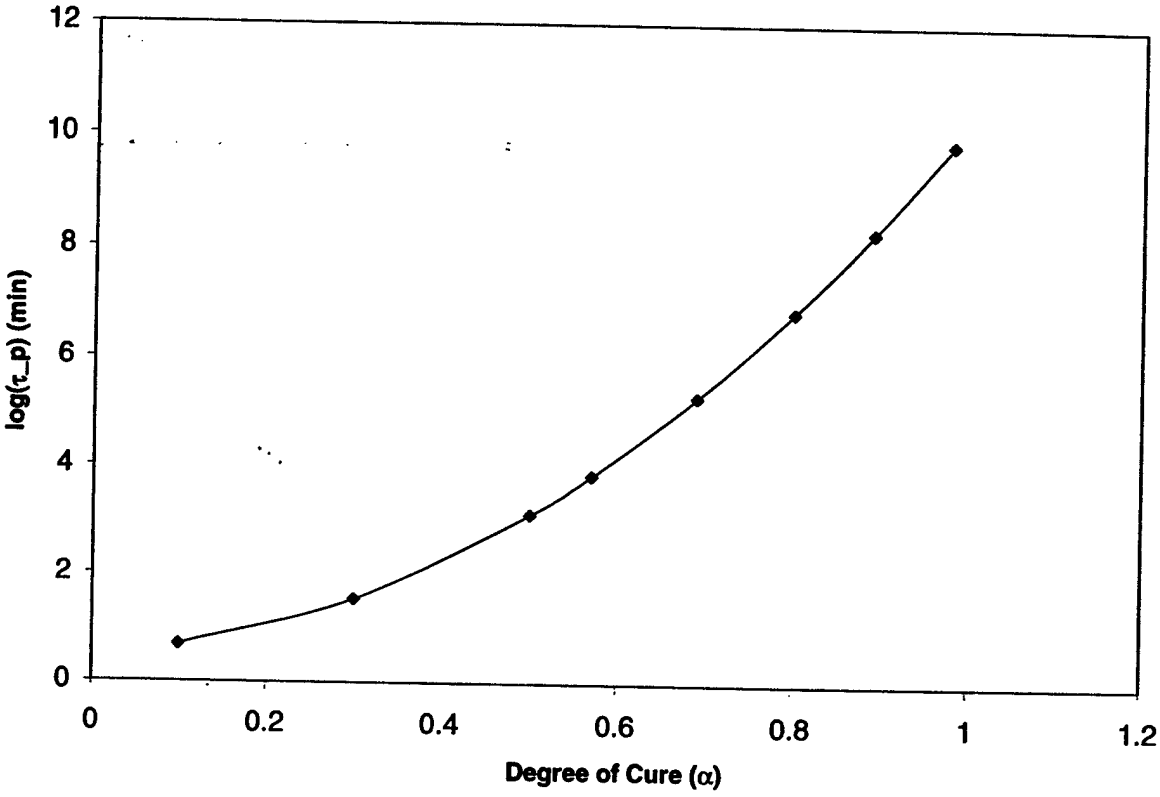

Figure 3.8: Peak Stress Relaxation Time for Different Degree of Cure

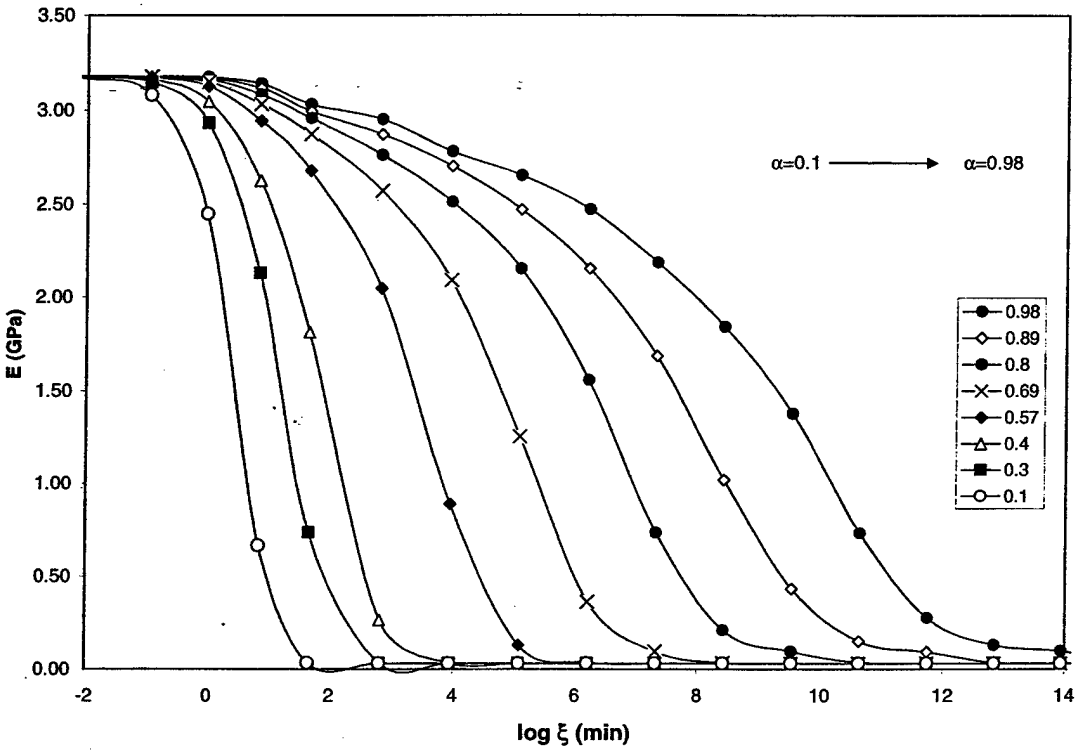

Figure 3.9: Resin Modulus Stress Relaxation for Different Degree of Cure

3.5.3 Composite Effective Properties

To define the composite material properties, the relaxation of the composite was assumed to follow the same behavior as the resin modulus. Because of this, Equation (3.14) was rewritten in the following equation to describe the composite modulus.

$$Q_{ij}(\alpha,\xi,T) = Q_{ij}^{\infty}(\alpha,T) + Q_{ij}^{*}(\alpha,T)\sum_{\omega=1}^{N} W_{\omega}(\alpha,T)exp\left[\frac{-\xi(\alpha,T)}{\tau_{\omega}(\alpha)}\right] \qquad (3.22)$$

Again, the assumptions that the weight factors and the composite unrelaxed and relaxed moduli are independent of degree of cure and temperature, Equation (3.22) reduces to:

$$Q_{ij}(\alpha,\xi,T) = Q_{ij}^{\infty} + E_{m}^{*}\sum_{\omega=1}^{N} W_{\omega}exp\left[\frac{-\xi(\alpha)}{\tau_{\omega}(\alpha)}\right] \qquad (3.23)$$

where Q_{ij}^{∞} is the fully relaxed modulus and $Q_{ij}^{*} = Q_{ij}^{u} - Q_{ij}^{\infty}$, in which Q_{ij}^{u} is the unrelaxed modulus. Q_{ij}^{u} is the elastic stiffness of the lamina and obtained from the elastic micromechanics model in Appendix A. The value of the fully relaxed stiffness, Q_{ij}^{∞}, is based on the unrelaxed stiffness (Q_{ij}^{u}) and a partition factor, R_f as seen in the following expression:

$$Q_{ij}^{\infty} = R_f Q_{ij}^{u} \quad (0 \leq R_f \leq 1) \qquad (3.24)$$

R_f describes the degree to which a material completely relaxes. If $R_f = 1$, then the material doesn't relax. If $R_f = 0$, then the material completely relaxes. For the graphite/epoxy composite studied in this case, $R_f = \frac{1}{7}$.

The elastic material properties of the graphite fiber and epoxy resin used in this study are in Table 3.2. The fully unrelaxed stiffnesses and other composite

Table 3.4: Elastic Composite Properties of AS4/3501-6

Q_{11} (GPa)	127.4
Q_{12} (GPa)	3.88
Q_{22} (GPa)	10.0
Q_{44} (GPa)	2.57
ϕ_{11} $(\mu\varepsilon/^oC)$	0.5
$\phi_{22} = \phi_{33}$ $(\mu\varepsilon/^oC)$	35.3
κ_{11} $(\mu\varepsilon)$	-167
$\kappa_{22} = \kappa_{33}$ $(\mu\varepsilon)$	-8810

properties were calculated the micromechanics model found in Appendix A. The results are presented in Table 3.4.

3.6 ABAQUS Implementation

3.6.1 Isotropic Viscoelasticity

For the viscoelastic analysis, two methods were attempted to simulate the residual stress and deformation development using the ABAQUS finite element software. For the first methodology, the viscoelastic function in ABAQUS was adapted to match the model found in Equation (3.15). The viscoelastic function in ABAQUS is limited to linear isotropic materials. Therefore, the following procedure can only be used to model the resin behavior. This procedure also required the use of the subroutines, UEXPAN, UFIELD, and UTEMP. Another method to describe the viscoelasticity of an orthotropic composite system is described in Section 3.6.3. In ABAQUS. the basic hereditary integral formulation for linear isotropic viscoelasticity is the following:

$$\sigma(t) = \int_0^t 2G(\tau - \tau')\dot{\epsilon}dt' + I\int_0^t K(\tau - \tau')\dot{\phi}dt' \tag{3.25}$$

where ϵ and ϕ are the mechanical deviatoric and volumetric strains, K is the bulk modulus, G is the shear modulus, and τ is the reduced time. The reduced time in ABAQUS is expressed as:

$$\tau = \int_0^t \frac{1}{A_\theta(\theta(t'))} dt' \tag{3.26}$$

where A_θ is the shift function modeled as the Williams-Landell-Ferry (WLF) equation. Rather than using the WLF equation to describe the shift function, the subroutine, UTRS, which is found in Appendix B, was generated to replace the WLF equation in ABAQUS with the shift function model presented in Section 3.5.2. The relaxation functions $K(t)$ and $G(t)$ can be defined as an exponential Prony series similar to Kim's viscoelastic model in Equation (3.15).

$$K(\tau) = K_\infty + \sum_{i=1}^{n_K} K_i exp\left[\frac{-\tau}{\tau_i}\right] \tag{3.27}$$

$$G(\tau) = G_\infty + \sum_{i=1}^{n_G} G_i exp\left[\frac{-\tau}{\tau_i}\right] \tag{3.28}$$

In Kim's model, the relaxation times τ_ω are functions of degree of cure. The relaxation time in ABAQUS does not permit field dependent relaxation times. As a result, a time-temperature-field superposition scheme had to be developed to shift onto the master curve at the reference degree of cure, $\alpha_{ref} = 0.98$. In order to shift onto the master curve, the modulus at the current degree of cure must equal the modulus at the reference degree of cure. For this to occur, the following expression must be true:

$$E_m(\alpha, \xi) = E_m(\alpha_{ref}, \xi') \tag{3.29}$$

where the superscript (') denotes the values at the reference degree of cure. In Equation (3.15), the only quantities that are cure dependent are the reduced (ξ) and relaxation (τ_ω) times. Therefore, Equation (3.30) must be true in order for Equation (3.29) to be satisfied.

$$\sum_{\omega=1}^{N} \frac{-\xi(\alpha)}{\tau_\omega(\alpha)} = \sum_{\omega=1}^{N} \frac{-\xi'(\alpha_{ref})}{\tau_\omega(\alpha_{ref})} \tag{3.30}$$

Using Equations (3.17), (3.19), and (3.21) into Equation (3.30), $log(a_T(\alpha_{ref}))$ is a function of the current degree of cure (α) and temperature (T) and the reference degree of cure (α_{ref}) as expressed in the following:

$$log(a_T(\alpha_{ref})) = H(\alpha, \alpha_{ref}, T) \tag{3.31}$$

$$H(\alpha, \alpha_{ref}, T) = \sum_{\omega=1}^{N} log\tau_\omega(\alpha) + loga_T(\alpha, T) - \sum_{\omega=1}^{N} log\tau_\omega(\alpha_0)$$

A plot of $H(\alpha, \alpha_{ref}, T)$ versus temperature for different degree of cure cases is presented in Figure 3.10 to illustrate the temperature-degree of cure superposition. Equation (3.31) can be expanded to yield the following noting that the temperature dimensions are in absolute temperature, K:

$$(c_1 exp\left[\frac{1}{\alpha_{ref}-1}\right] - c_2)(T' - 303) = H(\alpha, \alpha_{ref}, T) \tag{3.32}$$

Solving for the temperature needed for the master curve shift, T', Equation (3.32) becomes:

$$T' = \frac{H(\alpha, \alpha_{ref}, T)}{c_1 exp\left[\frac{1}{\alpha_{ref}-1}\right] - c_2} + 303 \tag{3.33}$$

As a result, the shift factor computed in the user subroutine, UTRS, and supplied to ABAQUS is the following:

$$a_T(\alpha_{ref}, T') = A_\theta(\theta(t')) = log^{-1}\left[\left[c_1 exp\left(\frac{1}{\alpha_{ref}-1}\right) - c_2\right](T' - 303)\right] \tag{3.34}$$

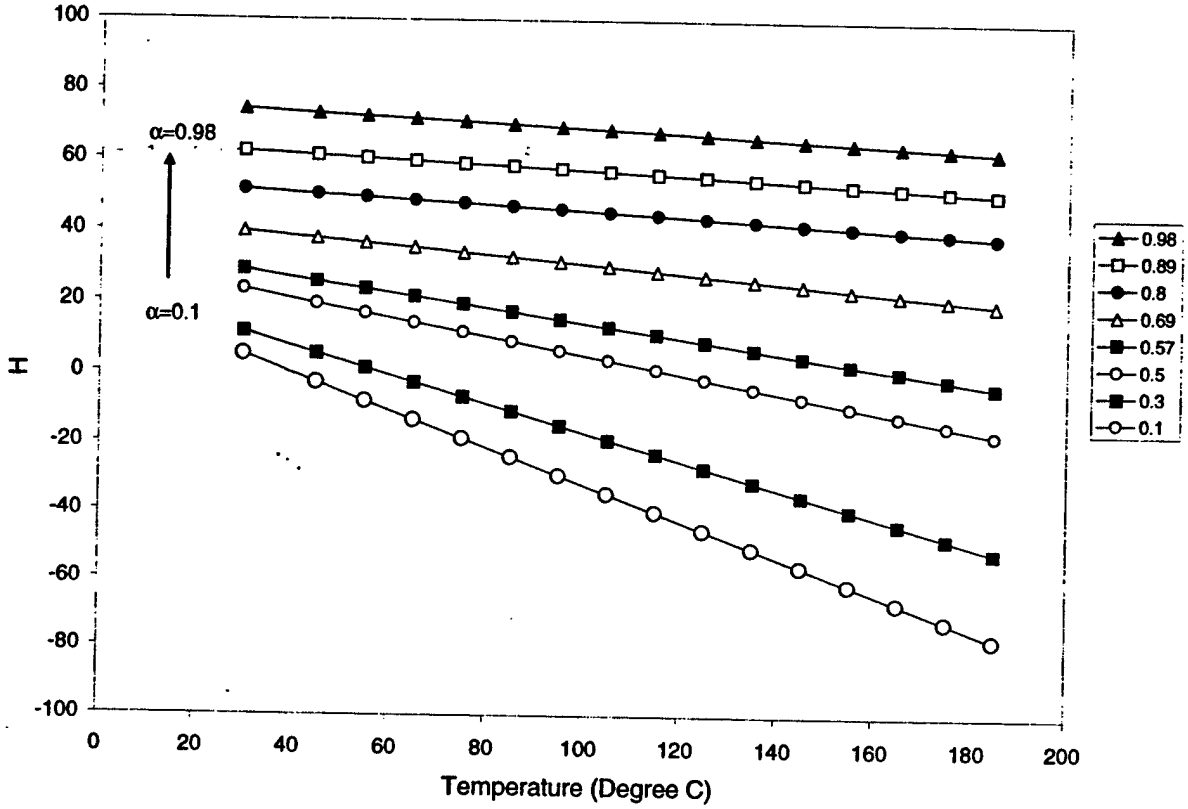

Figure 3.10: Plot of $H(\alpha, \alpha_{ref}, T)$ for Different Degrees of Cure

A schematic of the flow of variables in the user subroutine to obtain the proper shift to the master curve is presented in Figure 3.11.

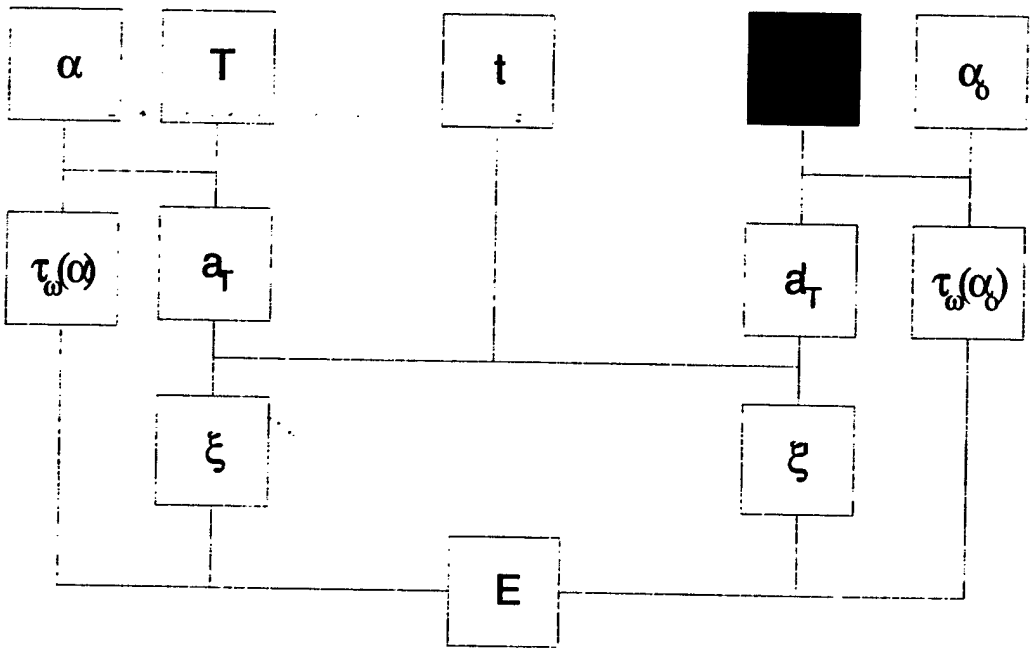

Figure 3.11: Flow of Variables to Shift to Master Curve for ABAQUS Viscoelasticity

3.6.2 Numerical Example

For this model, the same curve-shaped part as seen in the previous examples was used. Since the model can only be used to describe the matrix of the composite, the simulation was conducted in order to gain an understanding of the behavior of a viscoelastic material. Since the material is only the resin matrix, many of the mechanisms giving rise to residual stress, such as the mismatch in thermal coefficients and mechanical properties, are not present. As a result, the stresses evolved were only on the order of 0-135 kPa. Despite most negligible stresses, the transverse normal stress in the z-direction, σ_{33} reached a peak value of 135 kPa as seen in Figure 3.12. At the beginning of the cycle, the stress profile is dominated by the thermal expansion strains. As the composite hardens, the chemical shrinkage strains start to effect the stress development. The behavior of the stress profile toward the end of the simulation is similar to the advancement of degree of cure. From this observation, one can see the importance of chemical shrinkage contribution to residual stress and deformation development. The normal strain in the z-direction is presented in Figure 3.13.

Again, the three cases conducted for the thermo-elastic analysis were performed. From the isotropic viscoelasticity simulation, the most significant stress development did not occur along the fiber direction as previously seen in the thermo-elastic case. Figure 3.14 shows the normal stress (σ_{11}) for all three cases. In the case of thermal expansion only, the part reaches a maximum stress of -2.5 MPa. For the case where only there are only chemical shrinkage effects, the nor-

mal stress reaches a maximum of 4.5 MPa. The significant stress development in Case 1 and 2 shows the tremendous influence of thermal expansion and chemical shrinkage on the residual stress and deformation. If either mechanism is ignored, an incorrect stress state will result. From Figure 3.15, the strain for Case 3 is very small on the order of $4x10^{-4}$. The shear stress and strain for Case 3, σ_{23} and ε_{23} are plotted in Figure 3.16. The sharp dip in the shear strain at the beginning of the cycle as seen in the elastic case does not occur in this situation. The contour plots of the displacement and Von Mises stress at the end of the cure cycle is presented in Figures 3.17. A maximum displacement of $1.27x10^{-}4$ m, which is higher than the displacement in the elastic case, was experienced on the bottom face, particularly along outer edges. In contrast, the maximum stress was on the top face because of the constraint from the mold. Since this example only modeled the properties of the resin, the stress only reached a maximum Von Mises stress of 198 kPa.

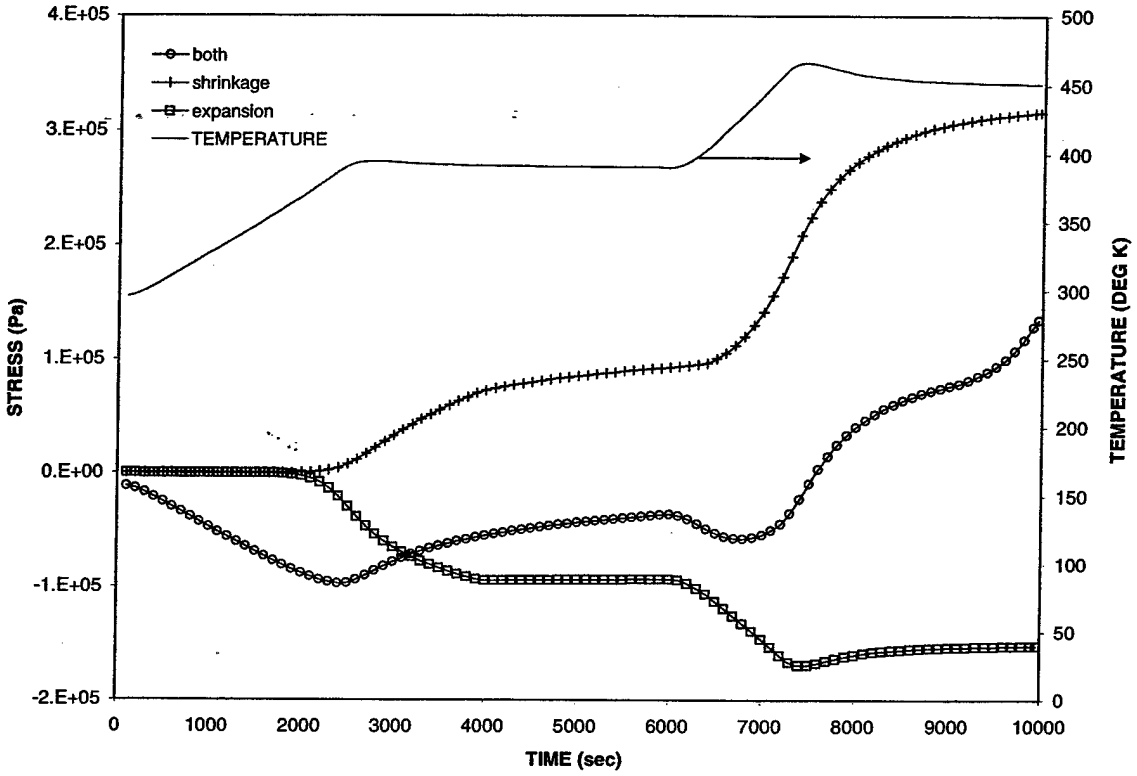

Figure 3.12: Isotropic Normal Stresses in Z-Direction (σ_{33})

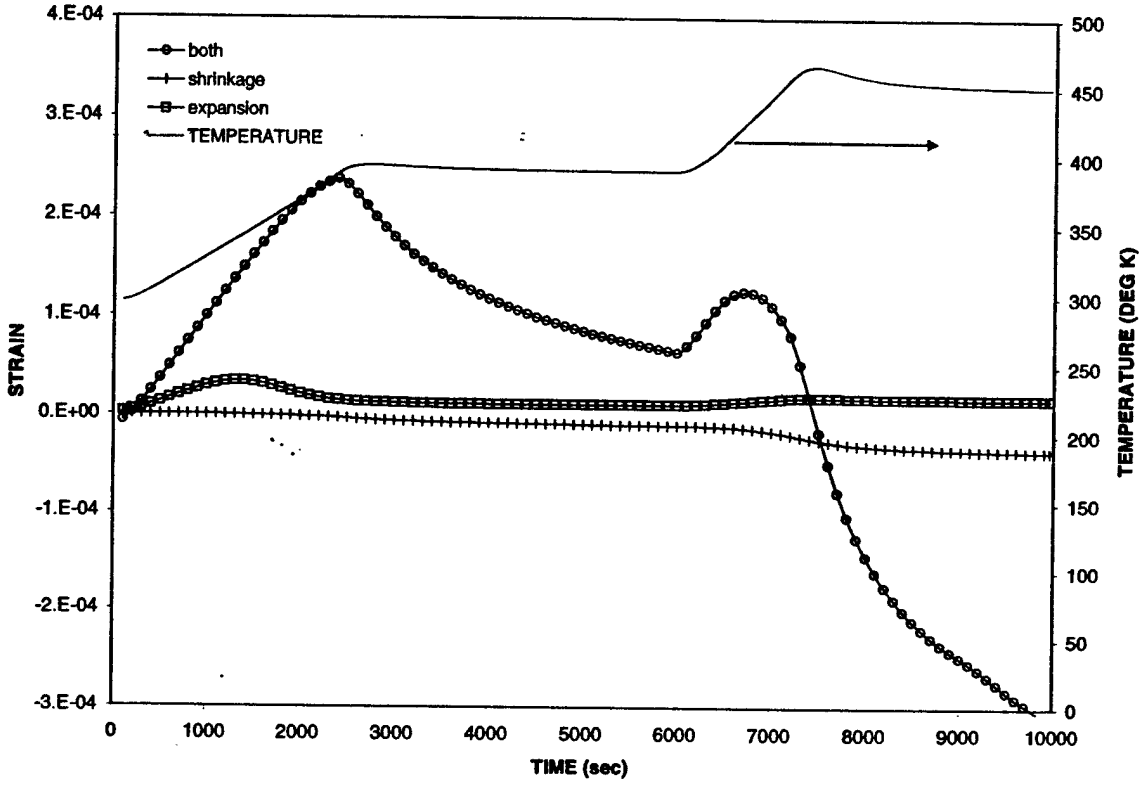

Figure 3.13: Isotropic Normal Strains in Z-Direction (ε_{33})

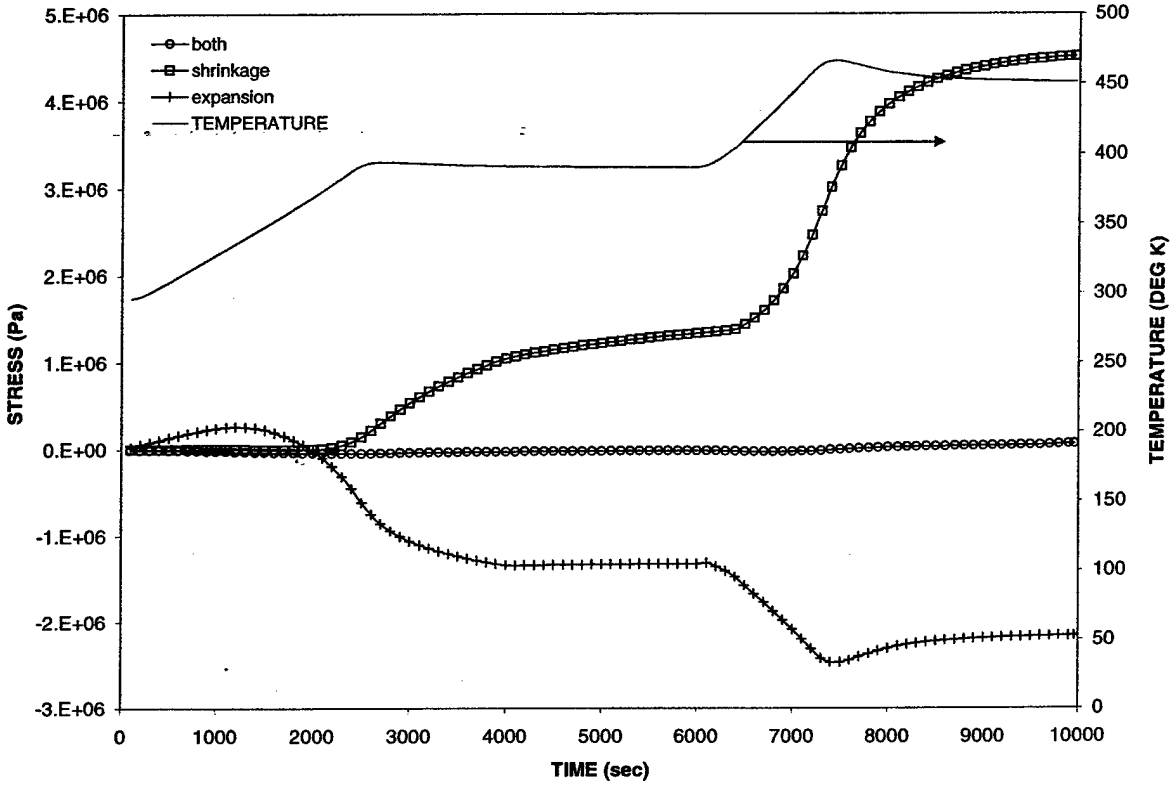

Figure 3.14: Isotropic Normal Stresses in X-Direction(σ_{11})

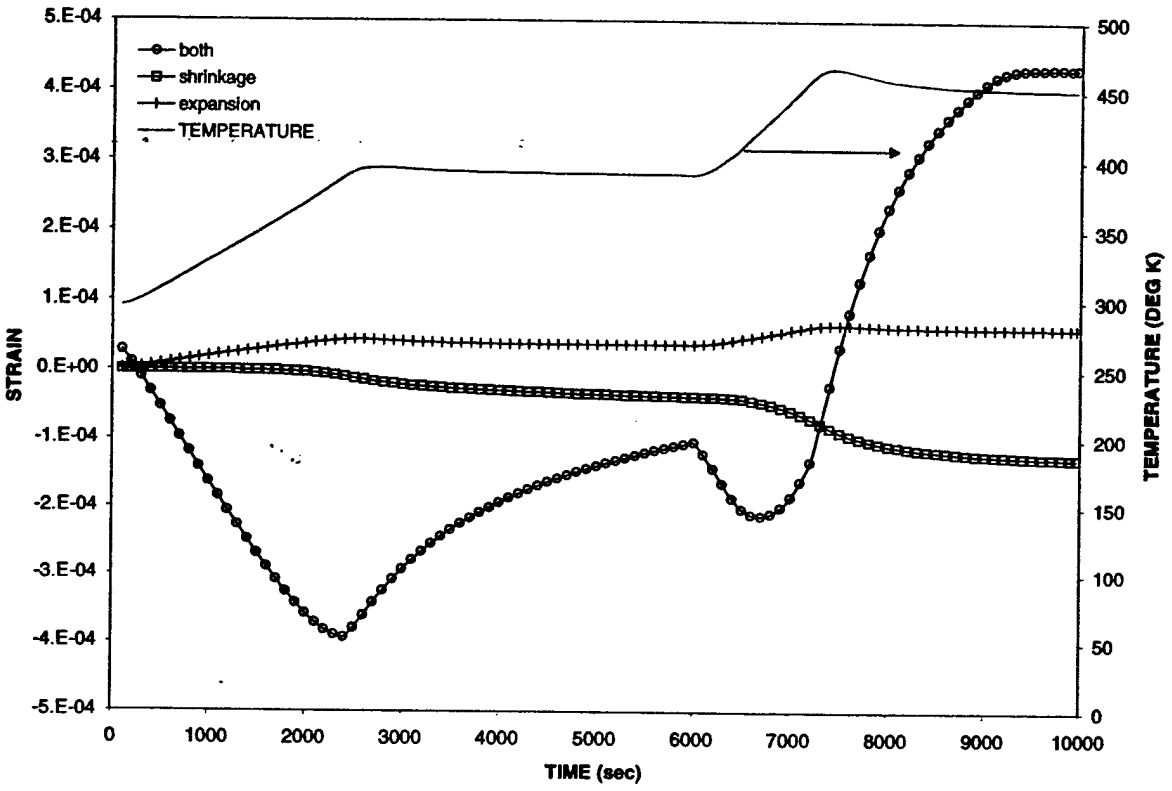

Figure 3.15: Isotropic Normal Strains in X-Direction (ε_{11})

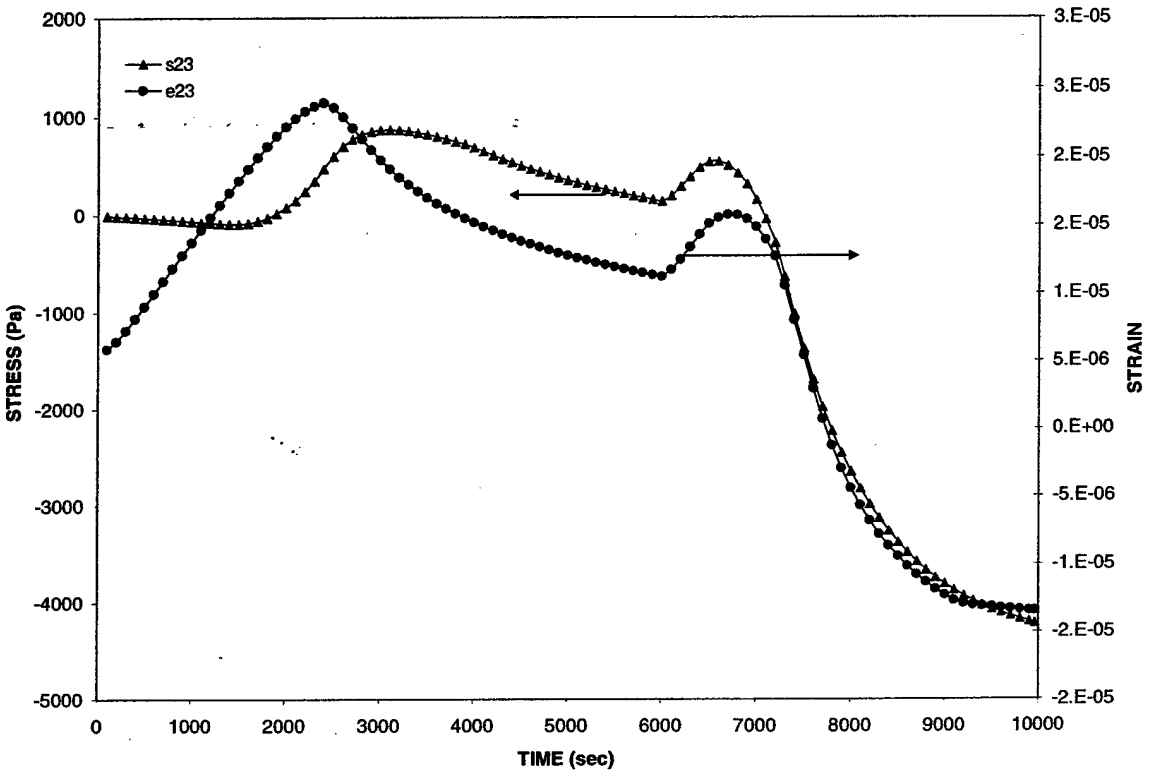

Figure 3.16: Isotropic Shear Stress and Strain

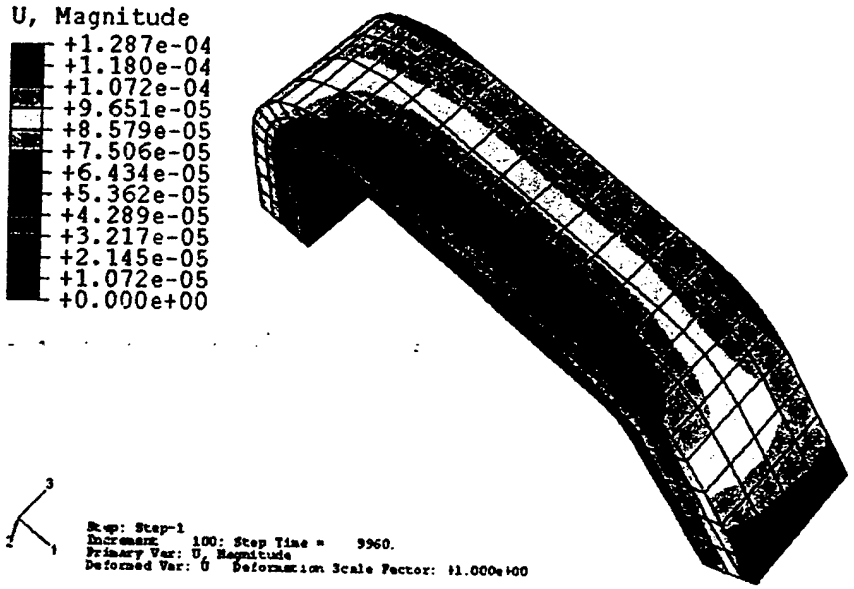

(a)

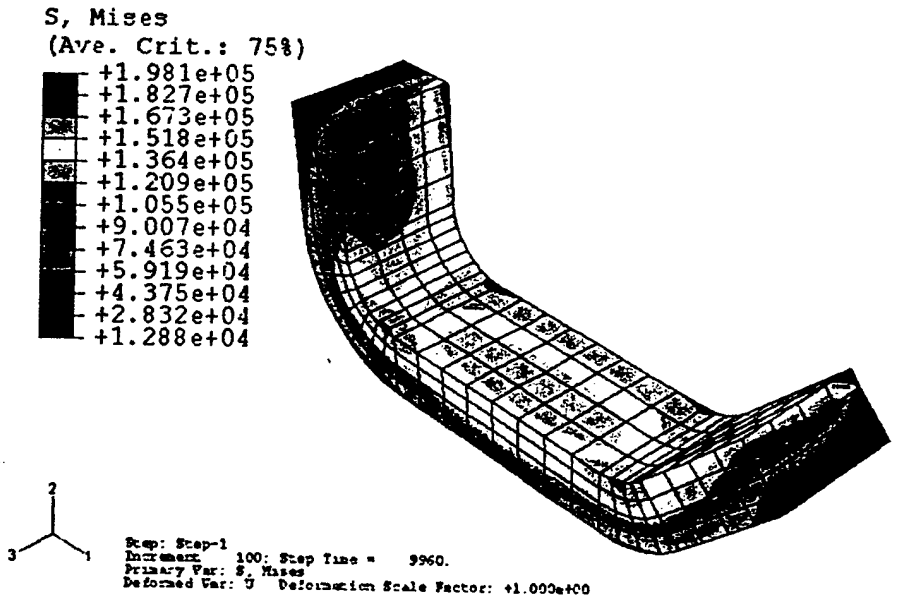

(b)

Figure 3.17: Isotropic: Displacement (a) and Von Mises Stress (b) Contours at t=9960 sec

3.6.3 Orthotropic Viscoelasticity

With the limitations of the viscoelastic function of ABAQUS, another approach was taken to describe the viscoelasticity of an orthotropic composite system as modeled in Section 3.5.3. A user subroutine, UMAT, (Appendix B) was developed to calculate the changing stress relaxation moduli at each time step. For this subroutine, the Jacobian matrix of the constitutive equation, Equation (3.23), is computed at every time step and the resulting stresses and deformations are provided by ABAQUS. This scheme also utilized the previous subroutines, UTEMP, UFIELD, and UEXPAN, to obtain the temperature and degree of cure history and to include the chemical shrinkage and thermal expansion strains.

3.6.4 Numerical Examples

For a completely orthotropic viscoelastic simulation, the user subroutine, UMAT, was developed. In this case, the residual stress and deformation were modeled in the following three steps:

(1) In-mold cure phase modeling

(2) Part Cooling

(3) Mold Constraint Removal

Like the isotropic case, the significant stress development occurred in the Z-direction. The plots of the normal stress and strain are found in Figures 3.18 and 3.19, respectively. The maximum normal stress attained was 2 MPa, which

is similar to the elastic case but along a different direction. The profiles of the isotropic and orthotropic case were similar along the Z-direction. From Figure 3.19, the strain along the Z-direction is dominated by the thermal expansion mechanism. For comparison, the plots of the stress and strain in the X-direction are also presented in Figures 3.20 and 3.21. In contrast to the isotropic case, there was some stress development along the fiber direction of about 400 kPa. The shear stress and strain, Figure 3.22, were the same as the isotropic case. From the plots of the contours of stress and displacement, Figure 3.23 for this case, the high stress portions on the part are in the regions where the part starts to curve. The maximum Von Mises stress was 23 MPa. The deformation results show that there are large deformations along the outer edge of the face despite the fact that a uniform pressure load was applied to it. These deformations may lead to cracks and delamination.

A simulation of the cool-down and mold removal was conducted for this case. Figure 3.24 shows the normal stresses up to the end of the cool-down phase. When the cool-down phase starts (at about 14,000 sec), the normal stress in the Z-direction ramps up to 6.5 MPa. This shows that there is a significant stress development during the cool-down phase, which is the area where many studies were conducted. However, there is still a significant stress development prior to cool-down that should not be neglected in a simulation of the manufacturing process.

Lastly, the mold removal was simulated by only constraining four nodes on the top surface of the geometry. Figure 3.25 shows the deformed shape superimposed on the undeformed geometry. The two ends of the geometry spring-forward and the overall thickness of the part has reduced. These effects lead to part dimensional instability. These results convey the importance of accurately simulating the manufacturing process of composites to minimize these effects.

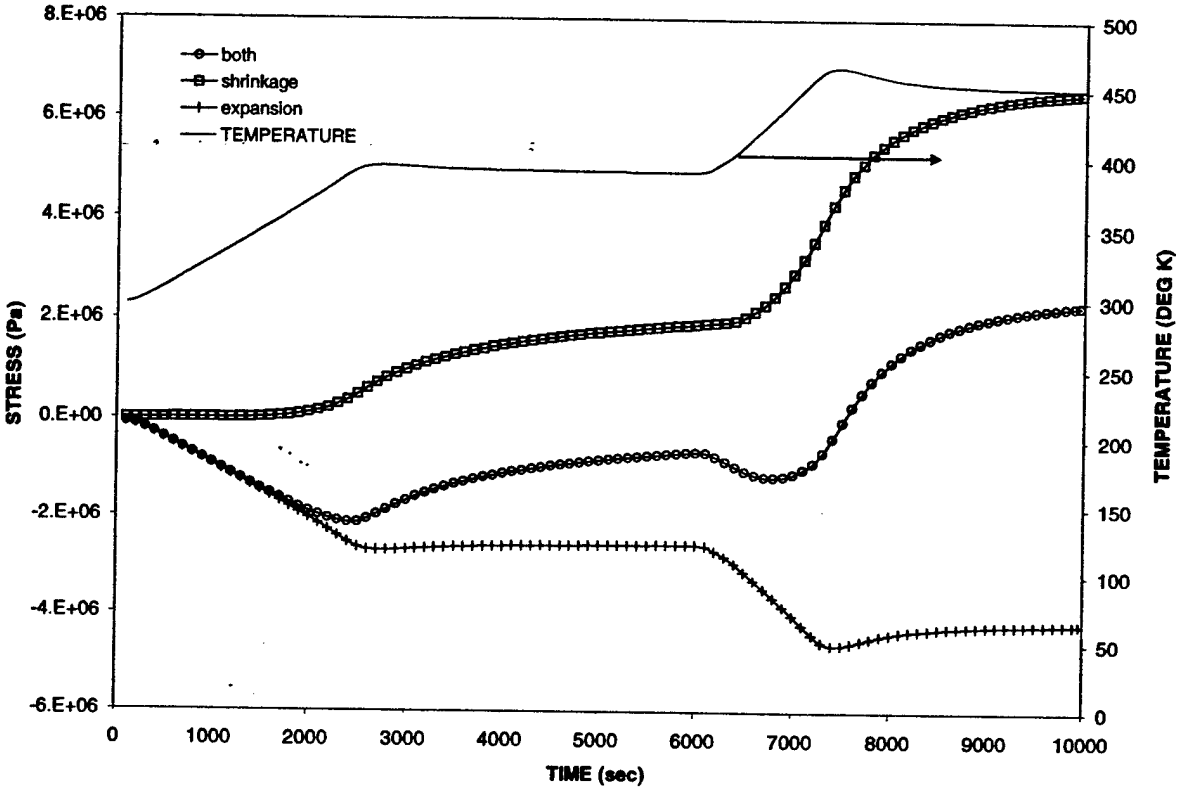

Figure 3.18: Orthotropic Normal Stresses in Z-Direction (σ_{33})

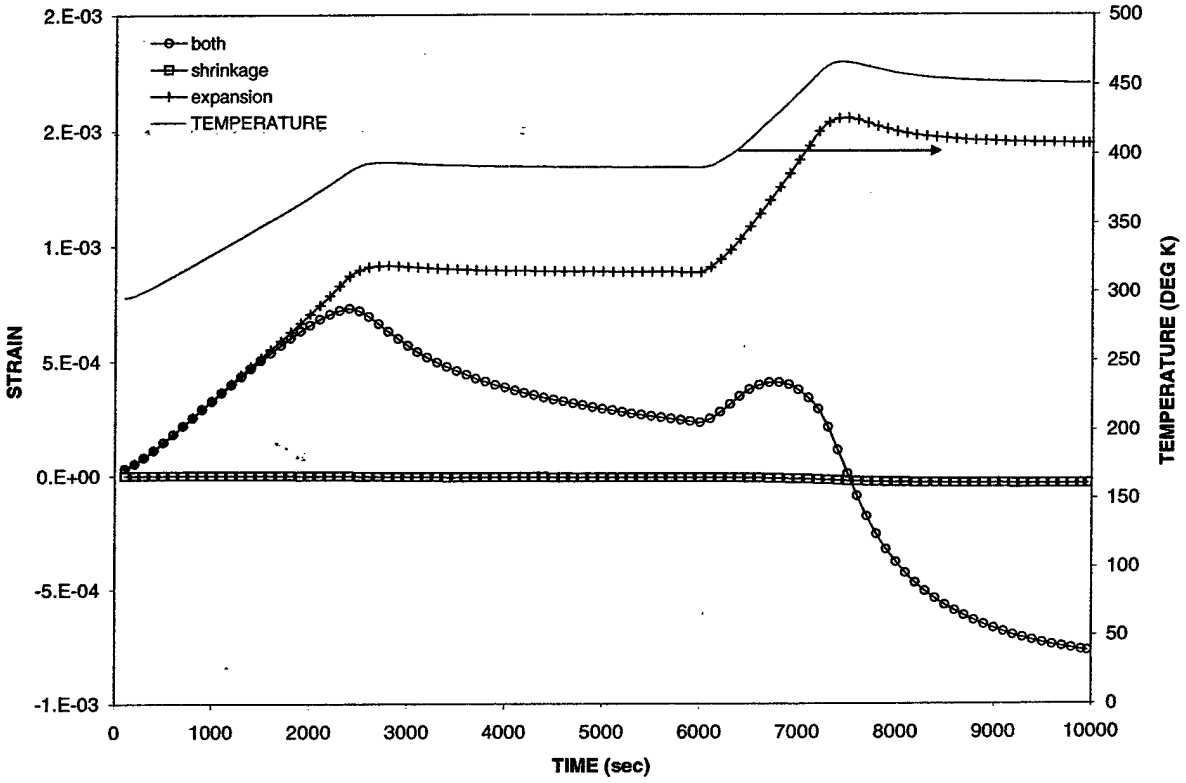

Figure 3.19: Orthotropic Normal Strains in Z-Direction (ε_{33})

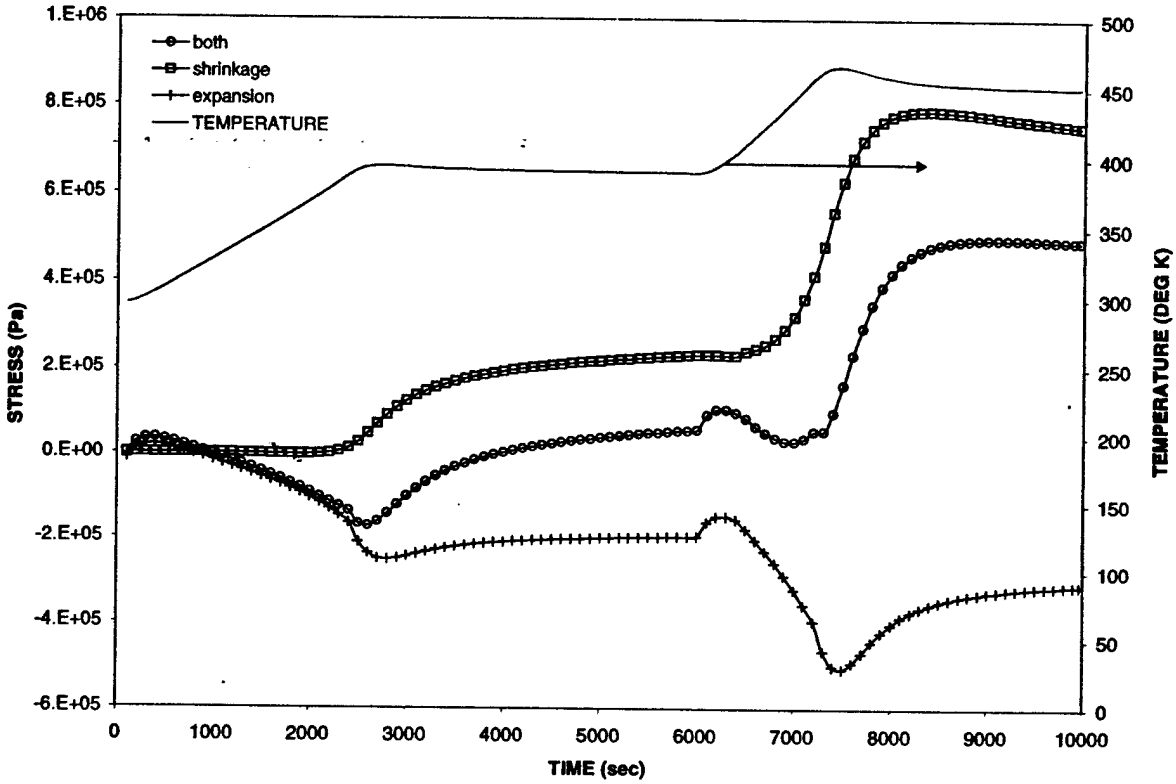

Figure 3.20: Orthotropic Normal Stresses in X-Direction(σ_{11})

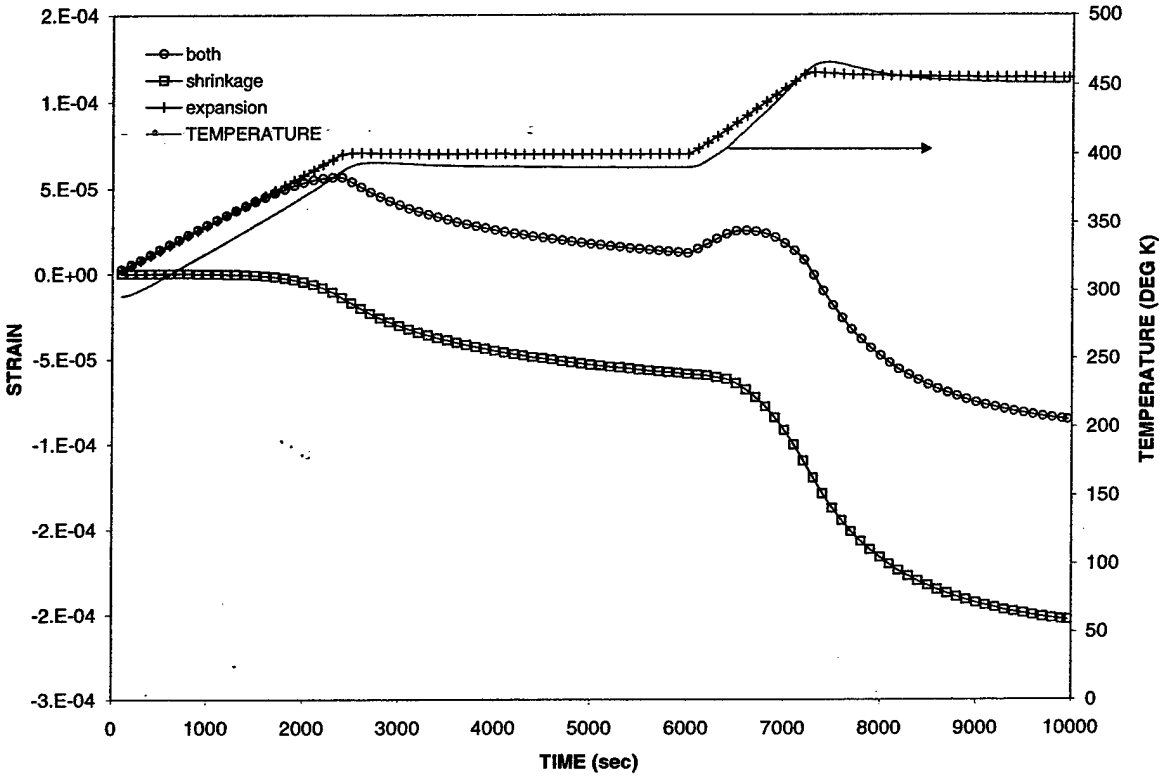

Figure 3.21: Orthotropic Normal Strains in X-Direction (ε_{11})

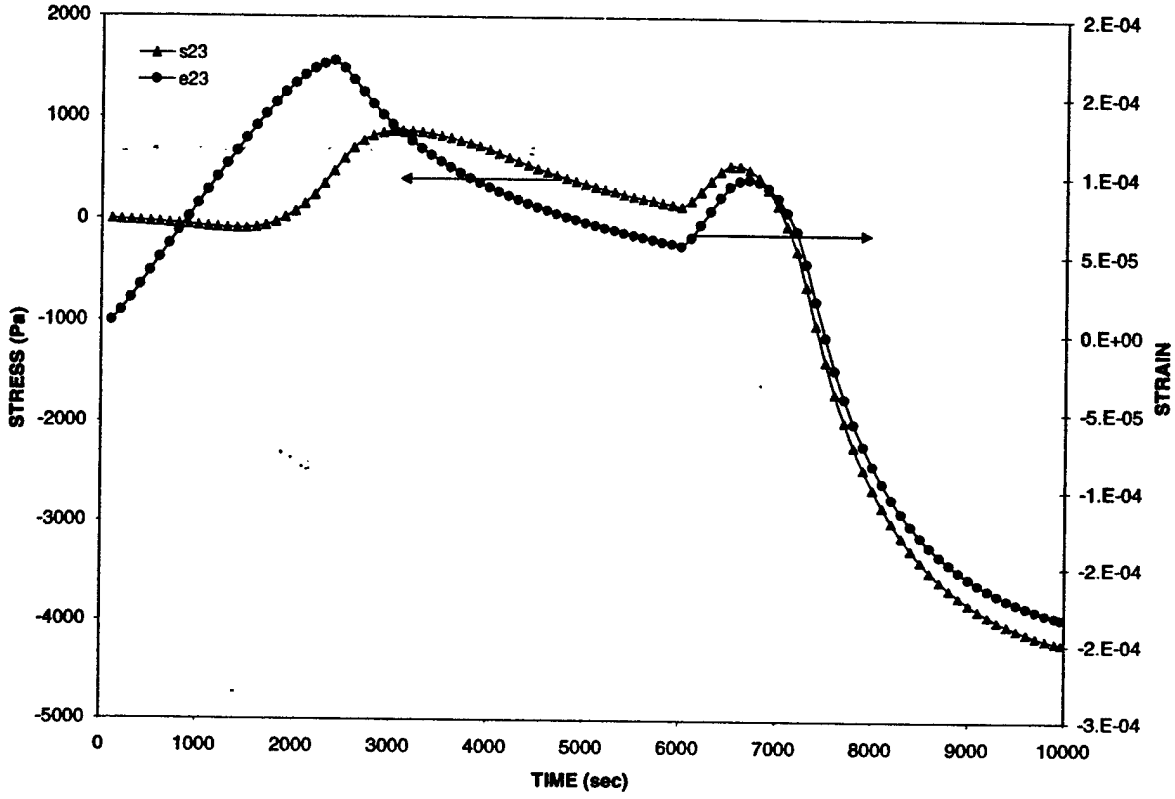

Figure 3.22: Orthotropic Shear Stress and Strain

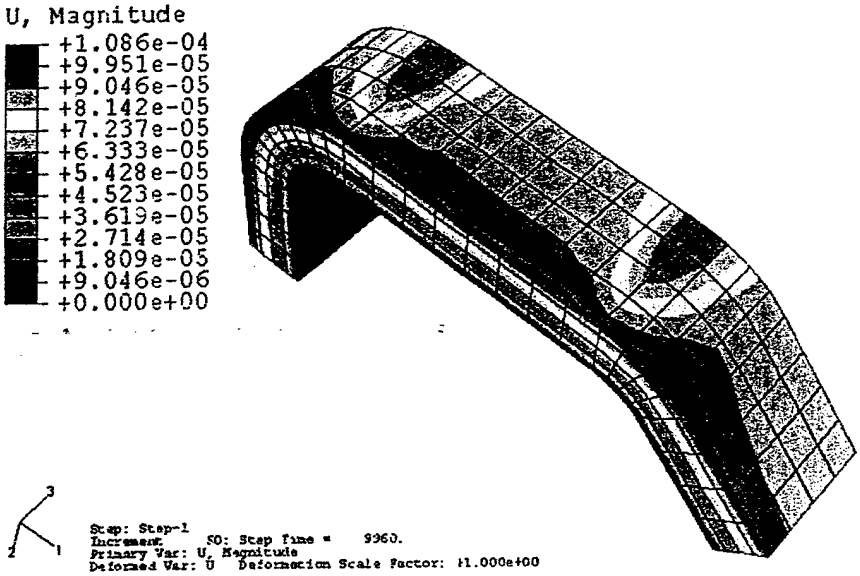

(a)

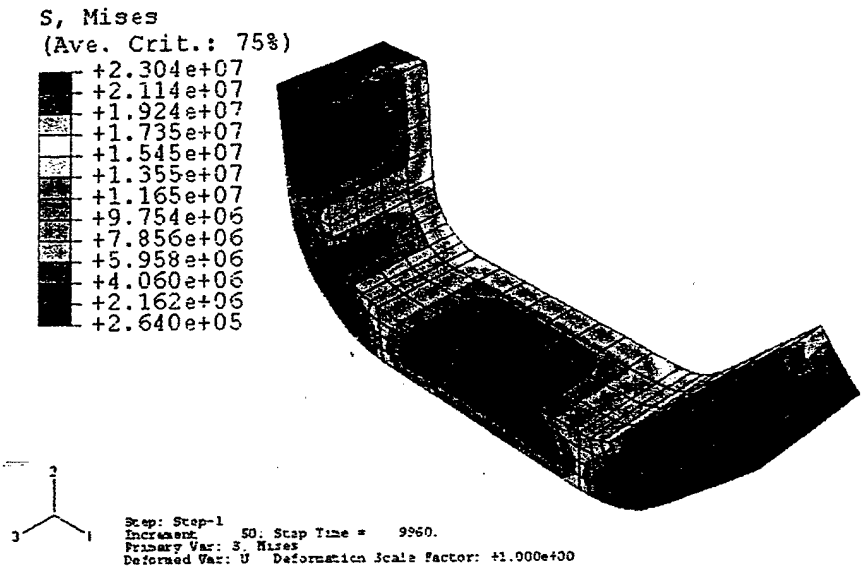

(b)

Figure 3.23: Orthotropic: Displacement (a) and Von Mises Stress (b) Contours at t=9960 sec

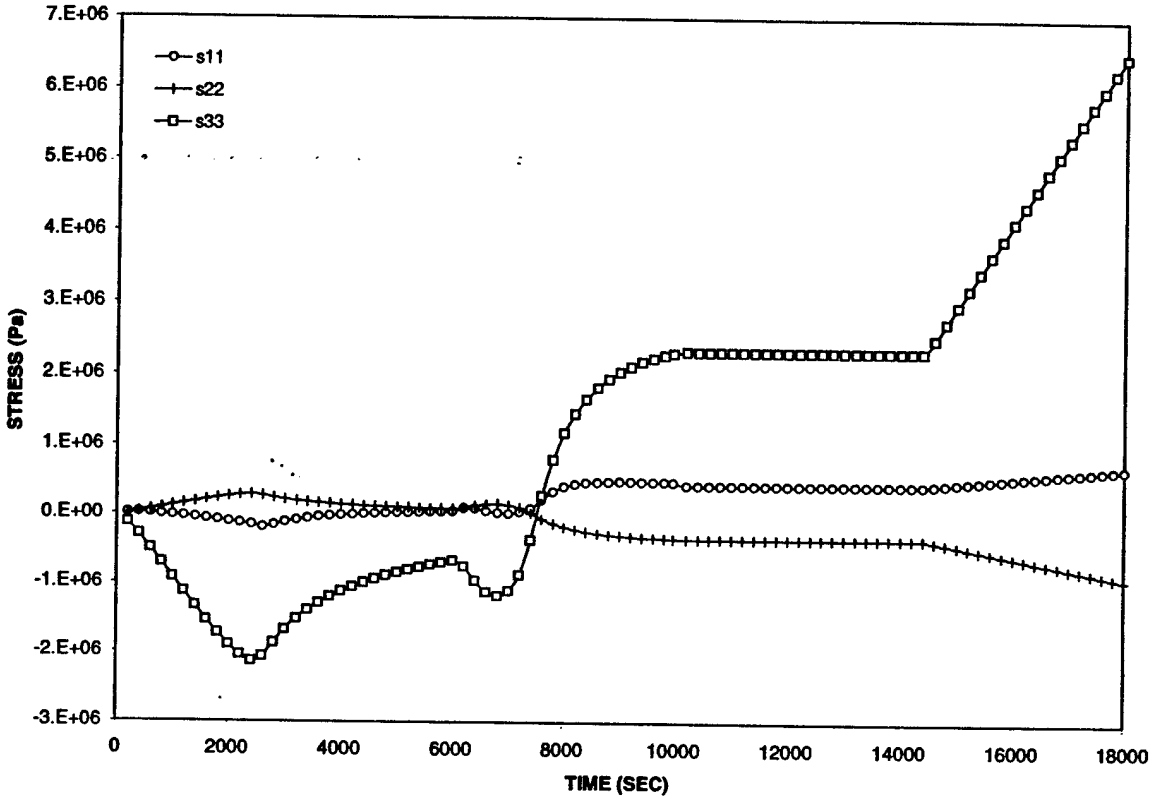

Figure 3.24: Orthotropic Normal Stresses up to Cool-Down

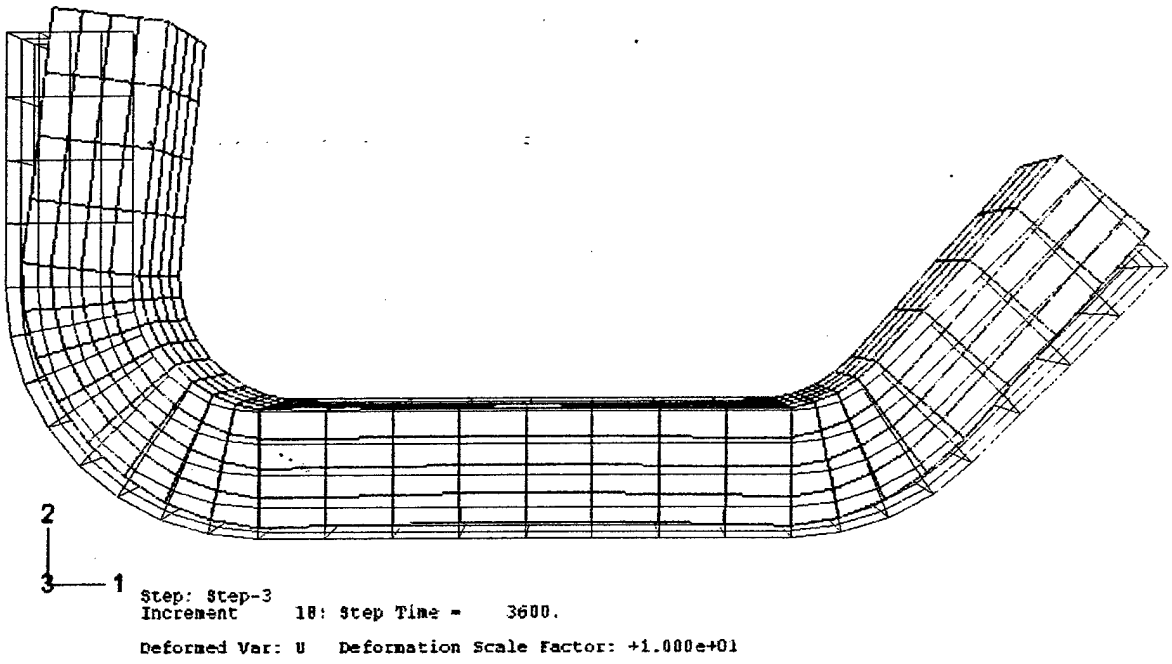

Figure 3.25: Orthotropic: Mold Removal Deformation, Magnification X10

Chapter 4

RESULTS AND DISCUSSION

A three-dimensional thermo-chemical cure simulation for polymer matrix composites is developed using the Galerkin finite element method. Several numerical examples are presented depicting the spatial and temporal gradients of temperature and degree of cure within a part. The developed methodology is capable of effectively solving large mesh problems with the resources of a personal computer. The results obtained from the present methodology were in good agreement with the experimental results available in the literature. Temperature and degree of cure gradients are illustrated for a typical composite part. The mesh sizes used in this effort are relatively small, and finer time-discretization, typically one second, is used. This is shown to capture the temperature variations due to the exothermic reaction in progress during the cure. While the temperature fields are predictable without the presence of internal heat of reaction, the heat generated typically presents a control problem during the manufacturing of these components. Prior studies indicate the use of simpler physical models or neural-networks based approximate methods to capture the physics of the problem in a predictive control strategy. The per time-increment computational burden is in

the order of 200 milliseconds for one second of simulation time. Therefore, the three-dimensional temperature and degree of cure field prediction with reasonable mesh sizes can be performed and embedded within the process control without, perhaps, resorting to approximate methods. The in-core memory requirement is quite affordable as the core size required for a 10,000 DOF problem is estimated to be roughly 32 MB. Thus the resources of a typical personal computer is adequate to perform the analysis.

The residual stress and deformation fields induced during manufacturing are driven by the the temperature and degree of cure distributions. Together with an appropriate constitutive relationship describing the mechanical behavior of the material during the cure process, the computed temperature and degree of cure distributions obtained from the cure simulation enable the prediction of the process induced residual stresses.

In simulating the process-induced stresses, several approaches were implemented including an elastic and viscoelastic formulation. The plots of stress and strain show a strong dependence on the temperature and degree of cure history. These stresses can lead to part warpage and subsequent failure. Therefore, in modeling the manufacturing process of composites, one must not neglect the process-induced stresses and deformations. In addition, the curing phase showed significant stress development. As a result, the stress development prior to cool-down should always be considered.

From the preceding study, a three-dimensional model and numerical simu-

lation of the process-induced stress was developed based on a constitutive model from the literature. The simulation is adaptable to include the use of other constitutive relations, material models, and fiber orientations and structures. This open simulation structure offers great flexibility and can be extended to simulate different types of composites and manufacturing processes.

The objective of the study was to develop a general platform to model and simulate the residual stress and deformation during cure. However, since the constitutive model used was obtained from the literature, a more comprehensive study into the viscoelastic behavior of composite materials is necessary in order to investigate the validity and reliability of the results. The results obtained and presented above were used only as a guide in the study of the mechanisms driving the residual stress development. This numerical analysis only serves as a platform to study the constitutive relationships. Moreover, the material behavior differs from material to material, which further increases the complexity of the problem. Extensive experimental testing of each material system at various temperatures and degrees of cure is necessary to accurately depict the viscoelastic behavior. In order to fully model the viscoelastic behavior of composites, experimental testing of the composite system should be conducted to obtain proper curves to model the shift function and reduced and relaxation times.

Using ABAQUS finite element software as the solver for the stress simulation had several limitations. As explained earlier, the ABAQUS viscoelastic function could only be implemented for an isotropic material with field independent relax-

ation times. As a result, the user subroutine, UMAT, needed to be developed. However, employing the UMAT subroutine requires extensive knowledge in the behavior of the material and the software. The inability to control the solving scheme of the software limits the range of problems that can be accurately modeled. Rather, the viscoelastic behavior should be simulated with a self-developed code to have a better control over the solving scheme. With a special purpose finite element code, the behavior can be modeled more accurately and there is more reliability in the results.

The issues involved in this current study is the subject of future work. An investigation into the validation and reliability of the results will be conducted through experimental material testing. Experimental testing is necessary especially for low cure states ($\alpha < 0.5$). The viscoelastic model used from the literature only had experimental validation for cure states above 0.5. Also, the development of an FEM code to overcome the limitations presented by ABAQUS will also be investigated. Modeling other manufacturing processes, fiber orientations and structures is also the subject of future research. In addition, the viscoelastic study will be applied to investigating the characterization of the physical aging and degradation of polymer matrix composites since they are similarly influenced by time and temperature.

Bibliography

[1] White, S. R. and Hahn, H. T. Process modeling of composite materials: residual stress development during cure. part i. model formulation. Journal of Composite Materials, 26(16):2402–2421, 1992.

[2] Kim, Y. K. Process-induced viscoelastic residual stress analysis of graphite-epoxy composite structures. PhD thesis, University of Illinois at Urbana-Champaign, 1996.

[3] Russell, J.D., Madhukar, M.S., Genidy, M.S., and Lee, A. A new method to reduce cure-induced stresses in thermoset polymer composites, part iii: correlating stress history to viscosity, degree of cure, and cure shrinkage. Journal of Composite Materials, 34(22):1926–1947, 2000.

[4] Loos, A.C. and Springer, G.S. Curing of epoxy matrix composites. Journal of Composite Materials, 17:135–169, 1983.

[5] Bogetti, T. A. and Gillespie, Jr., J. W. Two-dimensional cure simulation of thick thermosetting composites. Journal of Composite Materials, 25:239–273, 1991.

[6] Yi, S., Hilton, H. H., and Ahmad, M. F. A finite element approach for cure simulation of thermosetting matrix composites. Computers and Structures, 64(1-4):16–21, 1997.

[7] Park, H. C. and Lee, S. W. Cure simulation of thick composite structures using the finite element method. Journal of Composite Materials, 35(3):188–201, 2001.

[8] Zhu, Q., Geubelle, P. H., Li, M., and Tucker, C. L. Dimensional accuracy of thermoset composites: simulation of process-induced residual stresses. Journal of Composite Materials, 35(24):2171–2205, 2001.

[9] Cook, R.D., Malkus, D.S., and Plesha, M.E. Concepts and Applications of Finite Element Analysis, Third Edition. John Wiley and Sons, 1989.

[10] Teplinsky, Sh. and Gutman, E. M. Computer simulation of process induced stress and strain development during cure of thick-section thermosetting composites. Computational Materials Science, 6:71–76, 1996.

[11] Tang, L. Q., Pochiraju, K., Chassapis, C., and Manoochehri, S. Three-dimenisional transient mold cooling analysis based on galerkin finite element formulation with a matrix-free conjugate gradient technique. International Journal for Numerical Methods in Engineering, 39:3049–3064, 1996.

[12] Taya, M. and Arsenault, R. J. Metal Matrix Composites: Thermomechanical Behavior. Pergamon Press, 1989.

[13] Kim, Y. K. and White, S. R. Viscoelastic analysis of processing-induced residual stresses in thick composite laminates. Mechanics of Composite Materials and Structures, 4:361–387, 1997.

[14] Hahn, H. T. and Pagano, N. J. Curing stress in composite laminates. Journal of Composite Materials, 9:91–105, 1975.

[15] Hyer, M. W. Calculations of the room-temperature shapes of unsymmetric laminates. Journal of Composite Materials, 15:296–310, 1981.

[16] Zewi, I. G., Daniel, I. M., and Gotro, J. T. Residual stresses and warpage in woven-glass/epoxy laminate. Experimental Mechanics, 27(1):44–50, 1987.

[17] Jun, W. J. and Hong, C. S. Cured shape of unsymmetric laminates with arbitrary lay-up angles. Journal of Reinforced Plastics and Composites, 11:1352–1366, 1992.

[18] Radford, D. W. Cure shrinkage induced warpage in flat uni-axial composites. Journal of Composites Technology and Research, 15(4):290–296, 1993.

[19] Weitsman, Y. Residual thermal stresses due to cool-down of epoxy-resin composites. Journal of Applied Mechanics, 46:563–567, 1979.

[20] Weitsman, Y. Optimal cool-down in linear viscoelasticity. Journal of Applied Mechanics, 47:35–39, 1980.

[21] Hodges, J., Yates, B., Darby, M. I., Wostenholm, G. H., Clemmet, J. F., and Keates, T. F. Residual stresses and the optimum cure cycle for an epoxy resin. Journal of Materials Science, 24:1984–1990, 1989.

[22] Stango, R. J. and Wang, S. S. Process-induced residual thermal stress in advanced fiber-reinforced composite laminates. Journal of Engineering for Industry, 106:48–54, 1984.

[23] Kim, K. S. and Hahn, H. T. Residual stress development during processing of graphite/epoxy composites. Composites Science and Technology, 36:121–132, 1989.

[24] Bogetti, T. A. and Gillespie, Jr., J. W. Process-induced stress and deformation in thick-section thermoset composite laminate. Journal of Composite Materials, 26:626–660, 1992.

[25] White, S. R. and Hahn, H. T. Process modeling of composite materials: residual stress development during cure. part ii. experimental validation. Journal of Composite Materials, 26(16):2423–2453, 1992.

[26] Kim, Y. K. and White, S. R. Process-induced stress relaxation analysis of as4/3501-6 laminate. Journal of Reinforced Plastics and Composites, 16(1):2–16, 1997.

[27] Kim, Y. K. and White, S. R. Stress relaxation behavior of 3501-6 epoxy resin during cure. Polymer Engineering and Science, 36(23):2852–2862, 1996.

[28] White, S. R. and Hartman, A. B. Effect of cure state on stress relatxation in 3501-6 epoxy resin. Journal of Engineering Materials and Technology, 119(3):262–265, 1997.

[29] O'Brien, D. J., Mather, P. T., and White, S. R. Viscoelastic properties of an epoxy resin during cure. Journal of Composite Materials, 35(10):883–904, 2001.

[30] Simon, S. L., McKenna, G. B., and Sindt, O. Modeling the evolution of the dynamic mechanical properties of a commericial epoxy during cure after gelation. Journal of Applied Polymer Science, 76:495–508, 2000.

[31] Prasatya, P., McKenna, G. B., and Simon, S. L. A viscoelastic model for predicting isotropic residual stresses in thermosetting materials: effect of processing parameters. Journal of Composite Materials, 35(10):826–848, 2001.

[32] Wiersma, H. W., Peeters, L. J. B., and Akkerman, R. Prediction of spring-forward in continuous-fibre/polymer l-shaped parts. Composites Part A, 29(11):1333–1342, 1998.

[33] Yi, S., Hilton, H. H., and Ahmad, M. F. In Curing process induced viscoelastic residual stresses in polymer matrix lamiated composites, volume Proceedings of the ASME Materials Division, pages 65–76. American Society for Composites, November 1995.

[34] Yi, S., Hilton, H. H., and Ahmad, M. F. Nonlinear thermo-viscoelastic analysis of interlaminar stresses in laminated composites. Journal of Applied Mechanics-Transactions of the ASME, 63(1):218–224, 1996.

[35] Yi, S., , Chian, K. S., and Hilton, H. H. Nonlinear viscoelastic finite element analyses of thermosetting polymeric composites during cool-down after curing. Journal of Composite Materials, 36(1):3–17, 2002.

[36] Hilton, H. H. and Yi, S. Stochastic delamination simulations of nonlinear viscoelastic composites during cure. Journal of Sandwich Structures and Materials, 1:111–127, 1999.

[37] Zaoutsos, S. P., Papanicolaou, G. C., and Cardon, A. H. On the non-linear viscoelastic behaviour of polymer-matrix composites. Composites Science and Technology, 58:883–889, 1997.

[38] Papanicolaou, G. C., Zaoutsos, S. P., and Cardon, A. H. Prediction of the non-linear viscoelastic response of unidirectional fiber composites. Composites Science and Technology, 59:1311–1319, 1999.

[39] Chen, Y., Xia, Z., and Ellyin, F. Evolution of residual stresses induced during curing processing using a viscoelastic micromechanical model. Journal of Composite Materials, 35(6):522–542, 2001.

[40] Fisher, F. T. and Brinson, L. C. Viscoelastic interphases in polymer-matrix composites: theoretical models and finite-element analysis. Composites Science and Technology, 61:731–748, 2001.

[41] Bogetti, T. A. Process-induced stress and deformation in thick-section thermosetting composites. PhD thesis, University of Delaware, 1989.

[42] Whitney, J. M. and McCullough, R. L. Micromechanical Materials Modeling, Delaware Composites Design Encyclopedia, volume 2. Technomic Pub. Co., Inc., 1990.

[43] Russell, J.D. Cure shrinkage of thermoset composites. SAMPE Quarterly, 29:28–33, 1993.

Appendix A

Micromechanics Field Model

The following model from Whitney and McCullough [42] was used to compute the effective composite material properties based on the constituent properties and fiber volume fraction. A principal material coordinate system for unidirectional composites as seen in Figure A.1 was adopted where "1" or "L" corresponds to the direction along the fiber (longitudinal direction). The "2" or "T" direction is the transverse direction (perpendicular to the longitudinal direction). The model is formulated for an orthotropic material that is transversely isotropic; therefore, the properties in the "2" direction are the same as those in the "3" direction. The thermal expansion and chemical shrinkage coefficients were also computed using the micromechanics model. The subscripts f and m represent the fiber and matrix constituent properties, respectively, and ν_f is the fiber volume fraction.

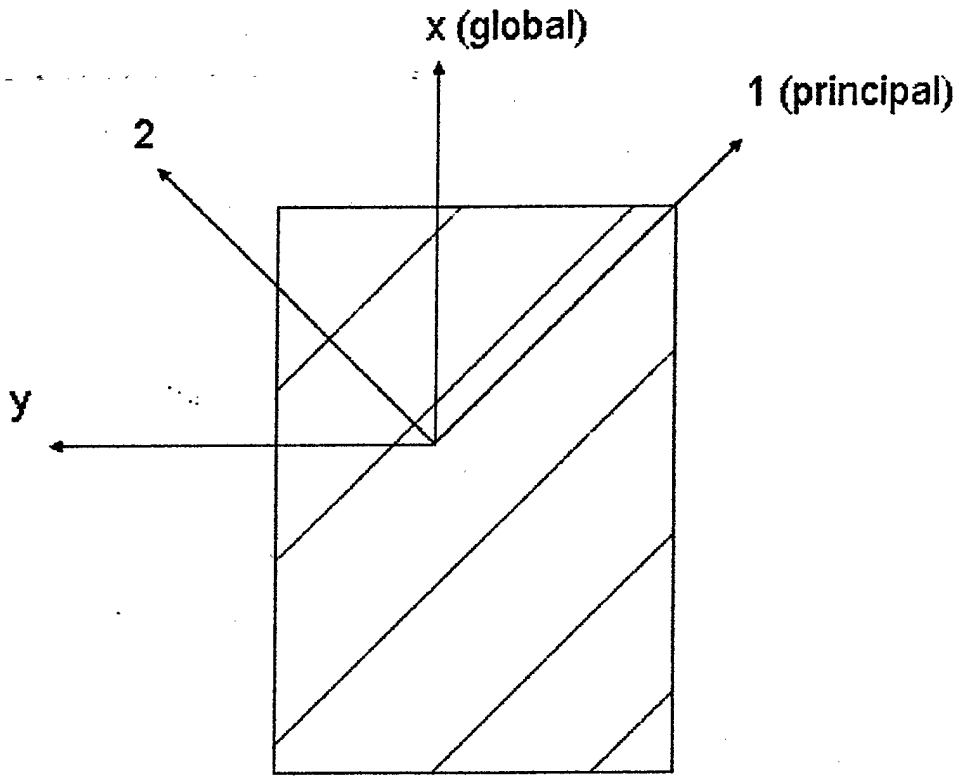

Figure A.1: Coordinate System of Composite System (Principal Directions)

A.1 Engineering Constants

Isotropic Plane Strain Bulk Modulus (Equation used to calculate the plane strain bulk modulus for the constituents- k_{Tf} and k_{Tm}.)

$$k_T = \frac{E_1 E_2}{2(1-\nu_{23})E_1 - 4\nu_{12}^2 E_2} \tag{A.1}$$

Longitudinal Young's Modulus:

$$E_L = E_1 = E_{Lf}\nu_f + E_{Lm}(1-\nu_f) + \frac{4(\nu_{LTm} - \nu LTf)^2 k_{Tf} kTm G_{TTm}(1-\nu_f)\nu_f}{(k_{Tf}+G_{TTm})k_{Tm} + (k_{Tf}-k_{Tm})G_{TTm}\nu_f} \tag{A.2}$$

Major Poisson's Ratio:

$$\nu_{LT} = (\nu_{12} = \nu_{13}) = \nu_{LT}\nu_f + \nu_{LT}(1-\nu_f) + \frac{(\nu_{LTm} - \nu_{LTf})(k_{Tm} - k_{Tf})G_{TTm}(1-\nu_f)\nu_f}{[(k_{Tf}+G_{TTm})k_{Tm} + (k_{Tf}-k_{Tm})G_{TTm}\nu_f]} \tag{A.3}$$

In-Plane Shear Modulus:

$$G_{LT} = (G_{12} = G_{13}) = G_{LTm}\frac{[(G_{LTf}+G_{LTm}) + (G_{LTf}-G_{LTm})\nu_f]}{[(G_{LTf}+G_{LTm}) - (G_{LTf}-G_{LTm})\nu_f]} \tag{A.4}$$

Transverse Shear Modulus:

$$G_{TT} = (G_{23}) = \frac{G_{TTm}[k_{Tm}(G_{TTm}+G_{TTf}) + 2G_{TTf}G_{TTm} + k_{Tm}(G_{TTf}-G_{TTm})\nu_f]}{[k_{Tm}(G_{TTm}+G_{TTf}) + 2G_{TTf}G_{TTm} - (k_{Tm}+2G_{TTm})(G_{TTf}-G_{TTm})\nu_f]} \tag{A.5}$$

Plane Strain Bulk Modulus:

$$k_T = \frac{(k_{Tf}+G_{TTm})k_{Tm} + (k_{Tf}-k_{Tm})G_{TTm}\nu_f]}{(k_{Tf}+G_{TTm}) - (k_{Tf}-k_{Tm})\nu_f} \tag{A.6}$$

Transverse Young's Modulus:

$$E_T = (E_2 = E_3) = \frac{1}{\frac{1}{4k_T} + \frac{1}{4G_{TT}} + \frac{\nu_{LT}^2}{E_L}} \tag{A.7}$$

Transverse Poisson's Ratio:

$$\nu_{TT} = (\nu_{23}) = \frac{2E_L k_T - E_L E_T - 4\nu_{LT}^2 k_T E_T}{2E_L k_T} \tag{A.8}$$

A.2 Expansional Strains

The forms of the following expressions were used to calculate the coefficients of thermal expansion and chemical shrinkage with ($\phi_1 = \epsilon_1^E$), etc.

Longitudinal:

$$\epsilon_L^E = \epsilon_1^E = \frac{\epsilon_{Lf}^E E_{Lf} \nu_f + \epsilon_{Lm}^E E_{Lm}(1-\nu_f)}{E_{Lf}\nu_f + E_{Lm}(1-\nu_f)} \tag{A.9}$$

Transverse:

$$\epsilon_T^E = \epsilon_2^E = [\nu_{LTf}\nu_f + \nu_{LTm}(1-\nu_f)]\frac{\epsilon_{Lf}^E E_{Lf} \nu_f + \epsilon_{Lm}^E E_{Lm}(1-\nu_f)}{E_{Lf}\nu_f + E_{Lm}(1-\nu_f)} \tag{A.10}$$

Appendix B

ABAQUS User Subroutines

B.1 UFIELD/UTEMP

```
c
c
c Thermo-kinetic viscoelastic subroutines
c

C
C
C
C
C
C
C
c
      SUBROUTINE UFIELD(FIELD,KFIELD,MSECPT,KSTEP,KINC,TIME,NODE,
     1 COORDS,TEMP,DTEMP,NFIELD)
C
        INCLUDE 'ABA_PARAM.INC'
C
      DIMENSION FIELD(MSECPT,NFIELD), TIME(2), COORDS(3),
     1 TEMP(MSECPT), DTEMP(MSECPT)
C
C
      COMMON /UTEMP_DATA/DATAVAL(2,2,5000),C_TIME(2),ATIM,BTIM,
     1  AINCRTIM,IFTIME,ICODE,MNODE
      CHARACTER FILENAM*256
      DATA IFTIME/0/
      CHARACTER CONFPATH*256,FILNAME*265
C
C do similar code to field for temperature, except read temperature from the v
tk files.
      IF(IFTIME.EQ.0)THEN
C
C
C  READ IN THE CONFIG FILE
C
        CALL GETENVVAR( 'this_dir',  CONFPATH, LENVVAR )
        FILNAME = CONFPATH //'\user.cfg'
         WRITE(*,*)'CONFPATH',CONFPATH,FILNAME
        OPEN(52,FILE=FILNAME,STATUS='OLD')
        READ(52,*)ATIM,BTIM
        READ(52,*)FSTTIME,SECTIME
        READ(52,*)MNODE
        CLOSE(52)

C READ IN 2 TIME STEPS
C
C
        AINCRTIM = SECTIME-FSTTIME
        icode = 1
c
c
c
        c_TIME(icode) = FSTTIME
        ifinc = ATIM*FSTTIME+BTIM
        call make_filename(filenam,ifinc)
        call read_vtk(filenam)
c
c
c
        ISINC = ATIM*SECTIME+BTIM
c
        call make_filename(filenam,isinc)
        icode = 2
        c_time(icode) = SECTIME
        call read_vtk(filenam)
```

```
          IFTIME = 1
        END IF
c
c See if the next step has to be read in.
c
        IF(TIME(2).GE.C_TIME(icode))THEN
         prev_time = C_TIME(icode)
         C_TIME(1)=prev_time
         ifinc=ATIM*C_TIME(1)+BTIM
         icode=1
         call make_filename(filenam,ifinc)
         call read_vtk(filenam)
         if(icode .eq. 1)then
            icode = 2
         else
            icode = 2
         end if
         C_TIME(icode) = Prev_time + AINCRTIM
         ISINC = ATIM*C_TIME(ICODE)+BTIM
        call make_filename(filenam,isinc)
         call read_vtk(filenam)
         END IF

c
c interpolate
c
c       WRITE(*,*)'ENTERING UFIELD'
c       WRITE (*,*) COORDS(1),COORDS(2),COORDS(3)
c       WRITE(*,*) 'WRITING CURE FROM UFIELD'
        AZ = (TIME(2) - c_time(1))/(c_time(2)-c_time(1))
        FIELD(1,1) = dataval(1,2,NODE)*(1-AZ) + dataval(2,2,NODE)*(AZ)
c       WRITE(*,*) 'KSTEP=',KSTEP,' KINC=',KINC
c       WRITE(*,*) 'TIME2=',TIME(2),' CTIME(1)=',C_TIME(1),
c      1    'CTIME(2)=',C_TIME(2)
c       WRITE(*,*) 'AZ=',AZ
c       WRITE(*,*) 'DATAVAL1=',dataval(1,2,NODE),
c      1    'DATAVAL2=',DATAVAL(2,2,NODE)
c       WRITE(*,*) 'UFIELD',FIELD(1,1)
c
        RETURN
        END

C
C
C
C
C
C
C
C Load in the temperature variations using UTEMP.
C
C
      SUBROUTINE UTEMP(TEMP,MSECPT,KSTEP,KINC,TIME,NODE,COORDS)
C
      INCLUDE 'ABA_PARAM.INC'
C
      DIMENSION TEMP(MSECPT), TIME(2), COORDS(3)
      COMMON /UTEMP_DATA/DATAVAL(2,2,5000),C_TIME(2),
     1    ATIM,BTIM,AINCRTIM,IFTIME,ICODE,MNODE
      CHARACTER FILENAM*256
C
C do similar code to field for temperature, except read temperature from the v
tk files.
C
```

```
      IF(IFTIME.EQ.0)THEN
C
C
C  READ IN THE CONFIG FILE
C
         OPEN(52,FILE='C:\RTM\Geu_ABQ\user.cfg',STATUS='OLD')
         READ(52,*)ATIM,BTIM
         READ(52,*)FSTTIME,SECTIME
         READ(52,*)MNODE
         CLOSE(52)
C READ IN 2 TIME STEPS
C
C
         AINCRTIM = SECTIME-FSTTIME
         icode = 1
c
c
c
         c_TIME(icode) = FSTTIME
         ifinc = ATIM*FSTTIME+BTIM
         call make_filename(filenam,ifinc)

         call read_vtk(filenam)
c
c
c
         ISINC = ATIM*SECTIME+BTIM
c
         call make_filename(filenam,isinc)
         icode = 2
         c_time(icode) = SECTIME
         call read_vtk(filenam)
         IFTIME = 1
      END IF
c
c See if the next step has to be read in.
c
       IF(TIME(2).GT.C_TIME(icode))THEN
        prev_time = C_TIME(icode)
        c_time(1)=prev_time
        ifinc=ATIM*C_TIME(1)+BTIM
        icode=1
        call make_filename(filenam,ifinc)
        call read_vtk(filenam)
         if(icode .eq. 1)then
            icode = 2
         else
            icode = 2
          end if
          C_TIME(icode) = Prev_time + AINCRTIM
          ISINC = ATIM*C_TIME(ICODE)+BTIM
         call make_filename(filenam,isinc)
          call read_vtk(filenam)
          END IF

c
c interpolate
c
c      WRITE(*,*) 'WRITING TEMPERATURE FROM UTEMP'
       AZ = (TIME(2) - c_time(1))/(c_time(2)-c_time(1))
       TEMP(1) = dataval(1,1,NODE)*(1-AZ) + dataval(2,1,NODE)*(AZ)
c      WRITE(*,*) 'TIME2=',TIME(2),' CTIME(1)=',C_TIME(1),
c     1    'CTIME(2)=',C_TIME(2)
c      WRITE(*,*) 'AZ=',AZ
c      WRITE(*,*) 'DATAVAL1=',dataval(1,1,NODE),
```

```
c     1     'DATAVAL2=',DATAVAL(2,1,NODE)
c      WRITE(*,*) 'TEMP',TEMP(1)

      RETURN
      END
c
c
c
      SUBROUTINE make_filename(filename,inte)
      Character filename*256
      CHARACTER IFBUF*30
      WRITE(IFBUF,fmt='(I30)')INTE
      ILEN = 1
      DO I = 1, 30
         IF(IFBUF(I:I).NE.' ')THEN
            ILEN = I
            GOTO 30
         ENDIF
      END DO
 30   CONTINUE
      filename = 'C:\RTM\Geu_ABQ\vtk
     1\rtm_'//ifbuf(ilen:30)//'.vtk'
      WRITE(*,*)'filename:',filename
      RETURN
      END
c
c
c
      SUBROUTINE read_vtk(filenam)
      INCLUDE 'ABA_PARAM.INC'
      COMMON /UTEMP_DATA/DATAVAL(2,2,5000),C_TIME(2),
     1     ATIM,BTIM,AINCRTIM,IFTIME,ICODE,MNODE
      character filenam*256,BUF*256

      open(53,file=filenam,status='old')
 100  CONTINUE
      READ(53,fmt='(A256)',END=200)BUF
      if(BUF(1:14).EQ.'SCALARS TEMPI_')THEN
         READ(53,fmt='(A256)')BUF
         WRITE(*,*)'READING TEMPERATURES',filenam
         DO I = 1, MNODE
            READ(53,*,END=200)DATAVAL(icode,1,I)
         END DO
      END IF
      if(BUF(1:14).EQ.'SCALARS CUREI_')THEN
         READ(53,fmt='(A256)')BUF
         WRITE(*,*)'READING CURES',filenam
         DO I = 1, MNODE
            READ(53,*,END=200)DATAVAL(icode,2,I)
         END DO
         GOTO 300
      END IF
      GOTO 100
 200  CONTINUE
      WRITE(*,*)'FILE ENDED ABRUPTLY'
 300  CONTINUE
      CLOSE(53)
      RETURN
      END
```

B.2 UEXPAN

```
c
c
c
c
c
c
c
c
c
      SUBROUTINE UEXPAN(EXPAN,DEXPANDT,TEMP,TIME,DTIME,PREDEF,
     1 DPRED,STATEV,CMNAME,NSTATV)
c
      INCLUDE 'ABA_PARAM.INC'
c
      CHARACTER*80 CMNAME
c
      DIMENSION EXPAN(*),DEXPANDT(*),TEMP(2),TIME(2),PREDEF(*),
     1 DPRED(*),STATEV(NSTATV)
c     composite
      DATA ALP11,ALP22,ALP33/0.5E-6,35.3E-6,35.3E-6/
c     DATA ALP11,ALP22,ALP33/0.0,0.0,0.0/

c     steel thermal expansion coefficients
c     DATA ALP11,ALP22,ALP33/13.9E-6,13.9e-6,13.9E-6/

      DATA VSHRINK1,VSHRINK2,VSHRINK3/-167e-6,-8810e-6,-8810e-6/
c     DATA VSHRINK1,VSHRINK2,VSHRINK3/0.0,0.0,0.0/
      DEXPANDT(1) = ALP11
      DEXPANDT(2) = ALP22
      DEXPANDT(3) = ALP33
      EXPAN(1) = DEXPANDT(1)*TEMP(2)+ VSHRINK1*DPRED(1)
      EXPAN(2) = DEXPANDT(2)*TEMP(2)+ VSHRINK2*DPRED(1)
      EXPAN(3) = DEXPANDT(3)*TEMP(2)+ VSHRINK3*DPRED(1)
c     write(*,*) 'TEMP',TEMP
c     write(*,*) 'cure',predef(1),dpred(1)
c     write(*,*) 'expan',expan(1),expan(2),expan(3)

      RETURN
      END
```

B.3 UTRS

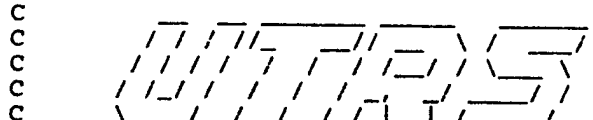

```
      SUBROUTINE UTRS(SHIFT,TEMP,DTEMP,TIME,DTIME,PREDEF,DPRED,
     1 STATEV,CMNAME,COORDS)
C
      INCLUDE 'ABA_PARAM.INC'
C
      CHARACTER*80 CMNAME
C
      DIMENSION SHIFT(2),TIME(2),PREDEF(*),DPRED(*),STATEV(*),
     1 COORDS(*)

C     user coding to define SHIFT(1) and SHIFT(2)

      DATA TW1,TW2,TW3,TW4,TW5,TW6,TW7,TW8,TW9/1.75E+03,1.75E+05,
     1  1.09E+07,6.62E+08,1.70E+10,4.77E+11,1.17E+13,1.99E+14,
     2  2.95E+16/

      DATA ALPREF/0.98/

c     WRITE(*,*)'ENTERING UTRS'
c     WRITE(*,*) COORDS(1),COORDS(2),COORDS(3)
c     WRITE(*,*)'TIME=',TIME(1),' DTIME=',DTIME

      TIME(2)=TIME(1)+DTIME
c     WRITE(*,*)'TIME=',TIME(2),' DTIME=',DTIME
c     WRITE(*,*)'TEMP=',TEMP,' DTEMP=',DTEMP
c     WRITE(*,*)'Field=',PREDEF(1),' DFIELD=',DPRED(1)

C     COMPUTE CONSTANTS
      FALPREF=0.0536+(0.0615*ALPREF)+(0.9227*ALPREF*ALPREF)
      R1=DLOG10(TW1*TW2*TW3*TW4*TW5*TW6*TW7*TW8*TW9)
      R2=-1.4*DEXP(1.0d0/(ALPREF-1.0d0))-0.0712
C         WRITE(*,*)R1
C         WRITE(*,*)R2

C     CALCULATE T' and aT'
      FALPHA1=0.0536+(0.0615*PREDEF(1))+(0.9227*PREDEF(1)*PREDEF(1))
C     WRITE(*,*) FALPHA1
      ALOGAT1=(-1.4*DEXP(1.0d0/(PREDEF(1)-1.0d0))-0.0712)*(TEMP-303)
C      WRITE(*,*)'ALOGAT1',ALOGAT1
      TPRIME1=((((FALPHA1/FALPREF)*R1)+ALOGAT1-R1)/R2)+303
c      WRITE(*,*)'TPRIME1=',TPRIME1
      SHIFT(1)=10**(R2*(TPRIME1-303))
      PREDEF2=PREDEF(1)+DPRED(1)
      TEMP2=TEMP+DTEMP
C         WRITE(*,*)DTEMP
C         WRITE(*,*)DPRED(1)
C         WRITE(*,*)PREDEF2
      FALPHA2=0.0536+(0.0615*PREDEF2)+(0.9227*PREDEF2*PREDEF2)
      ALOGAT2=(-1.4*DEXP(1.0d0/(PREDEF2-1.0d0))-0.0712)*(TEMP2-303)
c     WRITE(*,*)'1'
      TPRIME2=((((FALPHA2/FALPREF)*R1)+ALOGAT2-R1)/R2)+303
c     WRITE(*,*) 'TPRIME2',TPRIME2
      SHIFT(2)=10**(R2*(TPRIME2-303))
C      WRITE(*,*) 'TEMP1=',TEMP
C      WRITE(*,*) 'TEMP2=',TEMP2
C      WRITE(*,*) 'PREDEF1=',PREDEF(1)
```

```
C      WRITE(*,*) 'SHIFT(1)=',SHIFT(1)
C      WRITE(*,*) 'SHIFT(2)=',SHIFT(2)
C      WRITE(*,*)'EXITING UTRS'
       RETURN
       END
C
```

B.4 UMAT

```
C
C
C
C
C
C
C
C     STRESS(NTENS) - PASSED IN AS THE STRESSES TENSOR AT THE BEGINNING
C      OF THE INCREMENT, SIGMA_I_J. (THIS SHOULD BE UPDATED IN
C      THIS ROUTINE.)
C
C      STATEV(NSTATV) - SOLUTION DEPENDANT STATE VARIABLES.

C      DDSDDE(NTENS, NTENS) - JACOBIAN MATRIX Of THE CONSTITUTIVE
C      MODEL.

C      SSE - SPECIFIC ELASTIC STRAIN ENERGY.

C      SPD - PLASTIC DISSIPATION.

C      SCD - CREEP DISSIPATION.

C      RPL - VOLUMETRIC HEAT GENERATION PER UNIT TIME AT THE END
C      OF THE INC.

C     DDSDDT(NTENS) - VARIATION OF STRESS INCREMENTS WITH
C     RESPECT TO TEMPERATURE.

C      DRPLDE(NTENS) - VARIATION OF RPL WRT STRAIN INCREMENTS.

C      DRPLDT - VARIATION OF RPL WRT THE TEMPERATURE INCREMENT.

C      STRAN(NTENS) - TOTAL STRAINS AT BEGINNING OF THE INCREMENT.

C      DSTRAN(NTENS) - STRAIN INCREMENTS

C      TIME(1) - VALUE OF STEP TIME AT BEGINNING OF CURRENT INCREMENT

C      TIME(2) - TOTAL TIME AT BEGINNING OF CURRENT INCREMENT

C      DTIME - TIME INCREMENT

C      TEMP - TEMPERATURE AT START OF INCREMENT

C      DTEMP - INCREMENT OF TEMPERATURE

C      PREDEF - ARRAY OF INTERPOLATED VALUES OF PREDEFINED FIELD
C      VARIABLES.

C      DPRED - ARRAY OF INCREMENTS OF PREDEFINED FIELD VARIABLES.

C      CMNAME - NAME GIVEN ON *MATERIAL OPTION, LEFT JUSTIFIED.

C      NDI - NUMBER OF DIRECT STRESS COMPONENTS AT THIS POINT.

C      NSHR - NUMBER OF ENGINEERING SHEAR STRESS COMPONENTS AT
C      THIS POINT.

C      NTENS - SIZE OF THE STRESS OR STRAIN COMPONENT ARRAY
C      (NDI + NSHR)

C      NSTATV - NUMBER OF SOLUTION DEPENDANT STATE VARIABLES.

C      PROPS(NPROPS) - ARRAY OF MATERIAL CONSTANTS.
```

```
C       NPROPS - NUMBER OF MATERIAL CONSTANTS.
C       COORDS - ARRAY CONTAINING THE COORDINATES OF THIS POINT.
C       DROT(3,3) - ROTAION INCREMENT MATRIX.
C       PNEWDT - RATIO OF SUGGESTED NEW TIME INCREMENT TO THE
C       TIME INCREMENT BEING USED.
C       CELENT - CHARACTERISTIC ELEMENT LENGTH.
C       DFGRD0(3,3) - ARRAY CONTAINING DEFORMATION GRADIENT
C       AT THE BEGINNING OF THE INCREMENT
C       DFGRD1(3,3) - ARRAY CONTAINING DEFORMATION GRADIENT
C       AT THE END OF THE INCREMENT
C       NOEL - ELEMENT NUMBER
C       NPT - INTEGRATION POINT NUMBER
C       LAYER - LAYER NUMBER (FOR COMPOSITE SHELLS
C       AND LAYERED SOLIDS).
C       KSPT - SECTION POINT NUMBER WITHIN THE CURRENT LAYER
C       KSTEP - STEP NUMBER
c      KINC - INCREMENT NUMBER

      SUBROUTINE UMAT(STRESS,STATEV,DDSDDE,SSE,SPD,SCD,
     1 RPL,DDSDDT,DRPLDE,DRPLDT,
     2 STRAN,DSTRAN,TIME,DTIME,TEMP,DTEMP,PREDEF,DPRED,CMNAME,
     3 NDI,NSHR,NTENS,NSTATV,PROPS,NPROPS,COORDS,DROT,PNEWDT,
     4 CELENT,DFGRD0,DFGRD1,NOEL,NPT,LAYER,KSPT,KSTEP,KINC)
C
      INCLUDE 'ABA_PARAM.INC'
C
      CHARACTER*80 CMNAME
      DIMENSION STRESS(NTENS),STATEV(NSTATV),
     1 DDSDDE(NTENS,NTENS),DDSDDT(NTENS),DRPLDE(NTENS),
     2 STRAN(NTENS),DSTRAN(NTENS),TIME(2),PREDEF(1),DPRED(1),
     3 PROPS(NPROPS),COORDS(3),DROT(3,3),DFGRD0(3,3),DFGRD1(3,3)

      COMMON/TW/TWREF(9),TW(9)
      COMMON/WEIGHT/WEIGHT(9)

      COMMON/STIFF/QIJO(6,6),QIJINF(6,6),ILOAD

      DATA ILOAD/0/

      COMMON/SHIFT/ZETA(10000,9,2),KS,KI
      DATA KS,KI/0,0/

c     Number of Elements in Part
      DATA NELEM/448/
c     Reference Degree of Cure
      DATA ALPREF/0.98/

c     WRITE(*,*) 'ENTERING UMAT'
      IF(ILOAD.EQ.0) THEN
          DO I=1,6
              DO J=1,6
```

```
            QIJO(I,J)=PROPS(6*(I-1)+J)
            QIJINF(I,J)=PROPS(36+6*(I-1)+J)
            END DO
          END DO

          DO I=1,9
          TWREF(I)=PROPS(72+I)
          WEIGHT(I)=PROPS(81+I)
          END DO
c       ZETA INITITIALIZATION
        DO I=1,NOEL
            DO J=1,NPT
          ZETA(I,J,1)=0.0
          ZETA(I,J,2)=0.0
          END DO
        END DO

        ILOAD=1
        END IF


c        COMPUTE CONSTANTS FOR SHIFT FUNCTION
        ALPHA=PREDEF(1)+0.5*DPRED(1)
        TEMP_N=TEMP+0.5*DTEMP
        TIME_N=TIME(2)+0.5*DTIME
        FALPREF=0.0536+(0.0615*ALPREF)+(0.9227*ALPREF*ALPREF)
        FALPHA=0.0536+(0.0615*ALPHA)+(0.9227*ALPHA*ALPHA)
c       write(*,*) 'alpha=',ALPHA,' TEMP_N=',TEMP_N
c       write(*,*) 'FALPREF=',FALPREF,'FALPHA=',FALPHA

c       Reduced time multiplied by 60 to make units equivalent to seconds
        DO I=1,9
         TW(I)=60*(10**((FALPHA*DLOG10(TWREF(I)))/FALPREF))
        END DO
c       write(*,*) TW(1)

        SHIFT=10**((-1.4*DEXP(1.0d0/(ALPREF-1.0d0))-0.0712)*(TEMP_N-303))
c        WRITE(*,*) SHIFT
c       write(*,*) dtime
        IF((KSTEP.NE.KS).OR.(KINC.NE.KI)) THEN
            DO I=1,NELEM
                DO J=1,9
                ZETA(I,J,1)=ZETA(I,J,1)+ZETA(I,J,2)
                END DO
            END DO
        KS=KSTEP
        KI=KINC
        END IF


        ZETA(NOEL,NPT,2)=(1/SHIFT)*0.5*DTIME
c        ZETA_NOW=(TIME_N)+((1/SHIFT)*DTIME)
        ZETA_NOW=ZETA(NOEL,NPT,1)+ZETA(NOEL,NPT,2)


        TERM1=0
c       write(*,*) 'weight=',weight(1)
c       DO I=1,9
c           TERM=WEIGHT(I)*DEXP(-ZETA_NOW/TW(I))
c       write(*,*) 'term=',term
c           TERM1=TERM1+TERM
c       END DO

        DO I=1,6
            DO J=1,6
```

```
          DDSDDE(I,J)=QIJINF(I,J)+(QIJO(I,J)*TERM1)
          END DO
        END DO

        RPL=0
        DRPLDT=0

        DO I=1,6
c           STRESS(I)=0.0
            DDSDDT(I)=0
            DRPLDE(I)=0
            DO J=1,6
            STRESS(I)=STRESS(I)+(DDSDDE(I,J)*(DSTRAN(J)))
            END DO
        END DO


c       if ((NOEL.EQ.440).AND.(NPT.EQ.1)) then
c       WRITE(*,*)'temp',KINC,TEMP_N, TEMP
c       WRITE(*,*) 'cure', KINC, PREDEF(1), DPRED(1)
c       end if

c        IF ((NOEL.EQ.572).AND.(NPT.EQ.1)) THEN
c           WRITE(*,*) 'TIME=',TIME(2), DTIME
c           WRITE(*,*)'temp',KINC,TEMP_N, TEMP
c           WRITE(*,*) 'cure', KINC, PREDEF(1), DPRED(1)
c           WRITE(*,679) (TW(I),I=1,5)
c           write(*,680) (TW(I),I=6,9)
c           WRITE(*,*) 'NPT=',NPT
c           WRITE(*,*) 'KINC=',KINC,'','KSTEP=',KSTEP
c           WRITE(*,*)'ZETA_NOW=',ZETA_NOW
c           WRITE(*,*) 'aT',SHIFT
c           write(*,*)'ddsdde'
c           WRITE(*,677)((DDSDDE(I,J),J=1,6),I=1,6)
c677         format('A',6G12.5/,'B',6G12.5/,'C',6G12.5/,'E',6G12.5/
c       1 ,'F',6G12.5/,'G',6G12.5/)


c           WRITE(*,*)'dstrN(1)=', DSTRAN(1)
c           WRITE(*,678)(DSTRAN(I),I=1,6)

c           WRITE(*,*)'strN(1)=', STRAN(1)
c           WRITE(*,678)(STRAN(I),I=1,6)

c678        FORMAT(6(g12.5/))
c679       format('TW',(5g12.5))
c680       format('T2',(4g12.5))
c679      format('T1',G12.5/,'T2',G12.5/,'T3',G12.5/,'T4',G12.5/
c       1 ,'T5',G12.5/,'T6',G12.5/,'T7',G12.5/,'T8',G12.5/,'T9',G12.5/)
c           WRITE(*,*)'stress(1)=', STRESS(1)
c           WRITE(*,673)(STRESS(I),i=1,6)
c        END IF

        RETURN
        END
```